UNIVERSITÀ DEGLI STUDI DI PADOVA

Dipartimento di Tecnica e Gestione dei Sistemi Industriali

Corso di Laurea Magistrale in

Ingegneria dell'Innovazione del Prodotto

Investigation on the Recycling Process of Acrylonitrile Butadiene Styrene via Fused Filament Fabrication Technology

---

Relatore: **Prof. Giovanni Lucchetta**

Correlatore: **Prof. Ludwig Cardon**

Supervisore: **Dr. Rudinei Fiorio**

Laureando: **Pierandrea Dal Fabbro**

Accademic Year 2019/2020

ACKNOWLEDGEMENTS

First, I have to thank Prof. Giovanni Lucchetta and Prof. Ludwig Cardon for the opportunity I have been given and my supervisor Dr. Rudinei Fiorio, who has followed me, giving me the basis and the assistance for all my research.
I thank the researchers and technicians of the CMPT laboratory and of the TE.SI laboratory for their support, availability and patience towards me.
With gratitude I would like to thank my college from universities and Erasmus who have helped me to achieve my goal, motivating me and encouraging me.

CONTENTS

ABSTRACT

In this work the changing in the ABS properties due to the recycling process implemented in the FFF technology has been researched. It was a close loop process between the 3D printing process and the filament extrusion process, in order to obtain new printed parts for next recycling filament step. In each step, the rheological, thermal, chemical and mechanical properties have been investigated following the tests required by the ISO standards.

In the literature, it is well known that the degradation of acrylonitrile-butadiene-styrene mainly concerns the impact strength, and it is controlled by the polybutadiene phase. In the field of injection moulding, several studies associated the degradation of the polybutadiene to the cross-linking and the changing in the dispersion of the rubber phase inside the acrylonitrile matrix. The result is an increasing of the molecular mass and an increasing in the viscosity of the melt, on the other hand the degradation of the SAN matrix presents a decrease in molecular mass and a decrease in viscosity. In this way, the changing in the properties of the recycled ABS are the result of a match between the degradation of his two phases. To date, no research has been carried out on the changes of its the properties due to the recycling process with 3D printing.

The materials studied are a virgin ABS filament and a recycled ABS pellets for injection moulding. Two recycling processes were fully characterised and compared. They confirmed an expected decrease in impact resistance, an increase in tensile strength and a decrease in viscosity. Thermal, chemical and rheological properties were significantly more affected by the extrusion process than by the printing process.

Experimental work done at Center for Polymer and Material Technologies, CPMT, located in Ghent University's Tech Lane (Belgium) and at Laboratorio Te.Si, located in Rovigo (Italy).

The author is grateful to the European Union's Horizon 2020 Research and Innovation Program, which promoted the funding for this research by the grant number 730308 [1].

INTRODUCTION

Plastics are an important material in our economy, and modern daily life because they are found in everything, for example packaging, furniture, automobiles, micro devices and even biomedical components. Today it seems unimaginable a world without them. Their large-scale production dates back only to ~1950 [2]. The prevalence of plastics can be attributed to their highly desirable material properties, such as their lightweight, durability and amenability to be manufacturing using a diverse range of standardised processes.

Most plastics are not biodegradable and are made from oil.

According to the research article [2], it was estimated that 8,300 million metric tons (Mt) of virgin plastics have been produced until 2017 in the world. As of 2015, approximately 6,300 Mt of plastic waste had been generated, around 9% of which had been recycled, 12% was incinerated, and 79% was accumulated in landfills or the natural environment. If current production and waste management trends continue, roughly 12,000 Mt of plastic waste will be in landfills or in the natural environment by 2050 [2] (figure 0-1).

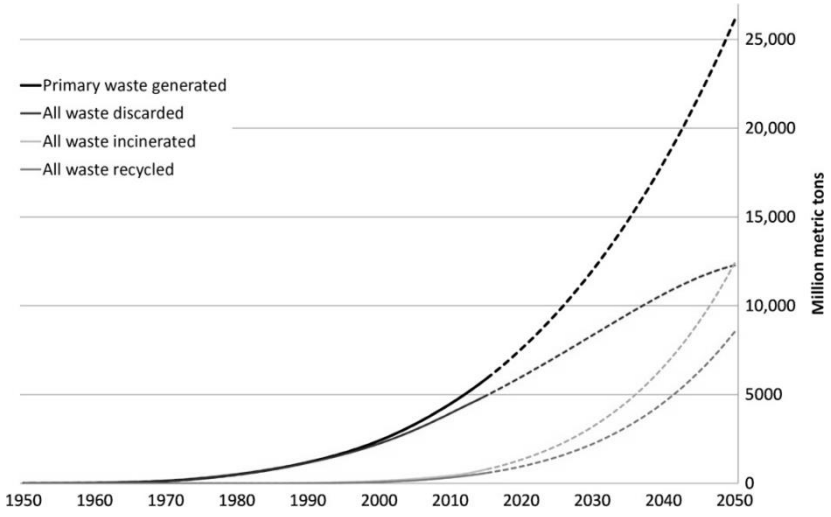

Figure 0-1 Cumulative plastic waste generation and disposal.

Therefore, plastic recycling is becoming increasingly important, not only due to finite fossil-based resources on our earth which are simultaneously used for energy generation, but from the resulting negative impact of our current actions on the environment.

Recycling will help to protect our environment, reduce marine litter, greenhouse gas emissions and our dependence to fossil fuels.

Action on plastics was identified as a priority in 2018 with the Circular Economy Action Plan by European Commission [3], to help European businesses and consumers to use resources in a more sustainable way. Better design of plastic products, higher plastic waste recycling rates, more and better quality recycles will help boosting the market for recycled plastics.

According to the article “Comparing environmental impacts of additive manufacturing vs traditional machining via life-cycle assessment” [4], manufacturing activities are responsible for 19% of the world’s greenhouse gas emissions and 31% of the United States total energy usage.

The AM technologies have been compared in the environmental impacts respect of a traditional CNC milling machine, using life cycle assessment [4]. The result shows the fused filament fabrication (FFF) machine had the lowest ecological impact per part of a CNC machine in the processing of plastics. Because AM builds parts by layering materials, it does not need to remove large amount of materials as in conventional subtractive manufacturing. But a significant volume of material is lost due to the use of rafts, supports and failed prints, leaving such volumes of material typically redundant. The quantity of support material could be influenced by the part orientation and other settings of the printing. Failed prints might be due to various reasons such as insufficient preheating time, inappropriate geometry of parts or printer malfunctions [5] material waste of FFF provides both cost and environmental concerns.

However, [5] quantifies the FFF material waste produced in a heavily used open shop is 34.6 % of the plastic used.

The filaments used in FFF printers are the same filaments produced during the extrusion phase of the classical industrial recycling process. Therefore, the use of these same processes with waste 3D printing recyclable plastics, otherwise destined for landfill, can generate filaments for re-use in FFF based 3D printers.

Despite the increase of materials used, the increase of the speeds for 3D printers and the relative market, there is not enough data available on the usable recycling materials.

1. ADDITIVE MANUFACTURING

Additive manufacturing formalized called rapid prototyping and popularly called 3D Printing, is a technology used in a variety of industries for rapidly creating a physical prototype before final release or commercialization, directly from digital model data [6]. The basic principle of this technology is that a model, initially generated using a three-dimensional Computer-Aided Design (3D CAD) system, can be fabricated directly without the need for process planning. Other manufacturing processes require a long analysis of the part geometry to determine the order in which different features can be fabricated, what tools and processes must be used, and what additional fixtures may be required to complete the part. AM needs only some basic dimensional details and a small amount of understanding as to how the AM machine works and the materials that are used to build the part.

The parts are made by adding material in layers; each layer is a thin cross-section of the part derived from the original CAD data and each layer must have a finite thickness to it; the resulting part will approximate the original data (figure 1-1).

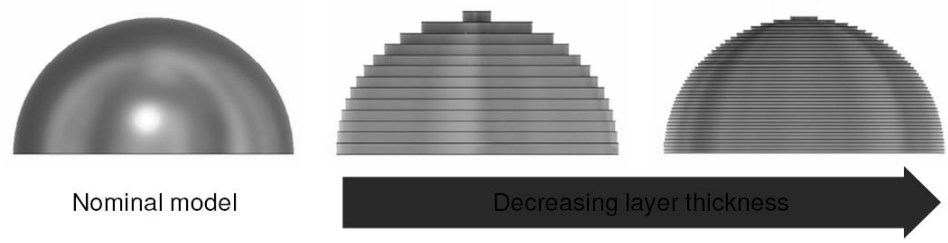

Figure 1-1 Thinner is the layer and closer is the final part will be to the original.

To date, all commercialized AM machines use a layer-based approach, and the major ways that they differ are in the materials that can be used, how the layers are created, and how the layers are bonded to each other, that determine factors like the accuracy of the final part plus its material properties and mechanical properties or how quickly the part can be made, how much post-processing is required, the size of the AM machine used, and the overall cost of the machine and process [6].

There are many commercially available 3DP technologies like fused filament fabrication (FFF), stereo lithography (SLA), inkjet printing, selective laser sintering (SLS), digital light manufacturing (DLP), selective laser melting (SLM), electronic beam melting (EBM), laminated object manufacturing (LOM), etc.

These technologies are categorized in base the architecture (Cartesian, Delta, Polar, Scara), the material used (thermoset polymer, thermoplastic polymer, metal, composite material, ceramic), the material consistency (liquid, filament, pellet, gel, powder), the material aggregation source (laser, heater nozzle, projector).
All A.M. required different state of starting materials and present advantages and disadvantages, in the table 1-2 it is illustrated the comparison of the common 3D printing techniques.

Table 1-2 Comparison of different prototyping techniques.

Techniques	**State of starting materials**	**Typical polymers**	**Working principle**	**Advantages**	**Disadvantages**
Extrusion-based FFF/FDM	Pellet, filament, gel material.	Thermoplastic.	Extrusion and deposition.	Low cost, good strength, multi material capacity.	Anisotropy, nozzle clogging.
Stereolithographic SLA/DLP	Photo-sensitive liquid resins.	Photo curable (epoxy or acrylate-based resin).	Laser scanning and UV introducing.	High printing resolution.	Material limitation, cytotoxicity, high cost.
Powder-bed fusion SLS/SLM/ DMLS/EBM	Powder.	PCL and polyamide powder.	Laser scanning and heat introducing.	Good strength, easy removal of support powder.	High cost, powdery surface.
Inkjet printing	Powder.	Binder jetting over powder material or material jetting DOD.	Drop-on-demand binder printing.	Low cost, multi-material capacity, easy removal of support powder	Clogging od binder jet, binder contamination.
3D plotting	Liquid or paste.	PCL, PLA, Hydrogel.	Pressurized syringe extrusion and heat or UV-assisted curing.	High printing resolution, soft materials capacity.	Low mechanical strength, slow.

1.1 Extrusion based technologies

Extrusion-based technology is currently the most popular additive manufacturing technology on the market [6] .

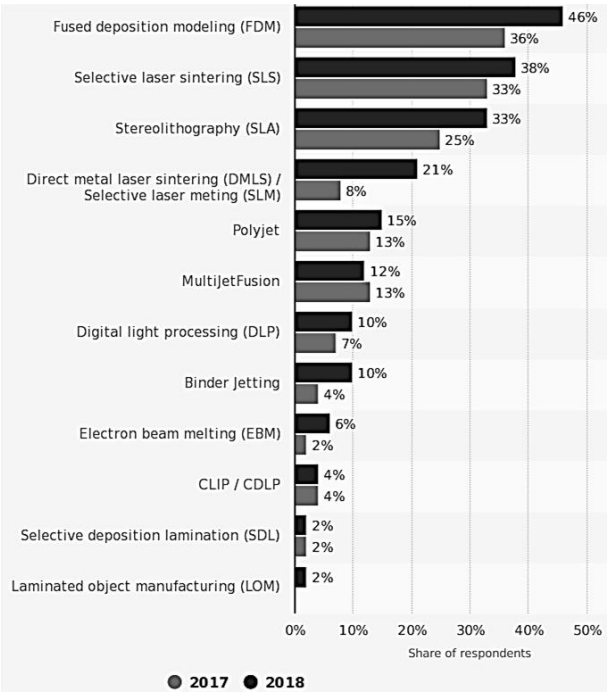

Figure 1-2 Worldwide- Sculpteo 2017 and 2018;

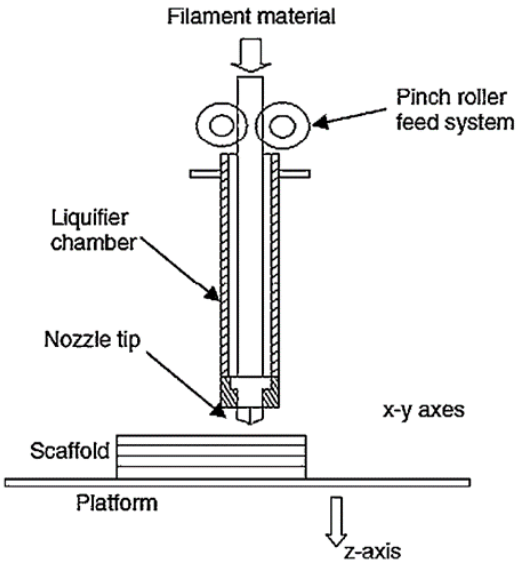

Figure 1-4 Schematic of extrusion-based systems.

There must be a chamber from which. the material is extruded and a continuous supply of material into (pellet, powder form, filament, rarely liquid) under gravity or with the aid of a screw or similar propelling process (figure 1.3).

The extrusion method works on the principle that material pass thought the chamber become a liquid and be push through the nozzle, it quickly solidifies following the extrusion and be liquid because of heat applied by heater between the chamber and the nozzle, the melt temperature should be constant.

The Input pressure is variable, and it changed ed regularly during a build, as it is tightly coupled with other input control parameters, but the more depend is from the kind of materials.

Extrusion-based systems use a platform that indexes in the vertical direction and the head is moved in the horizontal plane (or is the head is move in Z and the platform in XY) to allow formation of individual layers.

All AM systems must have a means for supporting free-standing and disconnected features and for keeping all features of a part in place during the fabrication process.

With extrusion-based systems such features must be kept in place by the additional fabrication of supports. Supports in such systems take two general forms:

- Similar material supports (only one extruder head);
- Secondary material supports (double or more extruder heads).

The variation in material properties can be exploited so that supports are easily to remove.

1.2 Fused Filament Fabrication

Fused Filament Fabrication (FFF), or Fused Deposition Modelling (FDM®) is a patented AM technology, and it developed by S. Scott Crump in the late 1980s and was commercialized in 1990 by Stratasys [7], which provided the basis for extrusion-based AM approaches (figure 1-4).

FFF technology builds parts layer-by-layer by heating and extruding thermoplastic materials in a highly controlled and automated manner, uses a heating chamber to liquefy polymer that is fed into the system as a filament.

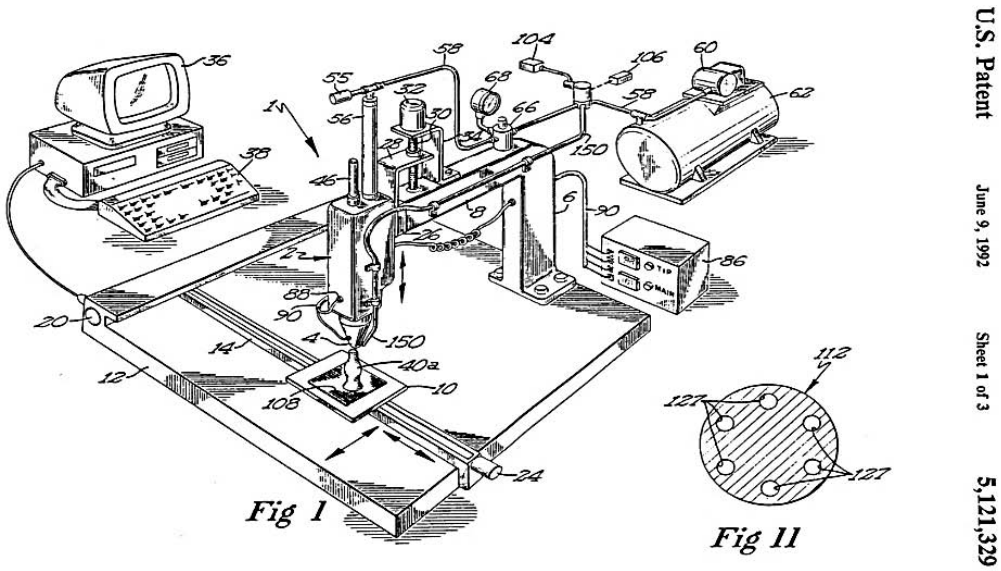

Figure 1-4 One of the images from the FFF patent that summarized the system by Stratasys (9 June 1992).

The filament is pushed into the chamber by a tractor wheel arrangement and it is this pushing that generates the extrusion pressure (figure 1-5).

The machine extrudes and deposits a semi-molten thermoplastic filament in a crisscross manner.

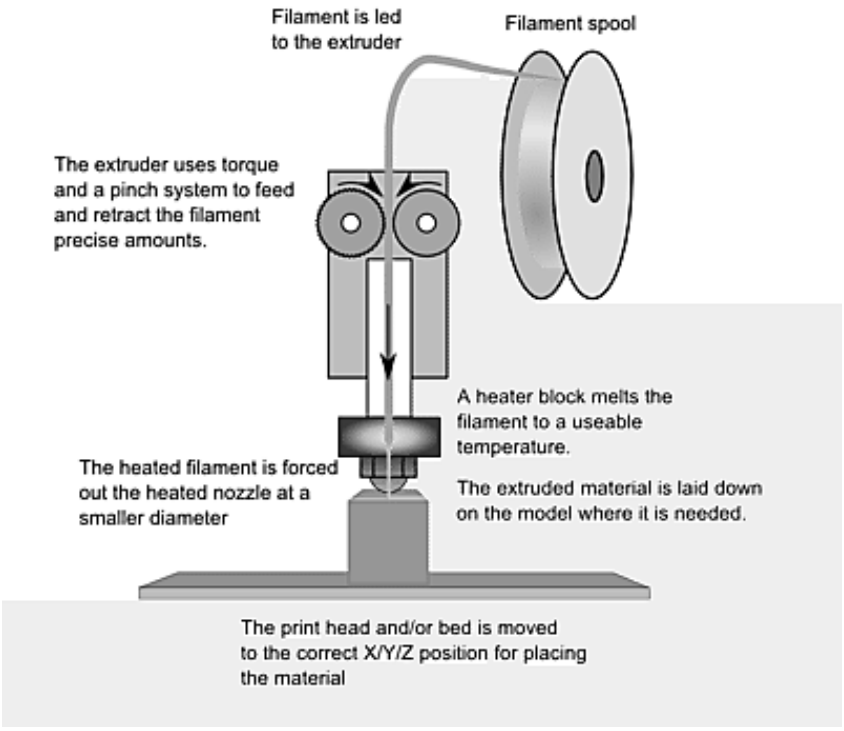

Figure 1-5 Schematic of fused modelling deposition systems.

The major strength of FFF is in the range of materials and the effective mechanical properties of resulting parts made using this technology.

The main drawback to use this technology is the build speed, depending on the inertia of the head. The inertia of the plotting heads means that the maximum speeds and accelerations that can be obtained are somewhat smaller than other systems another problem is the requires material to be plotted in a point-wise, vector fashion that involves many changes in direction.

Other disadvantages are in terms of build speed, accuracy, also that all nozzles are circular and therefore it is impossible to draw sharp external corners; there is a radius equivalent to that of the nozzle at any corner or edge. Internal corners and edges will also exhibit rounding. The actual shape produced is dependent on the nozzle, acceleration, and deceleration characteristics, and the viscoelastic behaviour of the material as it solidifies [5]. In the table 1-2 there are the advantages and disadvantages of this technology.

Table 1-3 Advantages and disadvantages FFF printer [8].

Advantages	Disadvantages
It is easy to change materials.	Support structures are required.
There is a good variety of materials available.	The process is slow on models of large mass.
Capable of fabricating functional parts.	The models have poor strength in the vertical direction.
Additive process with minimal wastage of building material.	Temperature fluctuations during production can lead to delamination.
The support material is easy to remove.	Restricted accuracy due to the diameter of the building filament.
Can use different type of material in the same part.	The process presents an unpredictable shrinkage.

The FFF machine are subdivided in desktop and industrial printer. The principle of function is the same and the main difference are in the dimension of the build volume, in the temperature reach by the bed and nozzle (that is influence the range of the material which can be used), in the cooling system, in the chamber that is able to change temperature and sometimes in the radiant heater inside, in the frame material, and of course the price.

The slicer software can be opensource or dedicated to the printer; anyway, the function and the parameters are almost the same.

An important project born on the FFF technologies it's the RepRap project [9], it has a huge influence over desktop 3D printing (figure 1-6).

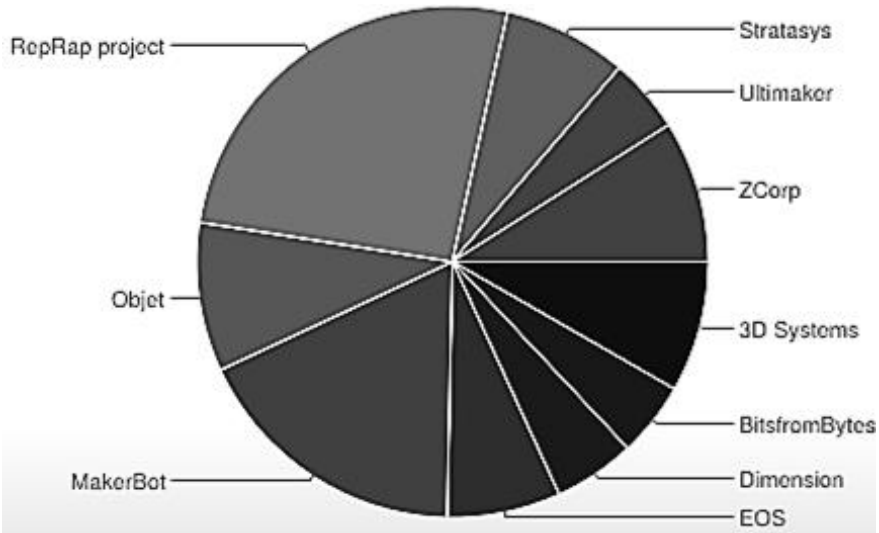

Figure 1-6 Source: Moilanen, J. & Vadén, T.: Manufacturing in motion: first survey on the 3D printing community, Statistical Studies of Peer Production.

RepRap is humanity's first general-purpose self-replicating manufacturing machine, and it is about making self-replicating machines. As an open design (Prusa i3, Hangprinter, Fisher, Snappy, Morgan, Ormerod, Mendel, Darwin) all of those produced by the project are released under a free software license, the GNU (General Public License). There is big community that evolve the printer's components in respect of the standard design. The Prusa i3 mk3s nowadays is always inside the first places in the rankings of best desktop printer.

1.2.1 General process

The working process of FFF can be generalized as three stages [5] (figure 1-7):

1. Pre-processing;
2. Processing;
3. Post-processing.

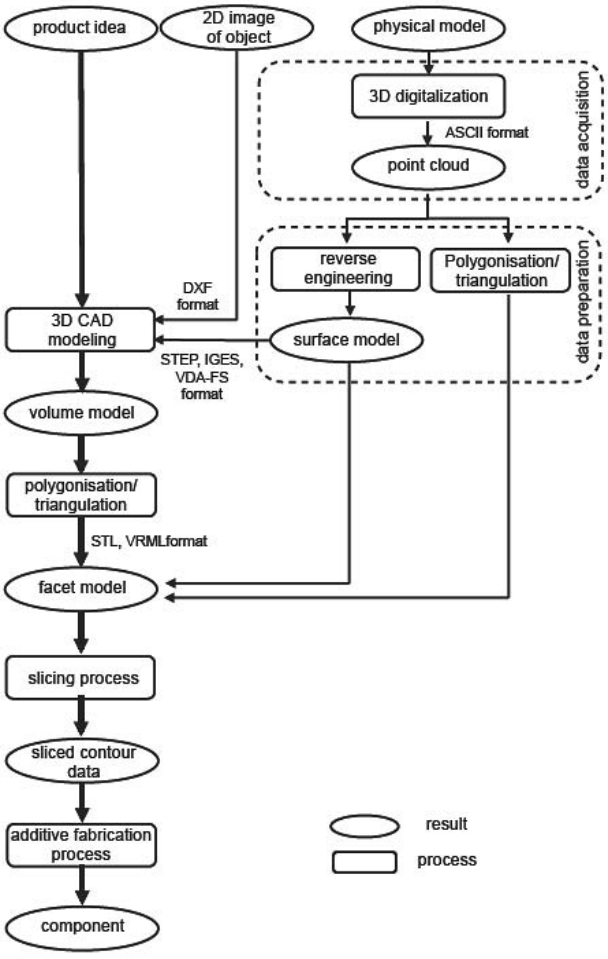

Figure 1-7 Schematic A.M. process system.

1.2.1.1 Pre-Processing

The AM parts must start from a software model that fully describes the external geometry of the product idea.

The first step is building a 3D model by CAD-3D software and export it in STL format (stereolithography file format), AMF (Additive Manufacturing File), OBJ or 3MF.

This format approximates the geometry of the CAD file to a finite element model, uses a simple triangular mesh to approximate the bounding surface of the part (figure 1-8).

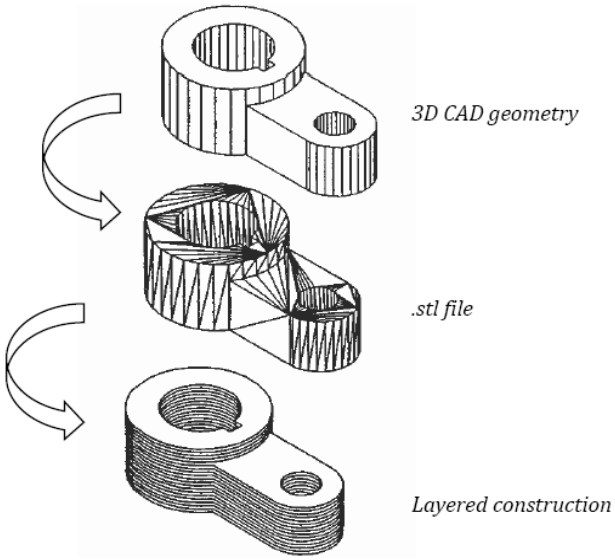

Figure 1-8 Steps from CAD file to printed.

The original CAD model and the STL generator can yield defects in the STL file that will affect the quality of the prototype or prevent its use, to fix these file problems, detection and repair software is available or sometimes is included in the Slicer software.

The Slicer software is required to convert a digital 3D STL/AMF/3MF/OBJ model into printing instructions. It means generate the machine code to manage the printing process, the so-called G-CODE (Geometric Code) and is a widely used in numerical control (NC) programming language. Its main function is to instruct a machine moving part how to move geometrically in 3 dimensions, or it can also instruct a machine to do non-geometric things, for example, G-code commands can tell a 3D printer to extrude material at a specified extrusion rate or change its bed temperature.

The trajectories definite from the slicer in the G-CODE are influenced to the technical characteristic of the machine, for example the dimension of the nozzle, that makes an approximation of the geometry of the part and the resolution of the object will be lower.

In every step from the 3D model to the final part, some information is lost due to the error of the conversion format to another format, the vectorized tool-path and the error of the 3d printer (figure 1-9).

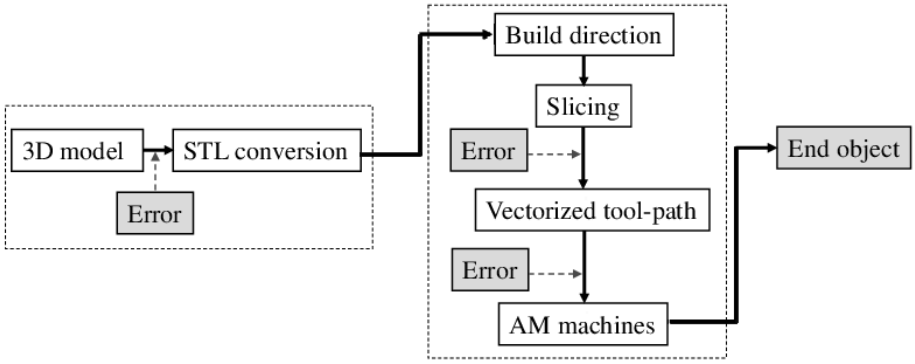

Figure 1-9 Sequence of the conversion cumulative errors.

There is many slicing software, many are opensource and the other are from the 3d printer manufacturers or of the software development companies.

The precision of the extrusion control is a complex trade-off, dependent on a significant number of parameters, the mains are:

- Machine Setting (printer dimension settings, printhead setting, motor setting, start and end of G-Code);
- Quality (layer height);
- Shell (wall thickness, top/bottom thickness);
- Infill (infill density, gradual infill steps);
- Support (type of support and location);
- Material (printing temperature, build plate temperature, diameter of filament, flow, retraction time and length);
- Speed (print speed, travel speed);
- Cooling (on/off fan, fan speed);
- Build Plate adhesion (none or skirt, brim, raft);
- Orientation and localization of the part.

After slicing, the slicer shows the preview of the 3D printing toolpaths, the estimation of building time and material amount required.

The control software must also determine how to fill the material within the outline. This is particularly crucial to this type of system since extrusion heads physically deposit material that fills previously vacant space, without compromising the material that has already been laid down and if the material is not laid down close enough to adjacent material, it will not bond effectively.

The outline is determined by extracting intersections between a plane (representing the current cross section of the build) and the triangles in the STL. These intersections are then ordered so that they form a complete, continuous curve for each outline (there may be any number of these curves, either separate or nested inside of each other, depending upon the geometry of that cross section).

The only remaining thing for the software to do at this stage is to determine the start location for each outline. Since the extrusion nozzle is a finite diameter, this start location is defined by the centre of the nozzle.

The stop location will be the final point on this trajectory, located approximately one nozzle diameter from the start location.

Since it is better to have a slight overlap than a gap and since it is very difficult to precisely control flow, there is likely a slight overfill and thus swelling in this start/stop region.

If all the start/stop regions are stacked on top of each other, then there will be a "seam" running down the part. In most cases, it is better to have the start/stop regions randomly or evenly distributed around the part to make not this seam obvious.

However, a seam is inevitable and having it in an obvious region will make it more straightforward for removing during the post-processing stage.

Determining the fill pattern for the interior of the outlines is a much more difficult task for the control software.

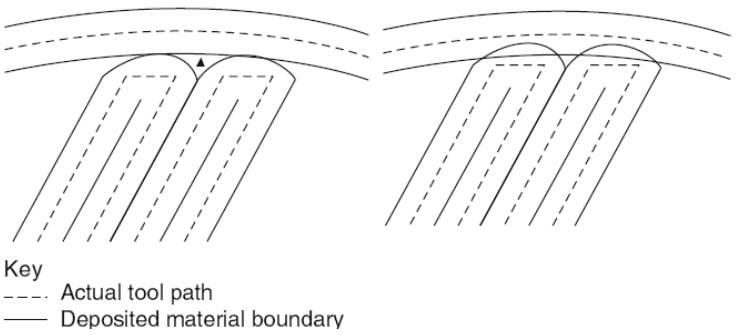

Figure 1-10 Extrusion of materials to maximize precision (left) or material strength (right)by controlling voids.

The first consideration is that there must be an offset inside the outline and that the extrusion nozzle must be placed inside this outline with minimal overlap (figure 1-10).
The software must then establish a start location for the fill and determine the trajectory according to a predefined fill pattern.
This fill pattern is like those used in CNC planar pocket milling, there is no unique solution to achieving the filling pattern.
Furthermore, the fill pattern may not be a continuous, unbroken trajectory for a shape or infill density and pattern (figure 1-11).

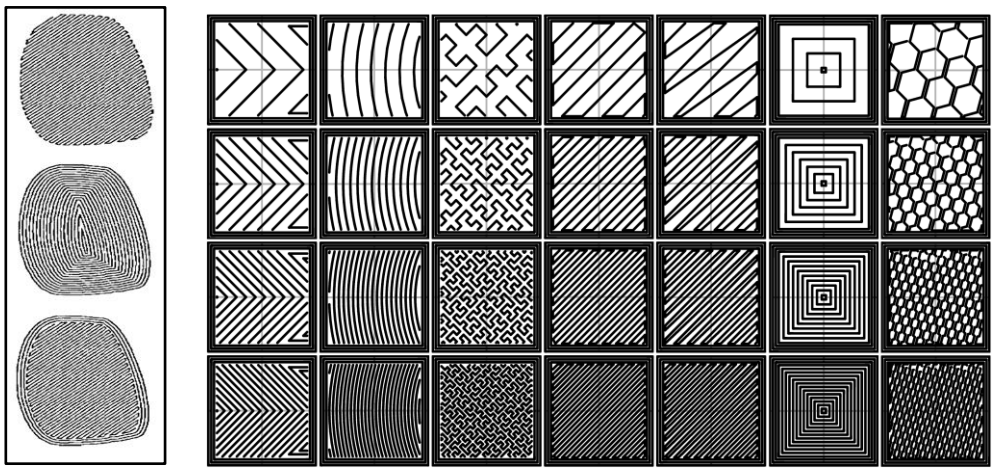

Figure 1-11 In the left different interior style raster, contour, raster/contour and in the right examples of different pattern and infill.

Placing extrusion paths over each other in a crossing pattern can help to distribute the strength in each part more evenly (figure 1-12).
The raster angle is the direction in which the infill is printed with respect to the orientation of the part and it is between 45° and -45°.

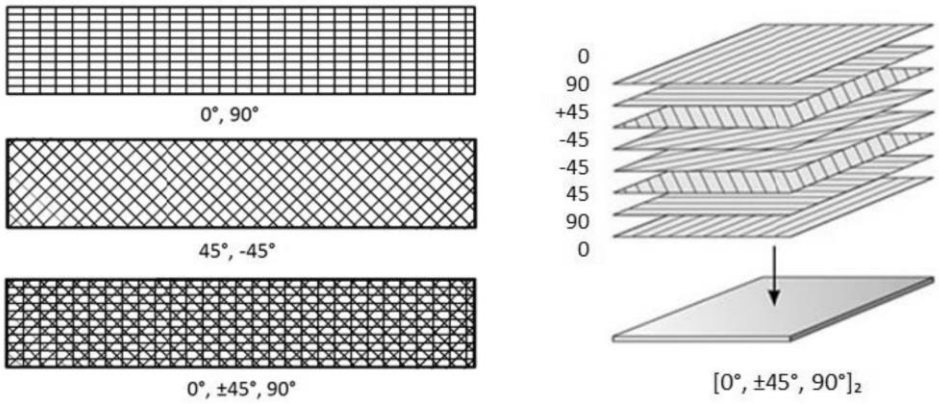

Figure 1-12 Example of different layer direction with the same path and infill.

The raster angle orientations influence the mechanical properties [10] (figure 1-13).

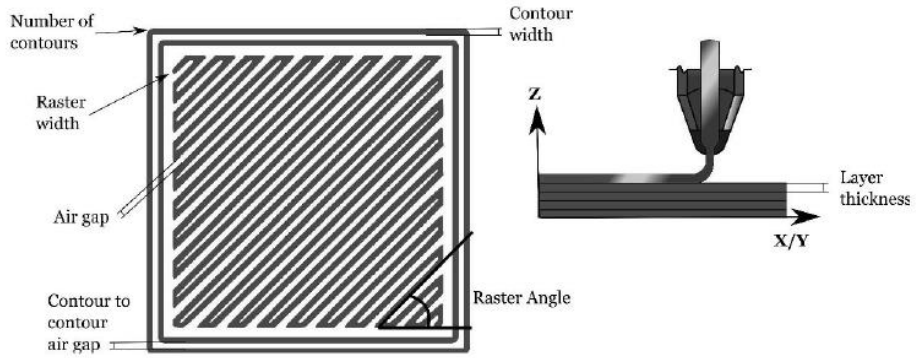

Figure 1-5 Infill setting and layer thickness.

Raster width is the width of the material bead used for raster, more is high more is density the part. Increment the density pattern of the part makes it stronger, but at same time there are some problem due to the printing process, the residual stress and contraction of the part increase with the increase of the density pattern and the part is addicted to warping next to the border.

Every additional weave pattern within a specific layer is going to cause a discontinuity that may result in a weakness within the corresponding part.

For complex geometries, it is important to minimize the number of fill patterns used in a single layer. Most outlines can be filled with a theoretically infinite number of fill pattern solutions. It is therefore unlikely that a software solution will provide the best or optimum solution in every case, but an efficient solution methodology should be designed to prevent too many separate patterns from being used in a single layer.

The weakness of the printer parts is due to the gaps between the layer (figure 1-14).

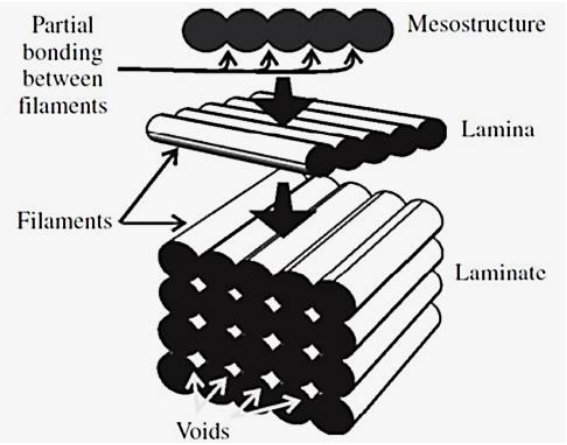

Figure 1-14 Structure of printed part and void due to the deposition strategy.

Since weave patterns achieve the best mechanical properties if they are extruded in a continuous path, there are many changes in direction.

Additionally, by changing the flow rate at these directional change regions, less or more material can be extruded into these regions to compensate for gaps and swelling.
This means that the material flow from the extrusion head should not be directly proportional to the instantaneous velocity of the head when the velocity is low, but rather should be increased or decreased slightly, depending on the toolpath strategy used.
Furthermore, if the velocity is zero but the machine is known to be executing a directional change in a weave path, a small amount of flow should ideally be maintained.
This cause the affected region to swell slightly and thus help fill gaps.
Obviously, care should be taken to ensure that excess material is not extruded to the extent that part geometry is compromised.

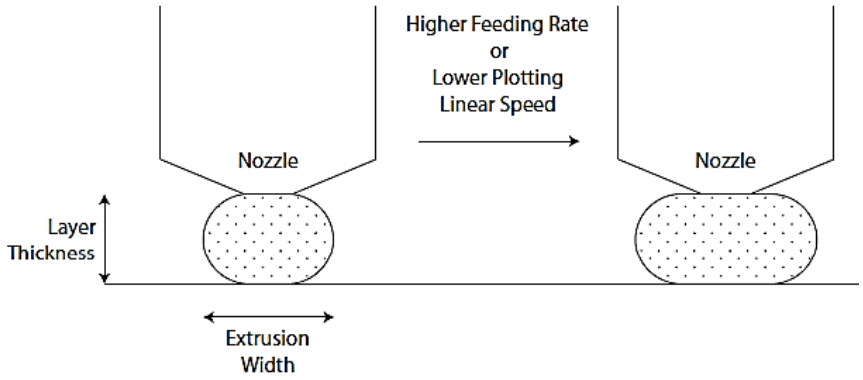

Figure 1-15 FFF extrusion width.

The figure 1-15 explains the influence of the feeding rate and linear movement speed, for a given layer thickness, on the extrusion width.
An increase in the feeding rate leads to an increase of the extrusion width, and similar scenario occurs vice versa when the linear plotting speed of the extrusion head, or nozzle, is decreased, for a given feed rate.
This means that the adjacent paths are very close to each other, resulting in an overlap of paths and excess of deposit filament or the adjacent paths distant from each other, resulting in gaps and minimal or non-existing bonding between them, which weakens the structural integrity of the part.
Thus, it becomes necessary to optimize the width of the path, by extruding more or less material via changing the feed rate/head's linear plotting speed ratio. Although thicker paths lead to a better bonding and thus better mechanical performance, it will most probably fail to meet the geometrical resolution.

The commons adhesion method is raft, brim (figure 1-16) or external adhesion material fixed on the bed (specific glue or scotch tape).

It is depending on the printing material and the dimension of the part and it is uses for preventing the warping and for help the adhesion of the first layer.

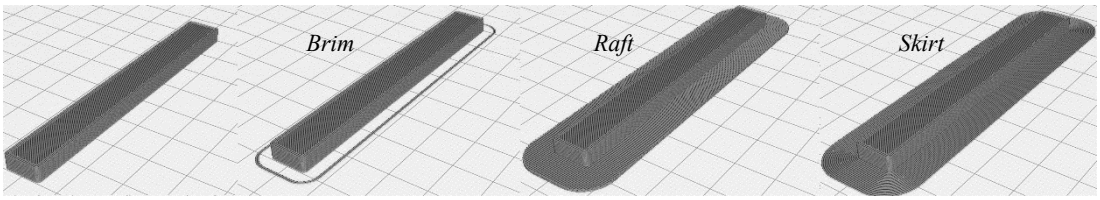

Figure 1-16 Comparison between the adhesion methods.

1.2.1.2 Processing

The printer head, or the plate, move along a toolpath forming the part.

The platform holds the part by an adhesion method.

The material is extruded in a semi-molten state and the newly deposited material fuses with adjacent material that has already been deposited, layer by layer.

1.2.1.3 Post-processing

The raft and support structure will be removed in this step.

The raft and the mesh like support material need to be broken away manually or by some chemical solvent.

Removing the raft or the supports manually probably results in parts deformation or even parts damage.

For the FFF machine with double liquefier, the support material can be built with another material and dissolved in detergent or water; in this way remove support is more safety and can preserve the part from the operator mistake.

1.2.2 Materials

In FFF process there are many properties of thermoplastic polymers that can contribute for a result appropriate in response at the required application (figure 1-17) [11].

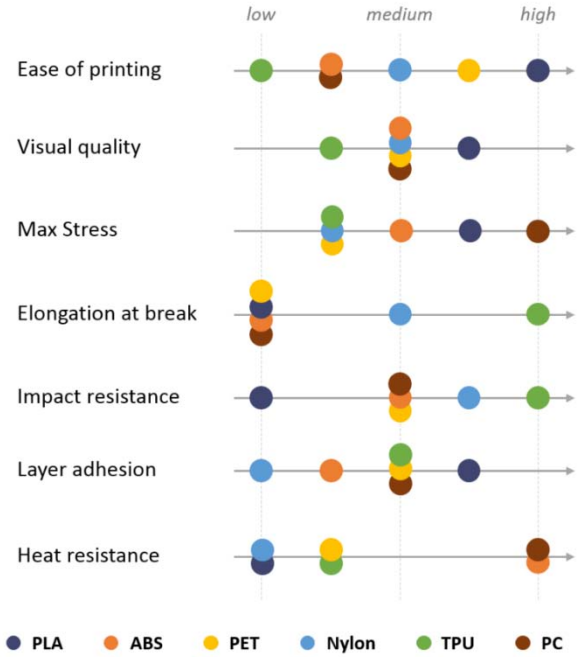

Figure 1-17 Rank of FFF most used polymers by 3DHUBS.

Using the data from Optimatter, 3DHUBS [11] ranked the polymers along the different criteria. Each material has been ranked along the following criteria on a 1 (low) to 5 (high) scale. These are relative grades for the FFF process, they would look quite different if other manufacturing technologies were considered.

The thermoplastics must be able to flow into the melt chamber in a controlled manner and then solidify in the deposition platform.

A polymer low melting temperature do not request a performant liquefier, but the polymer's utilization fields are very narrow.

The properties of interest include the melting temperature (T_m), glass transition temperature (T_g), and the coefficient of thermal expansion (CTE).

It is necessary to have a low coefficient of thermal expansion for reduce internal stresses caused during cooling and keep the final part dimensionally closer to the original 3D model.

A low glass transition temperature and CTE in thermoplastics is useful because it reduces problems such as residual stress warpage and helps bonding between layers, but a

too low T_g (elastomers) causes problems with the feeding system and material deposition. The T_g and the CTE relate to how much thermal stress is developed during printing which can affect bed adhesion.
Strong secondary bonding helps to have better layer-to-layer adhesion.
Solvent resistance, strength, and ductility are also important properties and are a function of the polymer chemistry and microstructure of the polymer.
The strength and ductility of the printed part are also directly affected by the chemistry and microstructure.
The T_m and the T_g are directly related to how easily polymer chains can slide past each other, at the molecular level. The T_g is the temperature for each plastic at which it is not yet melted, but at which it becomes easier for polymer chains to move, resulting in a large change in properties. Above T_g the plastic is flexible and ductile, and below T_g the polymer is stiffer and brittle like glass. In terms of chemistry, the factors that can affect these properties are the chemistry of the repeat unit backbone, pendant groups, and the polarity of the bonds. Large pendant groups make it easy for polymer chains to entangle which restricts motion of the chain polymer more raising T_g and T_m. Polymers with no aromatic rings in backbone tend to be more flexible and have a high elongation before fracture. Aromatic rings in the polymer backbone tend to increase the strength, stiffness, and T_g of the polymer, but reduces the amount of elongation before fracture.
They also improve flammability properties of a polymer but are susceptible to degradation from ultraviolet radiation.
Polar groups influence the resistance of a polymer to solvents as well. Polymers with more polar groups are more likely to dissolve in polar solvents, goods for the removable support structure. They also have the potential to participate in dipole or hydrogen bonding, a strong form of secondary bonding method that can increase strength of the polymer through crystallization. It also tends to make polymers stronger and more rigid, but more brittle.
Thermoplastic polymers can exhibit two types of microstructures, amorphous and crystalline, almost the thermoplastic properties depend from this. Amorphous structures have no identifiable order to the arrangement of the polymer chains and crystalline regions occur when the polymer chains align and pack tightly together. Polymers often exhibit a combination of amorphous and crystalline regions. The amorphous/crystalline

structure is controlled by many factors such as repeat unit chemistry, molecular weight, processing parameters, and loading. Anything that makes it harder for the chains to stack closely together such as pendant groups or stiff chains tend to cause the polymer to exhibit more amorphous structures. In terms of properties, amorphous regions tend to be more mobile and flexible and give the polymer increased ability to elongate. Semi-rystalline regions impart greater strength, stiffness, density, heat resistance and solvent resistance to a polymer, but lower its maximum elongation and optical transparency. For example, polymers with higher crystallinity, like PLA or PP, are more suited to products where hardness and rigidity are needed. On the other hand, products that need flexibility be more suited to amorphous polymers, like HIPS or ABS.

FFF works best with polymers that are amorphous in nature rather than the highly crystalline polymers. This is because the polymers that work better are those that are extruded in a viscous paste rather than in a lower viscosity form. As amorphous polymers, there is no distinct melting point and the material increasingly softens and viscosity lowers with increasing temperature. The viscosity at which these amorphous polymers can be extruded under pressure is high enough that their shape be largely maintained after extrusion, maintaining the extrusion shape and enabling them to solidify quickly and easily. Furthermore, when material is added in an adjacent road or as a new layer, the previously extruded material can easily bond with it.

The bonding between individual roads of the same layer and of neighbouring layers of FFF parts is driven by the thermal energy of the semi molten material. The required heat transfer is a function of the thermal properties of the liquefier, tip, and modelling materials, and the diameter of the filament. When the filament is deposited and is in contact with surrounding material, the interface's temperature is well above the material's glass transition temperature. This condition favours the rapid development of adhesive bonds. The bonding process can be described as shown in figure 1-18, the cross sections of filaments are idealized as circles.

Figure 1-18 Bonding process: surface contacting, neck growth, diffusion at interface.

The first step of the process is the establishment of interfacial molecular contact by wetting. The molecules then undergo motions toward preferred configurations to achieve the adsorptive equilibrium. Molecules diffuse across the interface, forming an interfacial zone, and/or react to form primary chemical bonds across the interface. The randomization of the chains can be reached only after extensive inter-diffusion of chain segments over the cross-section. In this zone the temperature of the filament is well above its glass transition temperature. So, the temperature of the filaments then rapidly decreases while a neck is formed between adjacent filaments

Anyway, the bonding zone between the layer present voids due to the deposition strategy. They are the most weakness factors for the mechanical properties and the main difference from the production from the injection moulding technologies (figure 1-19).

The higher material compaction in addition to the enhancement of the semi-crystalline structure in the injection moulding process give better mechanical properties in confront of the FFF technologies [10] (figure 1-20).

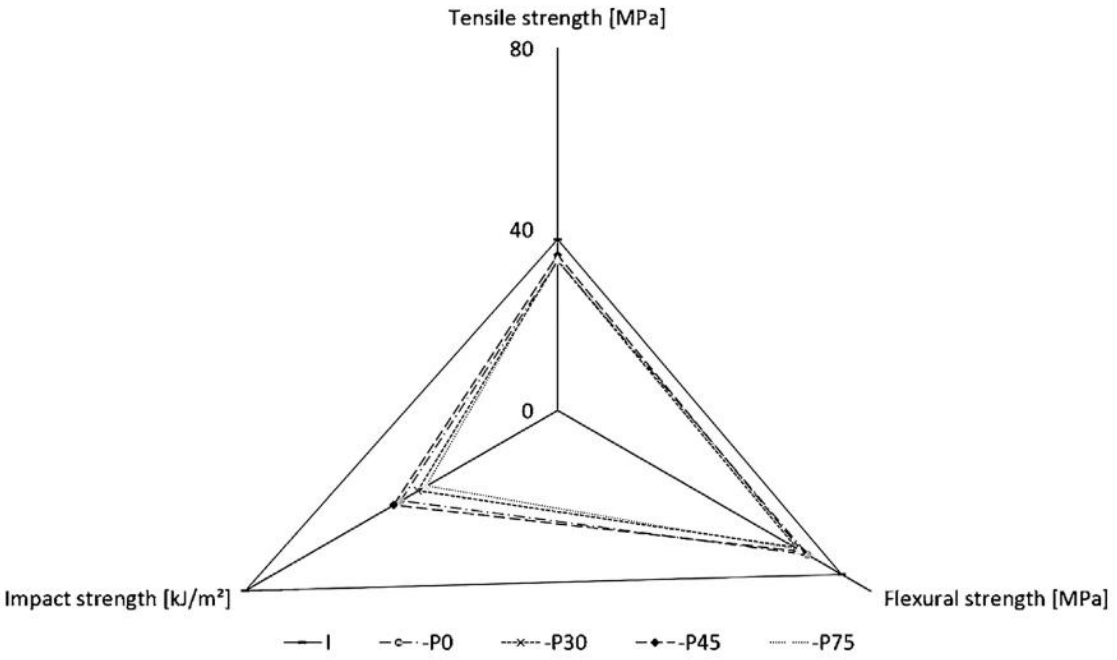

Figure 1-20 ABS mechanical proprieties of injection moulding and printer part with different raster angle and negative airgap [9].

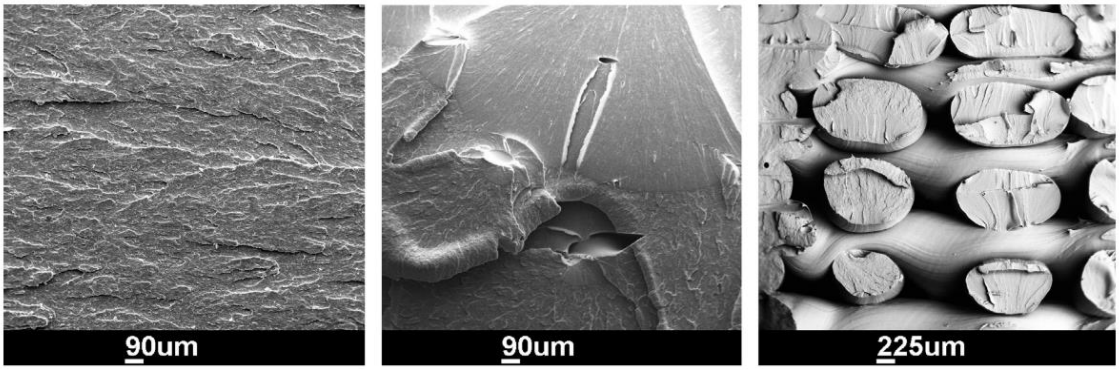

Figure 1-19 SEM of the fracture surface of tensile samples in ABS of injection moulded, printed part with negative gap and positive gap.

Increasing the nozzle temperature, the viscosity of the melt decreases and the polymer infiltrates better between the voids reducing the porosity, the bonding is better but the material thermo-degradation increase [12].

The cooling process is transient and physically complex in its nature [5].

The material of the filaments can be bio-based (like PLA) or completely synthetic (like ABS or PVA), there is a wide range of materials from standard to engineering-grade, also encompassing the most high-performance thermoplastic materials (Nylon 12, ABS, PLA, PTB, PC, PTEG ...).

Another family regards the composite materials, they have inside a thermoplastic matrix and a dispersion of short fibers, fibrils, nanofibers, carbon fillers and continuous fibers (carbon-fibers, fiberglass, carbon fillet, Kevlar-fibers, bio fibers, etc.), metal powders (aluminium, copper, etc.) and refractory material (graphene, ceramics, etc.), carbon nanotubes, etc.

Those reinforced materials provide comparably low thermal expansion, with higher control of the warpage problem, but they request special nozzle with high hardness and powerful extrusion system.

The diameter standard dimensions of the commercial filaments are: Ø 1.75 (mm) and Ø 2.85 (mm).

Almost all the commercial printer uses the Ø 1.75 (mm), and this is because it is preferred the bigger diameter for have a more constant flux, and a higher extrusion volume even if it requires more powerful filament pulling systems.

2.STYRENE BASED POLYMERS

ABS, HIPS, SBR, SAN are the most famous co-polymer or ter-polymer styrene based. The polystyrene was first commercially produced by Dow chemical company in 1937, and it was initially used because of its excellent dielectric and optical properties.
Styrene is produced from the ethyl-benzene by a process of dehydrogenation, is a linear hydrocarbon polymer.
It is hard, rigid and transparent with a low water absorption, good dimensional stability and isolation properties.
To improve the performance and properties of the PS (figure 2-1), various copolymers have been developed in which specific monomers are introduced together with the styrene:

- A-methyl-styrene to improve heat stability;
- Acrylonitrile to increase chemical resistance;
- Methyl-methacrylate to increase transparency;
- Di-methyl-ester to give greater stability to UV rays;
- Polybutadiene rubber as an anti-shock agent.

The addition of acrylonitrile, in contents of 20-30% by weight, should be emphasized to form SAN, a widely used material where high thermal properties are required; a content of about 50% in acrylonitrile shifts the glass transition temperature higher than 20°C. This material has a better chemical resistance especially to oils or greases, even if there is a risk of losing gloss (tends to yellow) and there is a reasonable increase in cost (40%). The acrylonitrile reduces cracking under stress but, in excessive proportions, reduces workability.
The addition of a certain amount of rubber (polybutadiene), in levels between 5% and 15%, leads to the formation of the anti-impact polystyrene (HIPS), which was first produced in 1960.
The properties of the product obtained depend on the type of rubber, the concentration and the size of the rubber particles.
The ter-polymer ABS is the combination of the good mechanical and chemical properties of the SAN with the impact resistance of HIPS (figure 2-1).

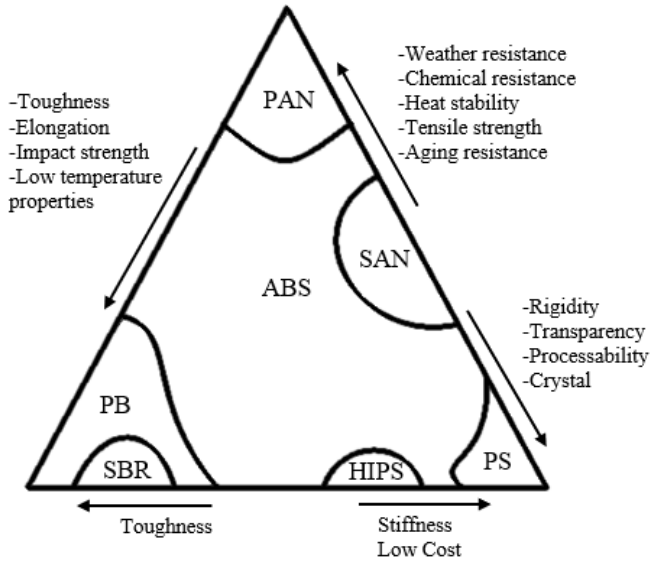

Figure 2-1 ABS proprieties.

The addition of dispersed polybutadiene in the form of particles into a rigid styrene-acrylonitrile matrix leads to the formation of a material with tensile strength and elastic modulus similar to the SAN polymer, but with a strong increase in impact toughness (table 2-1).

The first ABS plastics were produced in the fifties and today on a world scale, their production is a world scale, is around 11 million tons per year.

Table 2-1 physical properties of polystyrene and styrene copolymers.

Properties	**PS**	**SAN**	**HIPS**	**ABS**	**Unit**
Specific gravity	1.05	1.08	1.02-1.04	1.03 – 1.07	g/cc
Tensile Strength	32 - 57	57 - 76	16 - 40	25 - 52	MPa
Tensile modulus	2700 - 3500	3400-3900	1650-2550	2000 - 2700	MPa
Flexural modulus	3103 - 3448	3080 - 3560	1790-2690	2200 - 3030	MPa
Elongation at break	1 – 3.6	2 – 3.5	1 – 1.5	2 – 25	%
Impact Strength	13.3 - 24	13 - 24	48.1 - 219	104-320	J/m
Hardness Rockwell	60 - 84	80 - 83	45 - 88	105 - 112	
HDT (< 1.82 MPa load.)	76 - 108	99 - 110	69 - 101	93 - 104	°C
Glass Transition Temp.	74 - 110	115	93 - 105	105 - 115	°C
Dielectric Strength	19.7	12 - 16	11.8 - 105	16 - 31	KV/mm
Thermal expansion	7×10^{-5}	9×10^{-5}	7×10^{-5}	1×10^{-5}	$°C^{-1}$

2.1 Acrylonitrile Butadiene Styrene

This thermoplastic ter-polymer has an amorphous structure and is made of three monomers: acrylonitrile (C3H3N), butadiene (C4H6), and styrene (C8H8) (figure 2-2).

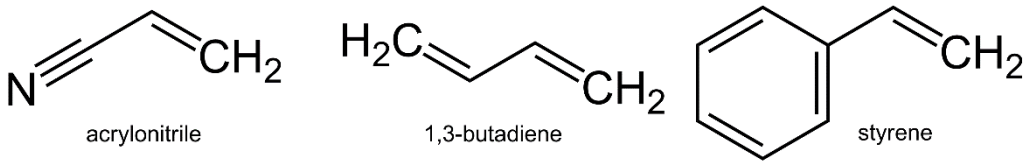

Figure 2-2 Monomers in ABS polymer.

Acrylonitrile is a synthetic monomer produced from propylene and ammonia; butadiene is a petroleum hydrocarbon obtained from the C4 fraction of steam cracking styrene monomer is made by dehydrogenation of ethyl benzene-a hydrocarbon obtained in the reaction of ethylene and benzene.

The glass transition of the elastomeric phase PB is around -90 (°C), for the matric phase (SAN) is around 110 (°C).

It is consisting in an continues rigid phase SAN (styrene-acrylonitrile copolymer) in which the elastomer phase (polybutadiene grafted with styrene and acrylonitrile) is finely dispersed in the form of spherical particles.

It can be considered a biphasic system in which there are rubber inclusions in a continuous and semi-crystalline matrix.

Due to many interspersed particles of rubbery polybutadiene, the material can absorb more mechanical energy and plastically deform without fracturing.

It is very sensitive to the rays UV and therefore limits the presence of ABS in outdoor environments.

It is a techno polymer designed for application requiring good impact resistance, toughness, rigidity, surface hardness, dimensional stability, heat resistance, aesthetic appearance.

ABS is resistant to aqueous acids, alkalis, concentrated hydrochloric and phosphoric acids, alcohols and animal, vegetable and mineral oils, but is attacked by concentrated sulfuric and nitric acids. It is soluble in esters, ketones, 1,2-dichloroethane and acetone.

The production of ABS is carried out according to two main methods [13]:

1. *Continuous mass polymerization*

Widely used to produce HIPS, provides in a single stage the simultaneous obtaining of both the matrix (acrylonitrile-styrene) and the rubber (butadiene), obtaining as final product ABS in granules.

Three main phases characterized the process:

- Process feed, the non-cross-linked polybutadiene rubber is dissolved in styrene and acrylonitrile monomers;
- Pre-polymerization, where the monomers are partially pre-polymerized by stirring the bath;
- Final cycle, the polymerization is completed with or without stirring.

At a certain degree of conversion, the thermodynamic balances that allowed the presence of a single phase at the beginning are modified by developing the phenomenon of phase separation. The SAN formed constitutes a separate phase with respect to the grafted polybutadiene and the monomers are arranged between the two phases, stabilising them. Subsequently, as a result of polymerization, a phase inversion develops: the SAN becomes the continuous phase and the polybutadiene the dispersed phase. The particles thus formed contain, in turn, conspicuous inclusions of rigid matrix, i.e. the structures generated at the beginning of the reaction are preserved during its entire development. The stirring conditions are fundamental because if the speed is too low the phase inversion does not occur or is delayed. The final size and composition of the dispersed phase particles is determined by the flow rate during the period immediately following the phase reversal. This process leads to a morphology called "slice of salame" because the gummy phase, following the rapid phase inversion, has significant (up to 80-90%) inclusions of rigid matrix within it and the average size of the gummy phase are larger than those obtained by polymerization in emulsion.

The continuous mass process does not use any material or additives extraneous to the reaction (such as water in the processes), thus allowing the reduction of the quantity of emissions drastically.

2. *Emulsion polymerization*

In this process there are two distinct moments to produce the rigid phase and the rubber phase. In fact, three basic stages can be distinguished:

- Preparation of rubber latex by emulsion polymerization;
- Copolymerization of styrene and acrylonitrile in the presence of rubber latex to produce "graft";
- Dispersion of the grafted rubber in the SAN copolymer.

From the first stage, a polybutadiene rubber is obtained, consisting of a dispersion of particles in an aqueous medium.

In the second stage, the reaction of the SAN chains to the rubber particles develops. This phenomenon occurs in the presence of substances, such as tensioactives, which are essential for the formation of an emulsion. Finally, by mixing, the grafted product is dispersed in the SAN homopolymer.

The polymeric chains grafted onto the rubber particles allow compatibility between the two different phases, ensuring the development of adhesion to the interface, which has a chemical nature and is ensured by the formation of physical cross-linking ('entanglements') between the grafted SAN chains and the rubber.

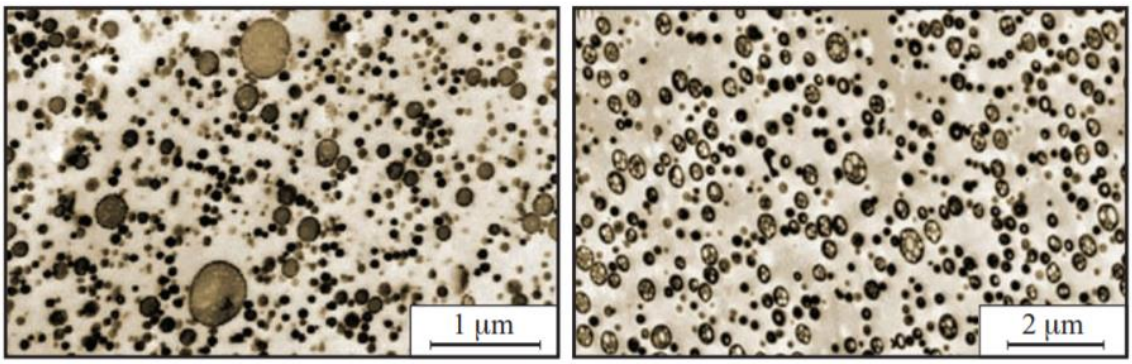

Figure 2-3 TEM image of ABS with process in emulsion (left), ABS product with process in mass (right).

This second methodology, which is more widely used than to the previous one, allows to obtain a more homogeneous rubber phase in the composition (almost no inclusions) and a homogeneous the size of particles (figure 2-3).

It is produced in a wide range of types (five main classes of ABS) that optimize impact resistance, resistance to temperature, fluidity or specific applications.

The properties depend on the percentual of each phase inside the ABS:

- Acrylonitrile 20 to 30% provides the resistance to heat and the tensile strength;
- Butadiene 20 to 30% provides brightness, moldability and stiffness, the toughness and the properties at low temperatures;
- Styrene 20 to 60% impact strength and stretching, stiffness, the transparency and the workability;

Processing of plastics at different temperatures enhance its basic properties, at high temperatures provide a better look but the impact properties decrease and vice versa. This thermoplastic material can be easily recycled and again mixed with virgin materials to form new plastic products.

ABS is the second most used material in the FFF world in according to the Belgium-based 3D printing material platform Filaments-directory [14] [15] (figure 2-4).

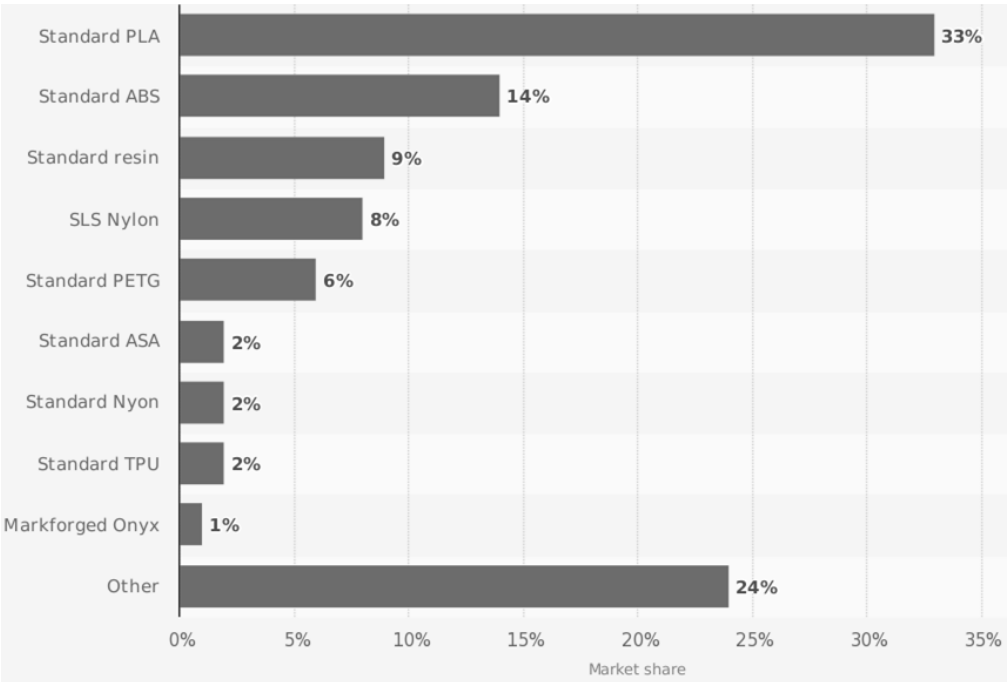

Figure 2-4 Worldwide most used 3D printing materials, as of July 2018, Source 3D Hubs.

Thanks to its properties, it is strongly suitable for the 3D printing, easily affordable and allows the modification and superficial treatment after printing (acetone treatment). It is proving to be a versatile material for the A.M.

The weakness points are its easily flammability when exposed to fire and his combustion gases, which are toxics (carbon monoxide and hydrogen cyanide).

2.2 Effect of reprocessing

The market demand for the acrylonitrile butadiene styrene resin is high and is continuously growing in recent years.

This material is considered a cheap engineering polymer in plastic manufacturing but the recycling process it's been come into practice. The recycled ABS can be used as a mixture of virgin material or in the product that doesn't required high mechanical properties.

There are many studies in literature about the evaluation of the properties after reprocessing ABS several times with injection moulding technologies, but not enough regarding the reprocessing with the addictive manufacturing technologies.

Boronat et al. [16] studied the effect of reprocessing cycle conditions (temperature and shear rate) on the properties of ABS. Two grades of ABS were injected and tested (high viscosity grade and low viscosity grade) and the results shows a different behaviour. The low viscosity grade showed a reduction of viscosity with increasing the number of processing cycles whereas the high viscosity grade, conversely, showed an increase of melt viscosity.

Perez et al.[17] studied the effect of reprocessing on the mechanical, thermal and rheological properties of ABS. The results showed that neither melt viscosity and tensile strength was significantly affected by the number of cycles, but the impact strength decreased slightly probably as a consequence of changes in the polybutadiene phase.

Karahaliou et all. [18] obtained the same results as Perez where the stability of ABS subjected to five extrusion cycle was investigated.

Also, Kim and Kang [19] reprocessed three ABS resins five time, they investigated the glass transition temperature of the SAN phase but without finding an important variation. The changes in the mechanical properties and the hardness was not important. However, impact resistance of all materials decreases, especially the impact resistance of ABS with the highest polybutadiene content. The reason for the decrease was again in the degradation of the polybutadiene component in ABS.

Mechanical properties of ABS are strongly affected by theirs phase morphologies [20][13]. In a recent study of Hirayama et al. [21] they compared ABS and HIPS virgin, recycled and the relative blend (figure 2-5).

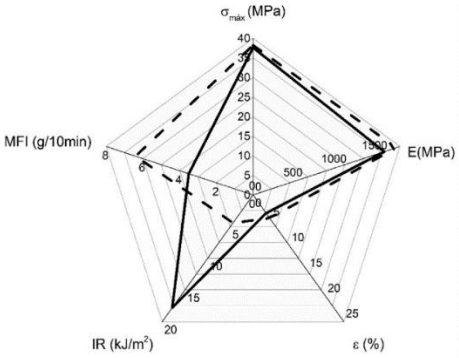

Figure 2-5 Mechanical and rheological properties for ABS: virgin (solid line) and recycled (dash line).

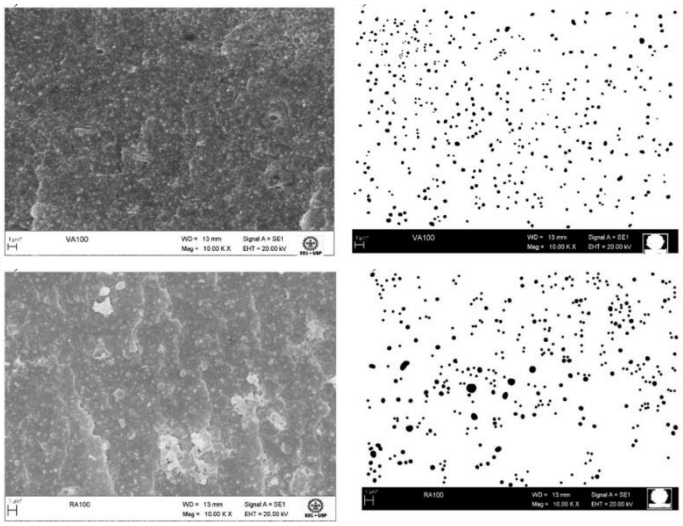

Figure 2-6 SEM images for virgin (above) and recycled ABS (non-treated image and treated image).

Thus, scanning electron (SEM) and treated the image with Image-J they evaluate morphological differences between virgin and recycled polymers (figure 2-6).

It is known the impact resistance of the ABS is only reached when the domains rich in polybutadiene present small dimensions [13][22].

As it shows in the virgin ABS, the dispersed phases are small, spherical, with uniform size and are regularly distributed in the material; while in the recycled ABS, the domains are slightly larger, with a bad distribution and a high size variation of dispersion phase [21]. The diameter of dispersed phase in the recycled ABS increase. Brittle polymer matrixes, such as PS and SAN, tend to fail by crazing, have low crack initiation energy and low crack propagation energy [23].

The yielding is important and depends of matrix-ligament thickness, during the fracture, thin ligaments may yield while thick ones may not. If the thick ligaments are surrounded by enough thin ones, the yielding of the thin one could also relieve the dilative stress and cause the thick ones to yield [24].

Therefore, both smaller diameter of rubber particle and thinner matrix-ligament thickness are the main important features that gives the peculiar mechanical properties [21], and in virgin ABS can explain the higher impact resistance for this polymer when compared to the recycled ABS.

In general, the ABS have several additives incorporated (flame retardants, colorants, stabilizers), they can influence the toughening mechanism of ABS, causing changes in

mechanical properties. The presence of additives or degradation products in the recycled ABS could cause changes in the phase equilibrium of the material, resulting in the morphological difference observed in the virgin and recycled ABS. Bai et all [25] investigated the effects of reprocessing on additives in ABS, they found that reprocessing ABS plastics leads to loss of some additives because of volatilisation, decomposition, or conversion. Reprocessing at a relatively low temperature can reduce the loss of additives in plastics.

Almost all the researches gave more important to the degradation of the polybutadiene, the changing of the rubber dispersion and the crosslinking as the result with an effective change in the mechanical and rheological properties of the polymer.

2.2.1 Thermomechanical degradation

As explained before, it is well known in literature that the polybutadiene controls the impact resistance and its degradation reduced this propriety, since it is a prime site for degrative attack at double bonds and tertiary carbon atoms.

The oxidative and thermo-oxidative degradation induce chemical changes in elastomers with polydienic structure leading to such as carbonyl and hydroxyl groups formation, lowering of the double bond content and an increase in the crosslink density [26].

The research of Xiaojuan Bai et all.[27] showed the significance of the loss of volatile molecules reduces and the importance of polybutadiene degradation increases by the reprocessing temperature and by the number of cycles.

These changes that occur during reprocessing alter the ABS morphology, reducing the interfacial bond strength between the SAN matrix and PB rubber particles, with significant effects on the mechanical properties, and more severe effect on impact properties than tensile properties (figure 2-7).

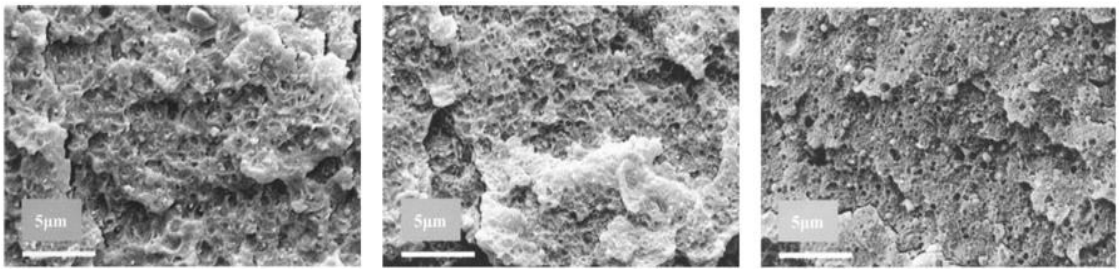

Figure 2-7 SEM image ABS morphology after reprocessing.

This is consistent with the changes outlined above, namely loss of small molecules, degradation of the polybutadiene phase and relatively little change in the SAN phase. Reduced numbers of small molecules and degradation of the rubber phase will both contribute to loss of impact resistance.

At the same time, since the load bearing SAN phase is relatively unaffected by the reprocessing, then the tensile properties also remain relatively unchanged.

It is known that high impact resistance of the ABS is reached when the domains rich in polybutadiene present small dimensions [13], diameter between 0.3-3.1 (nm) [22]. There is a critical rubber particle diameter in which a brittle-tough transition in polymer/rubber blends is verified; this parameter is directly related to the rubber volume fraction in the blend.

Other important factor is the critical matrix ligament thickness, it is independent of rubber fraction and particle size and is a characteristic property of the SAN matrix at a given mode, rate and temperature of deformation [24].

3.PREVIOUS STUDIES

Nowadays there are not studies about the reprocessing process of the ABS for the FFF, but there are studies regarding the poly(lactic acid) PLA recycling process.
Mazher et al. [28] investigated in the potentiality of the 100% recycled ABS in FFF, the mechanical properties of the recycled ABS resulting in a decrease in the ultimate strength but the superficial quality surface roughness analysis from the recycled filament was similar to the commercial filaments. The melt flow rate of the recycled material was lower than the virgin one. This was suspected to be due to thermal degradation of the recycled ABS and required the adjustment of the raster speed to avoid under extrusion problem during the printing process.

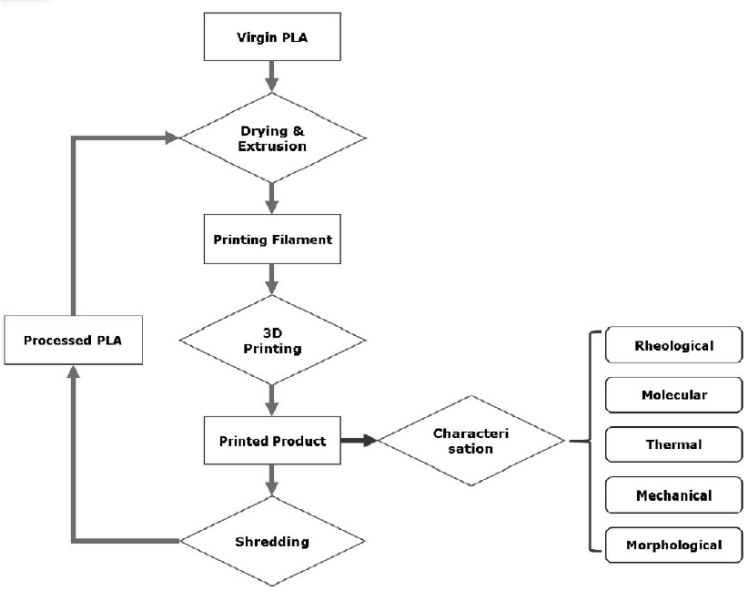

Figure 3-1 Scheme of close-looped recycling of PLA that used in 3D printing.

Peng Zhao et al. [29], studied a close-looped recycling of polylactic acid used in 3D printing (figure 3-1). The result shows a significant deterioration in the viscosity after the printing process, which made the material unsuitable for further reprocessing. Though mechanical performance deteriorated to a limited extent, significant decreases in rheological property conformed with losses in molecular weights. Chain scissions have triggered increases of crystallinity and compromised thermal stability. Noticeable deteriorations have also been observed in the FTIR spectra and SEM micrographs; the presence of carbonyl groups and surface pinholes, indicating that thermomechanical degradation has taken places during melt processing and it is responsible for decrements in the molecular weight of PLA.

Antonio Lanzotti et. all [30] compared the short-beam strength of virgin and recycled PLA; their result showed a significant decrease of the mechanical properties after the third recycling process.

Sancheza et all [31], proposed a methodology to characterize the recycling of polymers used as feedstock for open source3D printing machines, the methodology was applied to study the conditions for reusing PLA (figure 3-2, figure 3-3).

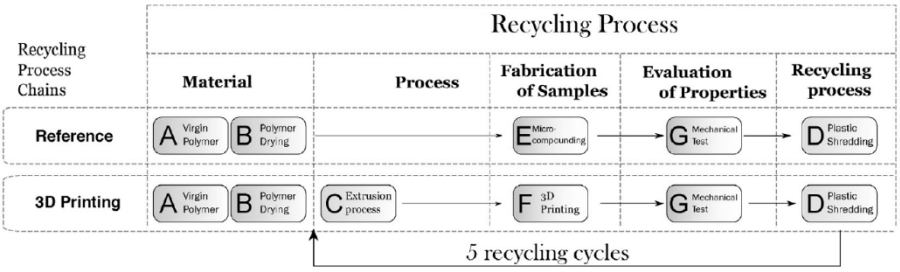

Figure 3-3 Methodologies for comparing the material degradation using a standard and 3D printing process.

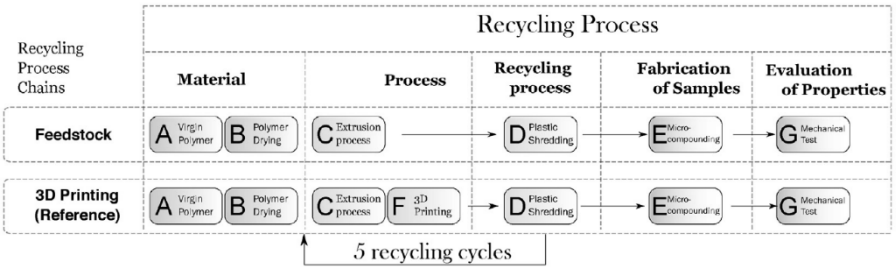

Figure 3-2 Methodologies to evaluate the impact of 3D printing process on material degradation.

The results showed that the elastic modulus for the samples made using micro injection moulding process presented a virtually constant value; for the printed samples, results high-lighted a relative and systematic increase in the elastic modulus as the number of recycling cycles increases. Their hypothesis to explain this behaviour is related to an appreciable reduction of internal defects (voids, pores) caused by the reduction in the material viscosity, which facilitates the homogenization of the deposited layers in the printing process; observed in the cross-section area of the recycled printed samples by an optical microscopy. The values of the others tensile properties, strain and strength, are decreasing every reprocessing steps.

Goutham Ra et all [32] studied the mechanical properties of recycled ABS blended with virgin, they used different percentual of recycled ABS inside the blend 20-30-40-50 %. The result showed that the ultimate tensile strength and the flexural strength are decreasing with the increasing of the recycled ABS percentual inside the blend.

4.MATERIALS AND METHODS

In this section it is discussed about the procedures followed during the thesis and it is presented the materials, the equipment and the relative setup used following the ISO standard.

The recycling process was in a close loop (figure 4-1), the main tasks are divided in rheological, thermal, chemical and mechanical characterization, printing process and filament extrusion process.

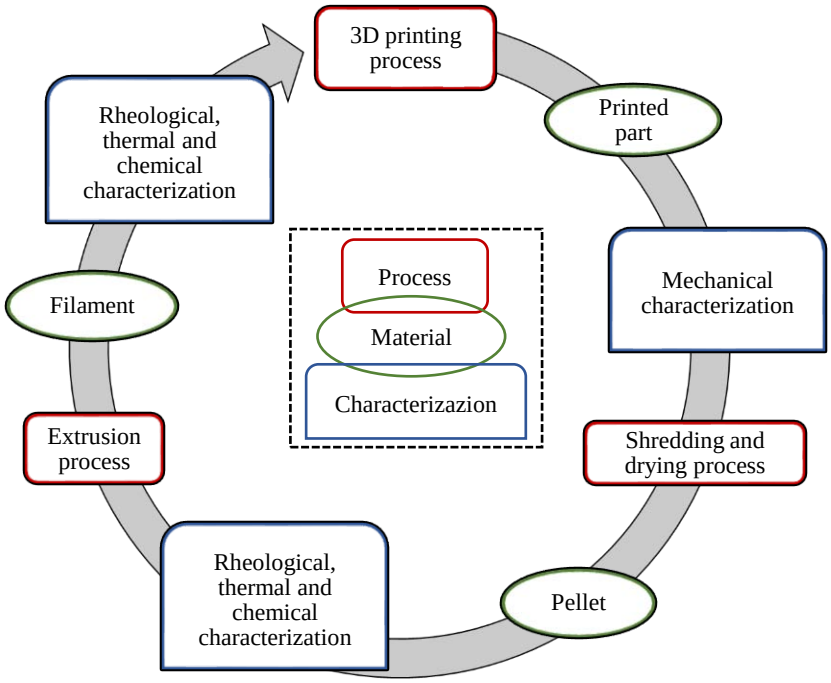

Figure 4-1 Close loop recycling process.

The focus of this research is in the changing of the ABS properties during the reprocessing. In the beginning were run the thermal characterization (melt flow rate (MFI), thermogravimetry (TGA) and differential scanning calorimetry (DSC)) and chemical characterization (Fourier transformed infrared spectroscopy (FT-IR)) for the started materials before the printing process. After each thermomechanical process (printing process or extrusion process) were investigated the thermal degradation of the material. For every recycled material the impact and the tensile properties were evaluated and the morphologies of the fracture surfaces of the samples was studied.

It was used two FFF printers, and apart the architecture the main difference between them is the radiant heaters and the hot chamber, so it was evaluated the impact of the radiant system on all the properties.

4.1 Materials

4.1.1 ABS ICE-Filaments

The virgin ABS filaments come from the ICE-filaments company, the diameter is 1.75 mm, natural white color with a low melt flow index.
Three spools of materials were used, the production code of two of them was the same. These two spools (production code 694) were used for the recycling with the radiant heater printer (Spiderbot), the last spool (production code 2414) was used in the standard one (Prusa).
In the attachment in table 8-1 [33] there are the properties from the data sheet.

4.1.2 ABS Sitraplas

The recycled ABS Sitraplas (S20/C905) is based on 100 % recycled ABS in pellet from Sitraplas. The pellet is for the injection moulding process and has a high melt flow index, low tensile properties and impact strength [34] (table 8-2).

4.2 Filament extrusion process

4.2.1 Shredding process

The shredding process makes the pellets from the filament or printed waste parts.
Two different shredding machines were used, one for the filament (figure 4-2 on the left), and one for the printer scabs (figure 4-2 Piovan MDS 340/150).
The principal problem in the shredding process is to obtain a regular pellets size, sometimes is needed to run more times the material to reduce the pellets size, otherwise there are problems during the feeding of the filament extrusion process.

Figure 4-2 Shredding machines.

Figure 4-3 Dryer machines.

4.2.2 Drying process

The drying process take-off the moisture from the pellets. ABS is a hygroscopic polymer and can absorb moisture from the external atmosphere. Even low percentage of humidity inside the polymers can negatively affect the rheological behaviour given problem during the characterization or the filament extrusion. It is required less than 0.2% moisture to avoid this problem. A convection oven and drying machine FarragTech Card 40E (figure 4-3) were used, for the pellets and the filament, before each melt process, at 80 °C for at the least 4 hours [35].

4.2.3 Filament extrusion process

The filament extrusion process can be summarized as in figure 4-4:

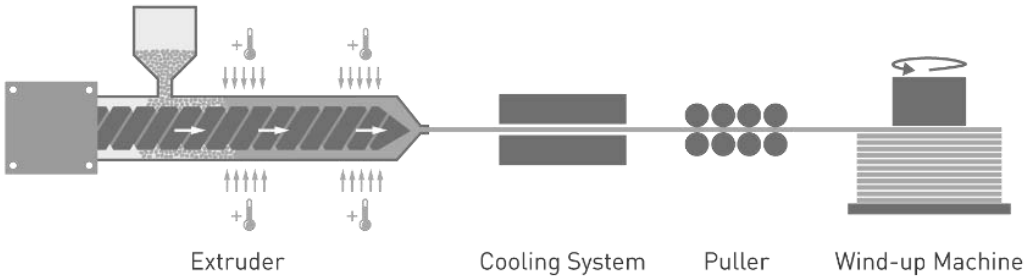

Figure 4-4 Filament extrusion process.

It was used a single-screw extrude (figure 4-5): Brabender Plastic Corder PL2000 (screw diameter of 19 mm and L/D of 25). The outgoing filament diameter (1.75 mm) is controllable trough the extruder screw speed and the puller system torque (figure 4-6).

Figure 4-5 Filament extrusion system.

Before each filament extrusion process the machine was cleaned with 100g of the same ABS pellets until the colour of the outgoing filament become acceptable.

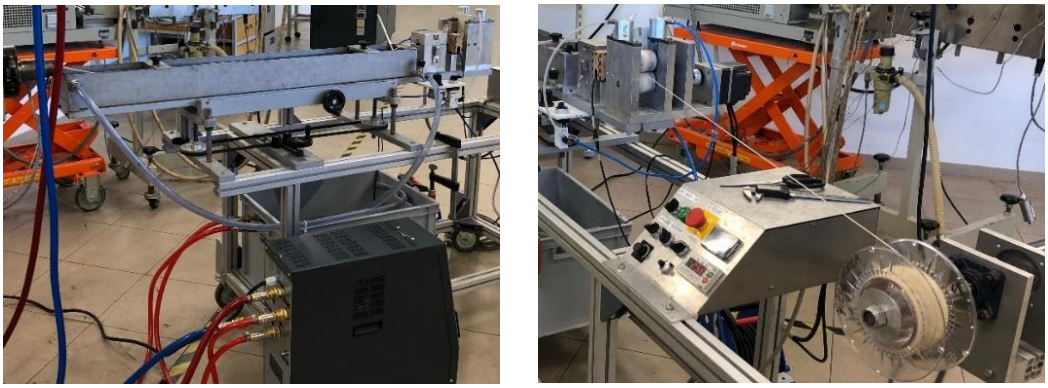

Figure 4-6 Cooling bath in the left and the pull system in the right.

The extruder machine has four controllable temperatures along the liquefier, the temperature profile used for each material is shown in table 4-1, T1 is the temperature near the hopper and T4 the temperature near the die (figure 4-7).

Figure 4-7 Extruder Brabender Plastic Corder PL2000.

Table 4-1 Temperature extruder machine.

T1 (°C)	210
T2 (°C)	220
T3 (°C)	230
T4 (°C)	230
R.P.M	30

The cooling system is a simple water bath (in the left in figure 4-4). The water is recycled with a pump inside a lower tank connected to the cooling tank, the return of the cooling liquid to the lower tank takes place by gravity.
In this lower tank there is a copper pipe that acts as a heat exchanger and there is connected a heater for injection molding moulds machine.

4.3 Rheological characterization

4.3.1 Melt flow rate

The melt flow rate MFR (or melt flow index MFI) is a measure of the flow of the melt of a thermoplastic polymer melt, it is measured in (g/10min). It is an indirect measure of molecular weight, where high melt flow rate corresponding to low molecular weight.

At the same time, it is a measure of the ability of the material's melt to flow under pressure, inversely proportional to viscosity. The equipment used is the Davenport MFI 10 (figure 4-8), was followed the ISO 1133-2 [36], the table 4-2 showed the setting.

Table 4-2 Melt flow index test setting.

Weight	10	Kg
Temperature	220	°C
Melt time	5	min
Cut-off time	10-30	s
Sample mass	4-8	g

Figure 4-8 Davenport MFI 10.

The cut-time depend on the rheological behaviour of the material, sometimes it needs a higher cut-time for have more control of the process during the test, because the outgoing filament it is cut manually.

The melt volume-flow rate (MVR) is expressed in cubic centimetres per 10 minutes and is given by the equation[36]:

$$MVR(T, m_{nom}) = \frac{A \times 600 \times l}{t}$$

where

- T is the test temperature (°C);
- m_{nom} is the nominal load (kg);
- A is the mean of the nominal cross-sectional areas of the cylinder and the piston head, in square centimetres and is equal to 0,711 (cm^2);
- *600* is the factor used to convert cubic centimetres per second into cubic centimetres per 10 minutes (600 s);
- l is the predetermined distance moved by the piston or the mean value of the individual distance measurements (cm);

- t is the predetermined time of measurement or the mean value of the individual time measurements (s);

The melt mass-flow rate (MFR) or MFI is expressed in grams per 10 minutes, is given by the equation [36]:

$$MFR(T, m_{nom}) = \frac{A \times 600 \times l \times p}{t}$$

where

- ρ is the density, in grams per cubic centimetre, of the melt at the test temperature and is given by the equation:

$$\rho = \frac{m}{A \times l}$$

- m is the mass (g) determined by weighing, of extrudate expelled by a piston movement of l (cm).

In the data sheet of the filament makers is common to find the MVR value. In this research is use the MFR value; the equation [36] that correlate those indexes is:

$$MFR = MVR \times \rho$$

4.3.2 Rotational rheometer

Rotational rheometers can measure viscosity, thixotropy, shear stress and strain. Steady, dynamic or transient viscosity measurements can be performed.

The equipment applies a torque to the top plate exerts a rotational shear stress on the material and the resulting strain or strain rate (shear rate) is measured. Instruments dedicated to this type of test have been designed to impose and control a strain for measuring a stress or to impose and control a stress for measuring a strain.

In order to measure all possible rheological properties, a wide range of measuring systems is available in the market, the choice of geometry depends on the consistency of the material, i.e. the elastic modulus.

For the ABS plastic is recommended to use the cone-plate measuring systems (ISO 3219) or the parallel plates measuring systems (ISO 6721-10) (figure 4-9).

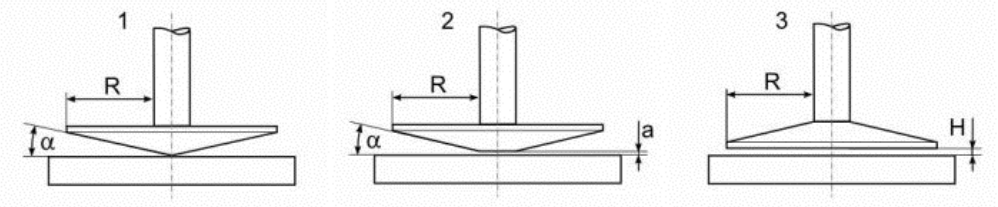

Figure 4-9 Cone-plate and parallel-plate geometries used with rotational viscometers.

The most widely used geometry for shear measurement of functions viscoelastic of the polymeric melts is the parallel plates. Parallel and cone plate geometries are suitable for polymer melts with sufficiently high elasticity and viscosity not to flow outside the area within they are to be confined.

There are two type of cone-plate, truncated cone and a normal one (figure 4-9). The first one is truncated at the top and the procedure involves approaching the plate and cone in such a way that, considering the ideal extension of the truncated cone part, the tip of the cone touches the surface of the plate. Since typically angles of the cone less than a tenth of a radian ($\alpha<6°$) are used, it is necessary to bring a distance a of a few tens of microns (usually 50 μm to 210 μm). The cone radius should be between 10 mm and 100 mm. For parallel plates, the standard demands that $H << R$. So, depending on the plate radius and the sample under test, H can range from 0.5 mm to 3 mm.

Viscoelastic behaviour is highly dependent on variables that are set before a test such as temperature, pressure, frequency and strain amplitude. Different methods are available to change one or more of these variables in ways that can be chosen according to the needs of the measurement operator, are mention the most used ones:

- Time sweep: frequency, temperature and amplitude of the deformation are maintained constant and the measurement is carried out at selected time intervals.
- Strain sweep: temperature and frequency are kept constant while viscoelastic functions are measured at variable strain amplitudes according to selected increments (or decreases).
- Frequency sweep: the temperature and amplitude of the deformation are kept constant while the frequency is changed in a selected range.
- Temperature sweep: the amplitude of the deformation and the angular frequency are constant while the temperature changes according to a programmed ramp that can be ascending or descending

In order to work where the material keep showing a linear viscoelastic behaviour (a Newtonian behaviour), it is advisable to check, by performing different strain sweeps, that the viscoelastic response is linear at the frequencies you want to use. In fact, the linear response zone of a polymer depends not only on the amplitude of the deformation, but also on frequency and temperature.

The model of the rheometer used is the ARES Rheometer by TA instruments (figure 4-10), the measuring system used were a parallel plates and cone-plate with a diameter of 25 (mm).The method of the test was dynamic frequency sweep test in strain-controlled, the measurement type was dynamic.

Figure 4-10 Rotational rheometer and cone-plate measuring system.

4.4 Thermal and chemical characterization

4.4.1 TGA-DSC measurements

For the test it was followed the ISO 11357 [37] with the equipment NETZSCH STA 449 F3 Jupiter (figure 4-11), is a simultaneous thermal analysis machine. It can run simultaneous application of thermogravimetry (TGA) and differential scanning calorimetry (DSC) to one and the same sample in a single instrument (table 4-3).

Figure 4-11 NETZSCH STA 449 F3 Jupiter.

Table 4-3 DSC and TGA possibilities.

DSC Possibilities	TGA Possibilities
Melting/crystallization behaviour	Mass changes
Solid-solid transition	Temperature stability
Polymorphism	Oxidation/ reduction behaviour
Degree of crystallinity	Decomposition
Glass transitions	Corrosion studies
Cross-linking reactions	Compositional analysis
Oxidative stability	Thermokinetics
Purity Determination	
Specific heat capacity	
Thermokinetics	

The test conditions are perfectly identical for the TGA and DSC signals (same atmosphere, gas flow rate, vapor pressure on the sample, heating rate, thermal contact to the sample crucible and sensor, radiation effect, etc.).
The software of NETZSCH recorded the diagrams and the NETZSCH Proteus Analysis software permits an analysis of the diagrams. It was used crucibles in Platinum before cleaned and burned with the Bunsen.
The first cycle was employed to eliminate the influence of thermal memory.
In each test it was inserted the sample just in one furnace, and the protective and purge gas was Nitrogen.
The limit temperature of this equipment is -50 °C, it is not possible to reach the glass transition temperature of the PB in the ABS (from -120 to -70 (°C)).

4.5 Chemical characterization

4.5.1 Fourier transformed infrared spectroscopy

The Fourier transformed infrared spectroscopy was used for the valuation of the ABS degradation.
The equipment used was the Brunker Tensor 27 (figure 4-12) and it was followed the ISO/CD 10640 [38].
Samples were studied in attenuated total reflectance (ATR) mode from 4000 to 600 cm^{-1}
The values of the absorbance were determinate using the baseline method.

Figure 4-12 Brunker Tensor 27.

Infrared spectroscopy is a vibrational spectroscopy in which absorption bands at specific wavelength allow to characterise chemical groups (functionalities) of a polymer structure (figure 4-12).

Different infrared technologies (transmission, reflection, photoacoustic, attenuated total reflection, micro-spectroscopy) can be used to be analyzed depending on the geometry of the specimen.

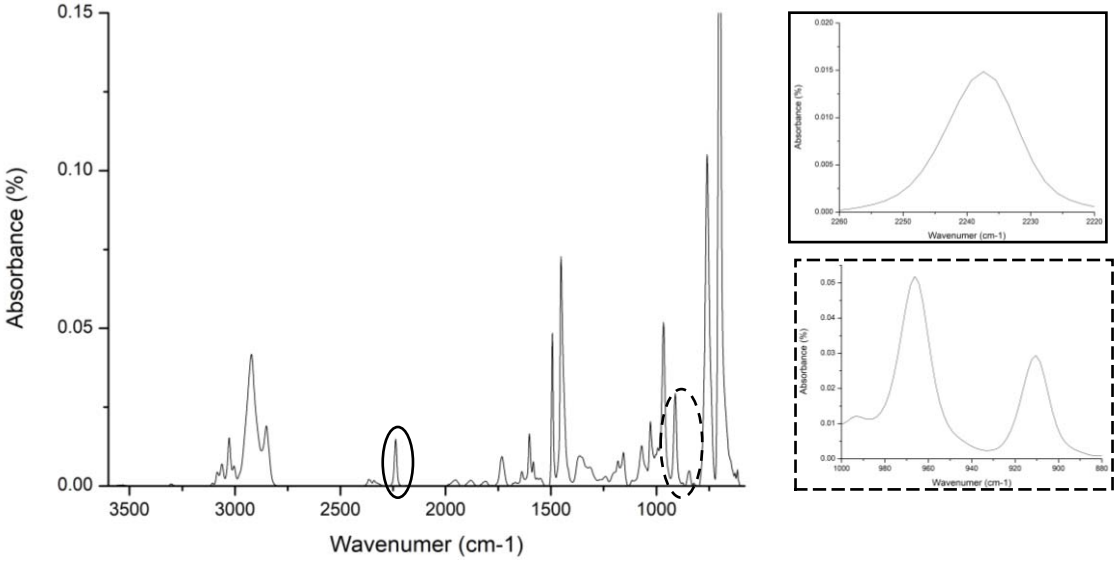

Figure 4-13 Absorption spectrum of a virgin ABS and the absorption peaks of PB and CN.

The polymer degradation can be characterized by:

- emergence of new absorption bands specific of the critical photo-oxidative products originated by the polymeric matrix: e.g. bands corresponding to chemical components including carbonyls or hydroxyls;
- decrease of a specific absorption band characteristic of a weak site of the polymeric structure: e.g. bands corresponding to urethane, ether, unsaturated functional groups.

The measuring, at specific frequencies of the mentioned bands, of the absorbance variation in relation with the initial state, allows to express the progression rate of the oxidation or, in the case of a kinetic analysis, the oxidation rate (table 8.6 in the attachment). The evaluated of the degradation of polybutadiene and polyacrylonitrile were used the rapport between the absorption peaks:

$$\frac{BD_1}{CN} = \frac{\%\ Absorbation\ 966.32\ (cm-1)}{\%\ Absorbation\ at\ 2237.4\ (cm-1)} \qquad \frac{BD_2}{CN} = \frac{\%\ Absorbation\ at\ 910.38\ (cm-1)}{\%\ Absorbation\ at\ 2237.4\ (cm-1)}$$

Before the test, the samples were dried for 4 hours at 80 °C and then were cut with a blade, the surface planarity of the samples in touch with crystal of the equipment has an influence on the results.

4.6 Printing process

In the printing process two different printers were used, the main distinction between them are the architecture (figure 4-14), the radiant heaters system and the hot chamber. The nozzle type used in each printer was the same: E3D-0.5 mm diameter (figure 8-1). The printer has a different feeding system, the delta has a bowden system and the cartesian a direct drive system, so the setting of the feeding system was different.

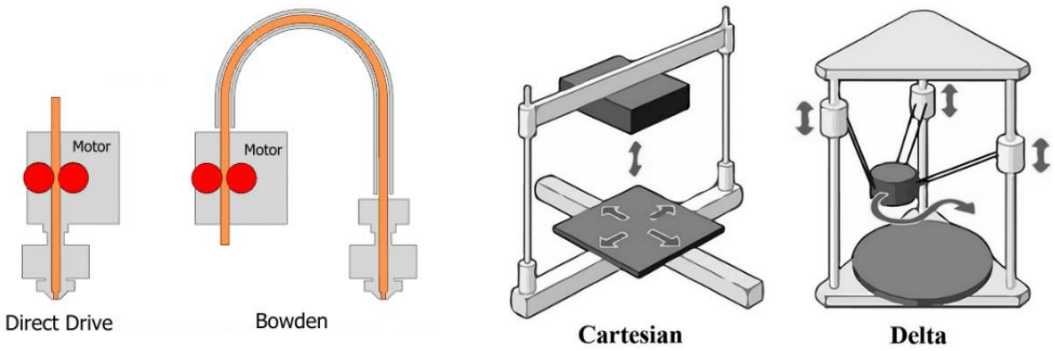

Figure 4-14 In the left the type of the feeding system and in the right FFF main architectures.

The printer used were a classic desktop cartesian printer the Prusa Mk3, the most famous RepRap desktop printer in the world, and the Spiderbot HT4.0, a special delta printer designed for work with the high-performance polymers.

4.6.1 Spiderbot HT4.0

The Spiderbot printer (figure 4-15) has a delta architecture [39], a infrared radiant heaters system and a temperature-controlled chamber.

The technical data sheet is in attachment (table 8-3).

The infrared radiants are placed all around the chamber towards the printing area, which greatly improves the layers bonding, print quality and reduces warping.

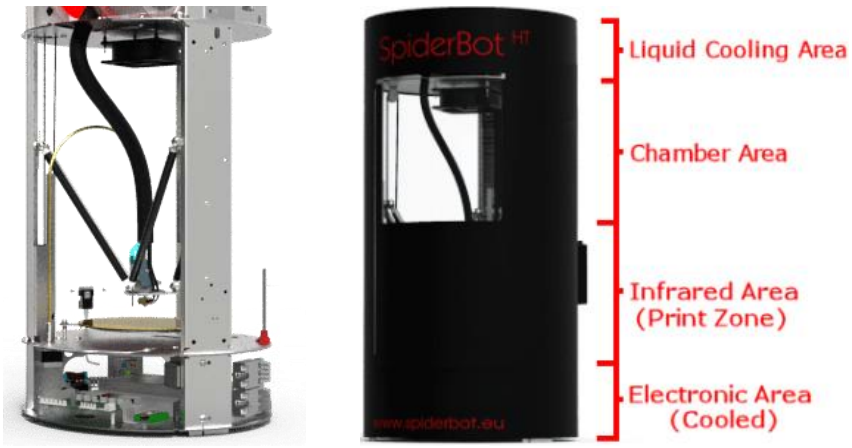

Figure 4-15 SpiderBot HT4.0.

High temperature resistant fans extract the excess heat generated by the radiants.
With delta technology, all three axes move simultaneously, the three motors simultaneously provide torque for movement on a single axis. This means less mass in motion. Z-axis movements are almost 30 times faster than a conventional XYZ architecture. The heated printing bed and the part itself remain fixed, only the print head is movable.
The printing bed is made of poly(ether-imide) (PEI) sheet.
The hot-end is cooled down by a liquid cooling system (figure 4-16), that improve the feeding system performance and maintain the nozzle in a temperature stable. The frame is in aluminium.

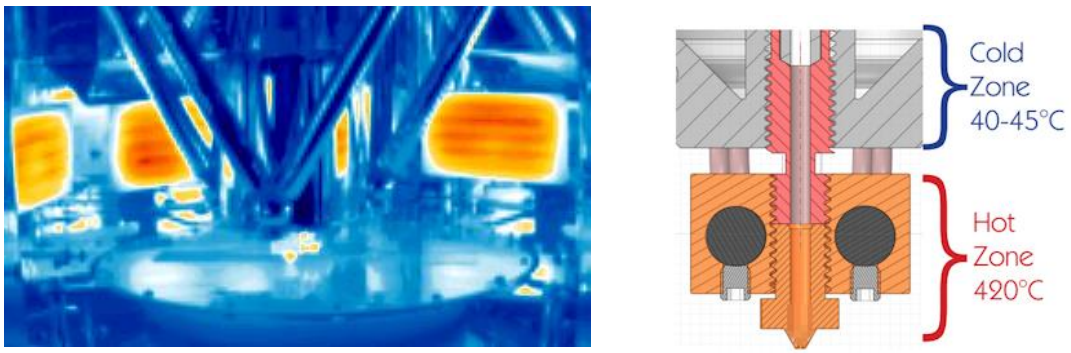

Figure 4-16 Printing head temperatures in the right, thermo camera image of the hot chamber in the left.

4.6.2 Prusa i3 Mk3s

The Prusa i3 is a cartesian RepRap 3D printer (figure 4-17), nowadays it is the most used 3D printer in the world [40].
With the cartesian technologies two axis are moving and the third one moves for change the work plane.
The extrusion system is direct, the pull system is the Bontech drive gear, the filament is driven from both sides.
The hot-end is E3D all-metal v6 hot-end air-cooled.
The bed coating is a smooth PEI sheet and the frame is made of aluminum.
The Prusa printer can works with all the Gcode made by the open-source slicer.
The technical data sheet is in attachment.

Figure 4-17 Prusa i3 Mk3s.

4.6.3 Printing process setup

It was used the printers with same slicer setting (table 8-5) and 3D models.
The nozzle temperature was selected after several tests to obtain the right compromise between the bonding and the thermal degradation.
The temperature of the bed is close to the T_g and was adjusted to have a good adhesion and prevent the warping (112 °C).
To have the same shear stress, in both printers it was used the standard nozzle, the layer height was 0.25 (mm) and the process deposition speed was the same.
It was used the open-source slicer CURA to generate the G-Code; for the printers was changed the machine setting correlate with the architectures and the retraction parameters (because of the different feeding system).
The deposition strategy was designed to have a good compromise with the tensile and impact properties.
The infill density was 100% and the pattern was “LINE “, the direction 45°/90°/-45°, since the first layer after the raft is imperfect, the first two layers were printed at 45° and then in an alternating direction. Several tests were run to selected the overlap in X-Y direction to reduce the porosity without compromising the final geometry (over-accumulation of material in the external surface).
The flow depends on the material viscosity and the average diameter of the filament, the initial flow was higher to increase the filling in the first layer surface and for improve the raft adhesion (depends on “raft air gap / initial layer z overlap” in table 8-5)
The movement speed of the printing head in the wall was selected in order to have good compromise between the bonding in the walls and infill and to reduce the material lost in the corner and external side of the part.
To avoid the warping problem and increase the bed adhesion it was used the raft for the adhesion method.
The raft parameters were improved for have good adhesion and an easy separation from the samples without damaging the external surface of the sample.
For the printer with the infrared radiant system it was added manually inside the G-code the temperature of the radiant heaters (224 (°C)), the real temperature perceived at the part is the half temperature of the radiant (112(°C)).This temperature was chosen in base of the SAN T_g (the same one used for the bed), after several tests was observe than

rising the radiant temperature over 224 (°C) improves the layer bounding but the part become too soft and the layer deposition was instable.
The chamber temperature depends on the radiant temperature, with 224 (°C) at the radiant the chamber temperature was at 55 (°C).
The cooling process was controlled with cooling ramp, a premature remove operation can distort the final shape of the printed part; but waiting longer can cause problem to remove the raft.
The cooling ramp was introduced at the end of the G-code by the activation of the radial fan on the top of the printer for 10 minutes (G4 S600, M107, M300 S300 P1000).
For the Spiderbot was chosen a cooling time of 10 minutes, that was enough to cooldown the part from 112 (°C) to 40 (°C).
For the Prusa it was waited 10 minutes before taking off the sample from the bed.
In the attachment there are the G-code used for the experiments.

4.7 Mechanical characterization

The techniques for measuring mechanical properties can be classified according to the methods of application of the deformation or the stress [41][42]:

- Static stress (non-impulsive test), constant deformation velocity:
  tensile test, compression test, flexion test and torsion test.
  Those tests allow to evaluate the mechanical properties in a polymer in terms of elastic modulus, tensile strength and deformation at break.
- Dynamic stress (impulsive test), increasing deformation with extreme rapidity:
  Izod method, Charpy method, tensile impact method, falling mass method. The energy that the sample absorbs in the break is measured.
- Constant stress or deformation over time:
  Creep test or stress relaxation, so in the sliding tests the deformation that a specimen undergoes over time is measured when it is subjected to constant stress, while in relaxation it is measured how stress varies over time to maintain constant deformation.
- Periodic deformation:
  Cyclic fatigue tests and dynamo-mechanical tests.

Fatigue tests define the number of cycles of application of a load, lower than the one-off breaking under static conditions, which cause the specimen to break. Dynamo-mechanical tests allow to evaluate the parameters that characterize the viscoelasticity of the polymeric material.

For this study were used the tensile static test and the impulsive test with the Charpy method, for evaluate and compare the different modulus, tensile strength, deformation at the break and the impact energy of the virgin and recycled ABS. The same deposition strategy and the same printing condition were used for to perform the comparation.

Figure 4-18 Tensile bone and impact bar with notch.

The presence of defects in the sample, inside or in the surface, act as a concentration of tensions which can greatly reduce the mechanical properties (figure 4-19).

In compliance with the ISO standard (figure 4-18), all the samples used were kept in a metrology room (50 % humidity and (20 C °)) for at least 48 hours.

Each sample was produced, storage and tested under the same conditions.

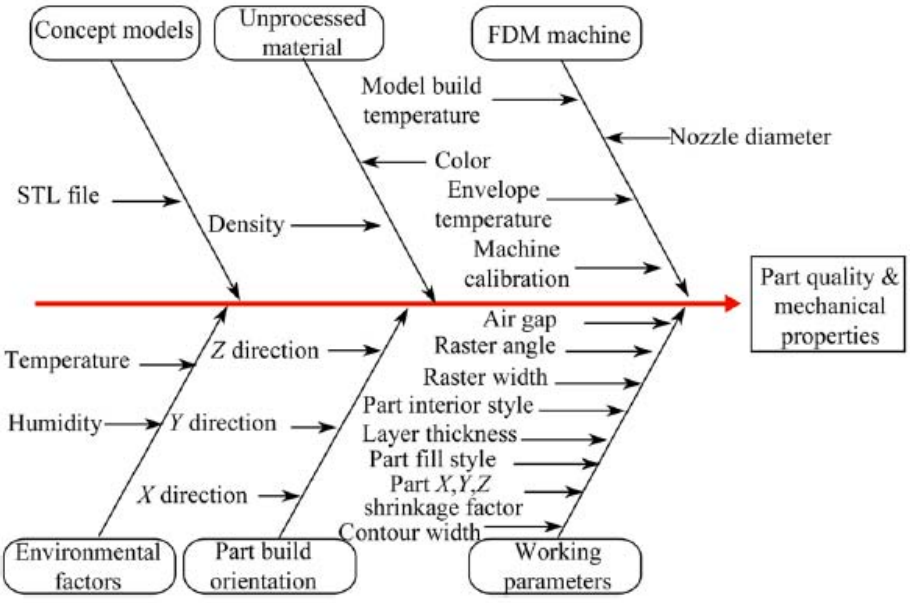

Figure 4-19 Cause and effect diagram of FFF process parameters.

4.7.1 Tensile test

The normative referred for this mechanical test is ISO 527 [43][44].

The tensile test consists in placing at the least 5 samples standardized in an axial effort, gradually increasing until it breaks, by a tensile machine (dynamometer).

The test is performed by fixing the ends of the specimens one to a fixed clamp and the other to a movable clamp that moves with an established constant speed. Under the tensile stress, applied gradually and continuously the sample elongates and shrinks.

The shape of the specimen favours the deformation and the rupture of the same in its central part and avoids the breaking at the ends where the material is weakened due to the action of the clamping pressure.

The initial length (gauge length L_0) is modified by the application of the force during the test and is measured at the fixed graft using a transducer.

The tensile stress is plotted as a nominal stress as a function of the nominal deformation, using the area of the original cross section A_0, the original length L_0, and the variation in length resulting from traction as reference data.

The length of the sample is determined in real time by the distance of the cracks in the instrumental structure or, more correctly, through an extensometer. It is an accessory connected to the central part of the specimen that measures the variation in distance between two points in the direction of the effort. It is removed, to preserve its integrity, during the test before the final breaks after yield stress, awarding strain measurement task to the clamps.

The shape of test sample (figure 4-20), suggested by normative ISO for the thermoplastic and thermoset material are 1A and 1B, the last one is referred to the samples obtained by mechanical machining; was used the 1A (Table 4-4).

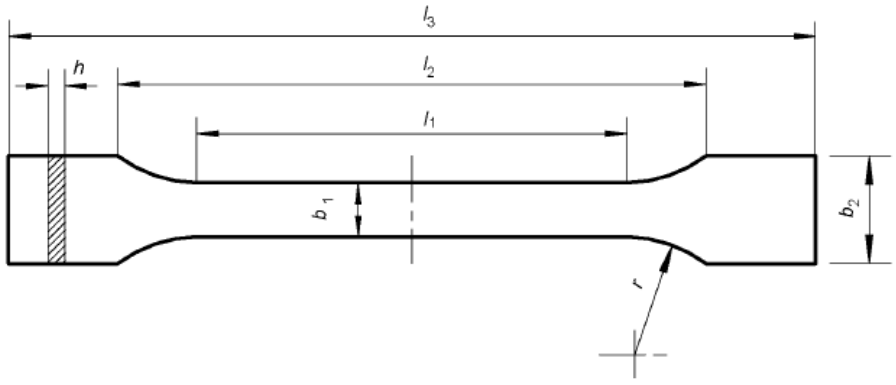

Figure 4-20 ISO standard tensile sample.

Table 4-4 ISO specimen parameters.

Specimen type	1A	
Overall length l_3	170	mm
Length of narrow parallel-sided portion l_1	80 ± 2	mm
Radius r	24 ± 1	mm
Distance between broad parallel-sided portions l_2	109,3 ± 3,2	mm
Width at ends b_2	20 ± 0,2	mm
Width at narrow portion b_1	10 ± 0,2	mm
Preferred thickness h	4 ± 0,2	mm
Gauge length L_0	75 ± 0,5	mm
Initial distance between grips L	115	mm
Modulus determination in base of tensile strain	From 0.05 to 0.25	%
Velocity for modulus determination	1	mm/min
Velocity test after the modulus determination	50	mm/min
Remove time for extensimeter in base of tensile strain	3-5	%

The tensile machine (figure 4-21) used was the INSTRON 5565, with the extensometer dedicated.

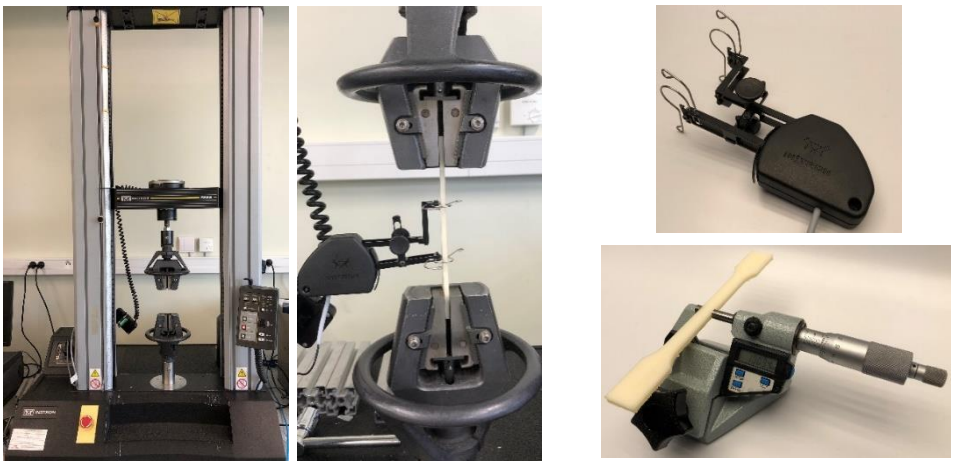

Figure 4-21 Tensile test equipment.

The software Bluehill was used to control the machine and for the post-processing.
The real dimensions of the cross section of the dogbones (thickness and width) were taken with a micrometer and introduced into the software; then was fastened the sample to the machine clamps, the extensometer was positioned, and the load was reset.
The mechanical properties are provided from the software: tensile stress at yield, tensile stress at maximum load, tensile stress at break, strain at yield, tensile strain at break, elastic modulus and the relative load-elongation diagram.

The sample break zone must be inside the gauge length L_0 in respect of the ISO standard, in other case (figure 4-22) that samples data were discarded.

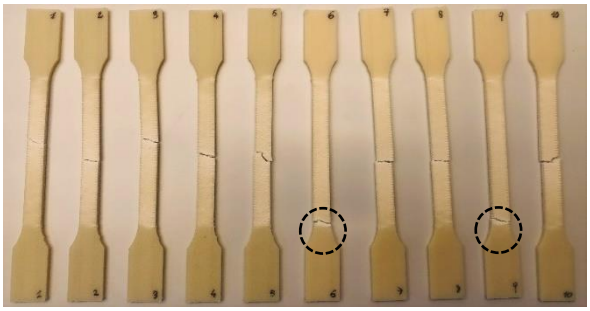

Figure 4-22 Tensile dogbones fracture zone.

4.7.2 Impact test

To determinate the impact strength was followed the ISO 179 [45].

The specimen, supported as a horizontal beam resting on the extremities, is broken by a single oscillation of the pendulum, with the impact line in the middle between the two supports and struck on the opposite side of the notch.

The standard requests at the least 10 samples.

The rapid stress test, or impact test, measured in a very short time a stress exceeding the breaking stress.

The breaking strength, expressed as energy needed to break up per unit area (kJ/m^2), is defined as the material's resilience and can also be obtained from the area subtended to the stress-strain curve obtained from the tensile test. The test determines the amount of energy absorbed by a material during fracture. Impact velocity imposed by normative is 3 (mm/s) and the dimensions of specimens (figure 4-23) is shown in the follow table.

Table 4-5 Impact test parameters.

Method designation	ISO 179-1/1eC	
Specimen Type	1	
Blow direction	Edgewise	
Notch type	C	
Notch Base radius *rn*	0,10±0,02	mm
Remaining width *bn* at the notch base	8,0±0,2	mm
Length *l*	80,0±2	mm
Width *b*	10,0±2	mm
Thickness *h*	4,0±0,2	mm
Span *L*	62+0,5	mm

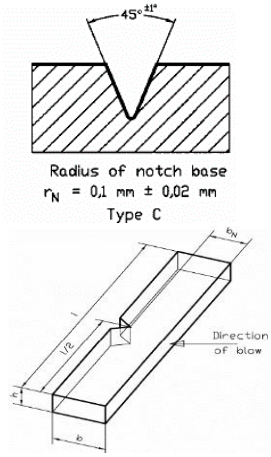

Figure 4-24 Notch impact bar setting.

The samples were printed without notch, it was made manually with a specific standard notch machine (above in the right on the figure 4-24).It was used the Tinius Olsen Model Impact 503 (figure 4-24 in the left), without extra weight in the pendulum. In the setting of the Charpy machine were insert the real dimension of the sample cross section with the notch (width and thickness) measured using a micrometer.

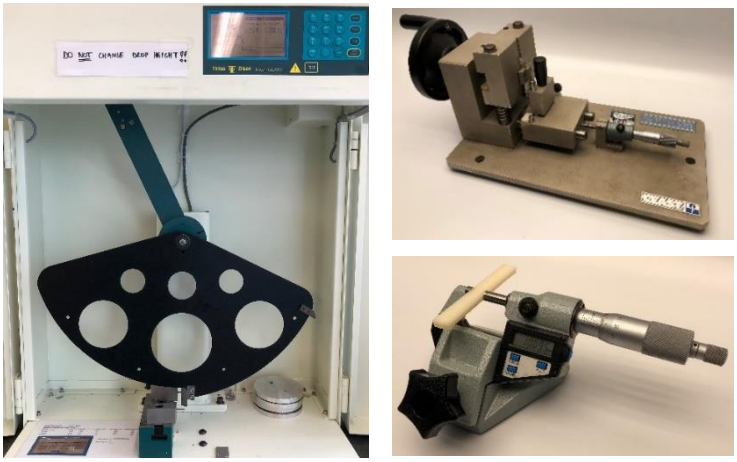

Figure 4-25 Impact test equipment.

4.7.3 Morphological characterization

The evaluation of the internal surface (void, bonding between layer, defects), the fracture surface of the mechanical samples was run by the digital microscope.
The test samples were brake in the middle and refine with the Microtome (figure 4-25).
The morphology between the two ABS phases was analysed with the scanning electron microscope using also the energy dispersive spectroscopy detector.

4.7.3.1 Digital microscope

A digital microscope is an optical microscope equipped with a digital camera, the image of the sample is observed, collected and analysed directly by the dedicated software.
The microscope observations of the specimen's cross-section were running by the Keyence digital microscope VHX 500F using the x30 of magnification (figure 4-25).

Figure 4-26 In the left the optic microscope, in the right the microtome.

4.7.3.2 Scanning electron microscope

A SEM scans a focused electron beam over a surface to create an image. The electrons in the beam interact with the sample, producing various signals that can be used to obtain information about the surface topography and composition [46].

The main SEM components include (figure 4-26): source of electrons, column down which electrons travel with electromagnetic lenses, electron detector, sample chamber, computer and display to view the images.

The electrons are produced at the top of the column, accelerated down and passed through a combination of lenses and apertures to produce a focused beam of electrons which hits the surface of the sample witch is mounted on a stage in the chamber area and, unless the microscope is designed to operate at low vacuums, both the column and the chamber are evacuated by a combination of pumps.

The position of the electron beam on the sample is controlled by scan coils situated above the objective lens, these coils allow the beam to be scanned over the surface of the sample that enables information about a defined area on the sample.

Depending upon the accelerating voltage and sample density, the signal come from different penetration depth. So, as a result of the electron-sample interaction, several signals are produced and detected by appropriate detectors to distinguish secondary electrons, backscattered electrons, or characteristic x-rays: backscatter electron detector (BSD), energy dispersive spectroscopy (EDS), secondary electron detector (SED); different information regarding the material can be evaluated.

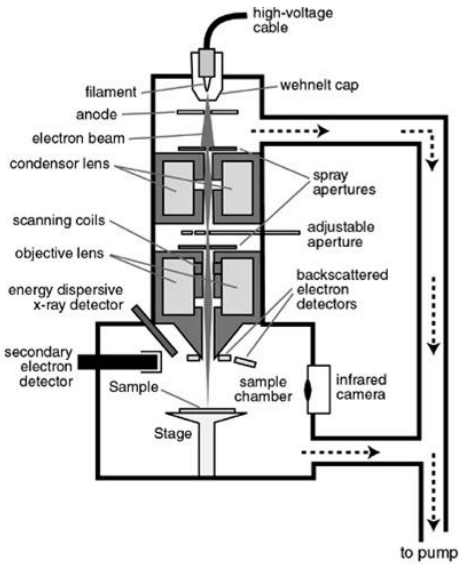

Figure 4-27 Scanning electron microscope.

5.RESULTS

In this session the results obtained from the characterization, along the reprocessing of the virgin filaments of ABS ICE-filaments up to the third recycling are presented.
It is also characterized the recycled ABS pellets of Sitraplas, used to produce the filament, up to the printing parts. The following sub-chapters are divided by material.

5.1 ABS ICE-Filaments

The follow results are obtained from the recycling process for the virgin ICE-Filaments ABS and they are subdivided in base of the printer. The virgin ABS used for both printers comes from the same filament productor. It is the same model, but the production code is different: the 694 production code was used for the Spiderbot and the 2414 for the Prusa.
The data from each recycling process are presented according to the variation of rheological, thermal, chemical and mechanical properties respect of the virgin filament.
Each recycle loop has been examined from the filament to the parts subsequently printed, where the material necessary for the next cycle was obtained.

5.1.1 Spiderbot

5.1.1.1 Rheological characterization

The ABS ICE-Filaments 694 virgin has a low melt flow index (MFI) , the same value of the data sheet from the filament manufacturer. (table 5-1)

Table 5-1 Rheometer setting for ABS 694 ICE-Filaments.

Cut time: 30 (s)	MFI (g/ 10 min)
Virgin	5.50 ± 0.15
Virgin printed part	6.38 ± 0.26
Recycled 1	6.13 ± 0.12
Recycled 1 printed part	6.20 ± 0.21
Recycled 2	5.83 ± 0.06
Recycled 2 printed part	6.63 ± 0.12
Recycled 3	6.23 ± 0.11
Recycled 3 printed part	6.18 ± 0.11

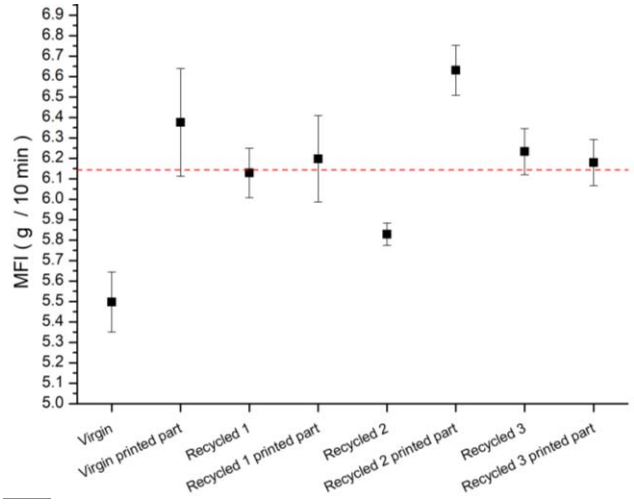

Figure 5-1 Trend MFI results ABS 694 ICE-Filaments.

In the figure 5-1 the trend of the MFI is not clear trend but the average value from the first up to the third printing process (6.14 g/10 min) is higher than the virgin one.
The rheometer test was done in dynamic mode, the settings are reported in table 5-2.

Table 5-2 MFI ABS 694 ICE-Filaments.

Measuring system	Height (mm)	Temperature (°C)	Strain (%)	Frequency range (rad/s)
cone-plate	0.0473	235	5	0.1-100

The results showed are the average of two test of the same material.
Increasing the frequency, the viscosity decreases and the modulus G' and G'' increase in each material and vice versa. The rheometer data gives more useful information of the viscosity change than the melt flow index and regarding the change in the molecular mass during the recycling loop through the modulus G' and G'' (figure 5-2).
As it is shown in figure 5-2, the viscosity decreases up to the third recycle and then increase after the last printing process.

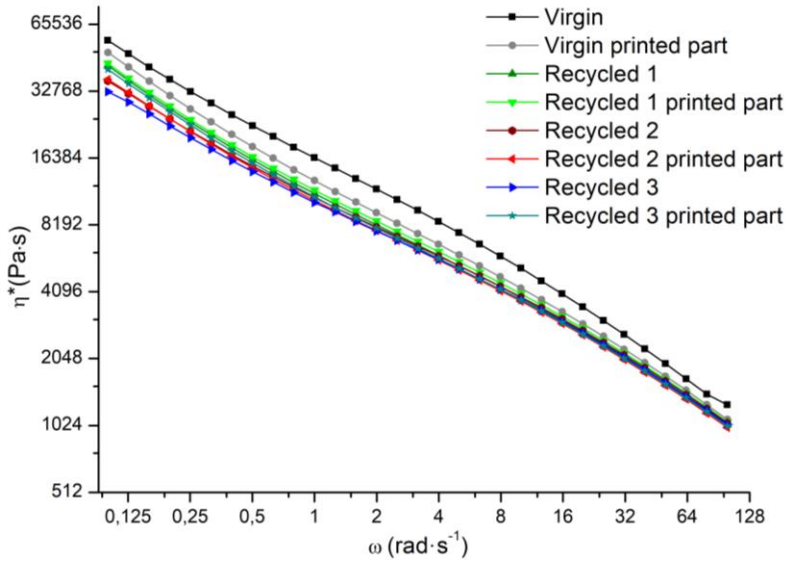

Figure 5-2 Viscosity curves ABS 694 ICE-Filaments.

The virgin material after the printing process has the higher drop of the viscosity and both of the modulus G' and G'', in accordance with the MFI result.
From the first recycle up to the third recycled filament the change in the rheological behaviour is more influenced by the extrusion process than by the printing process.
Indeed, the viscosity curves of the first and second recycled materials and the relative printed part are almost overlap.
The ABS of the last printing process have a controversial result: the viscosity raises up close to the one of the first recycled ABS and the modulus G', in the low frequency, is similar to the ABS from the virgin printing part.

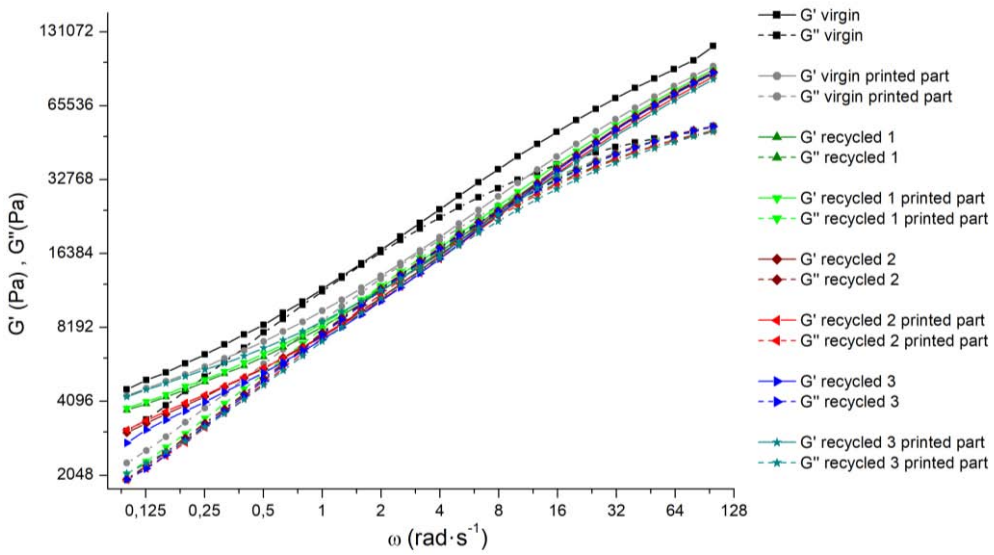

Figure 5-3 Storage modulus G' and loss modulus G'' curves ABS 694 ICE-Filaments.

The trend in figure 5-3 of the G' and G'' curves is the same of the viscosity, the curves are shifting down each recycle. In figure 5-5 the crossover points between those curves, compared to those of the virgin materials, are going to the right after the first printing process and then are moving to the left until the third recycle.

The point regarding the printed part of the third recycled ABS behaves in the opposite order and it is positioned close to the virgin printed material.

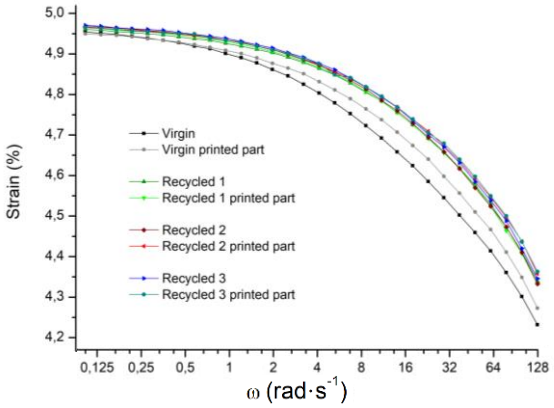

Figure 5-4 Strain in dependence of frequency ABS 694 ICE-Filaments.

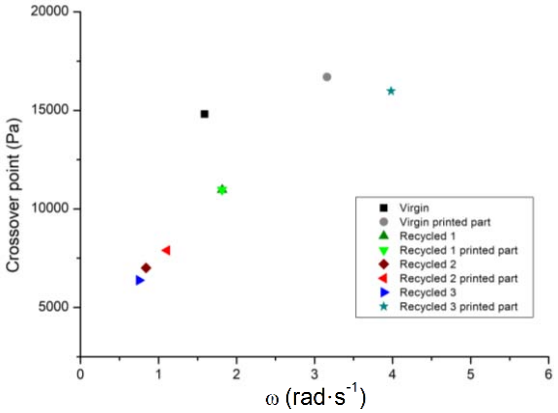

Figure 5-5 Cross over points ABS 694 ICE-Filaments.

There were some difficulties with the measuring system of the rheometer because of the high viscosity of this ABS. The time required to reach the standard space between the cone and the plate was around half hour and sometimes the tests failed because it was not possible to arrive at the measure.

Also, the percentage of strain was not maintained constant, at the medium-high frequency, due to a limit of the maximum toque of rheometer motor.

The recycled materials gave less problem because the viscosity was lower than the virgin, so the strain was more constant (figure 5-4).
Even if there is the strain nonlinear in the medium and high frequency the results are trustable thanks to the Cox-Merz rule [47].

5.1.1.2 Thermal characterization

The DSC-TGA analysis was run to compare the third recycled printed material with the virgin one. The temperature range of the analysis was from 30 °C to 900 °C, the ramp was of 10.0 (°C/min).
The glass transition of the PB was not investigated.
There is no evidence changing in the thermal properties between the virgin and the third recycled. In the figure 5-6 below it is visible the TGA curves almost overlap above the glass transition temperatures of the SAN phase where the T_G of the recycled material is 6.7 °C higher than the virgin (table 5-5).

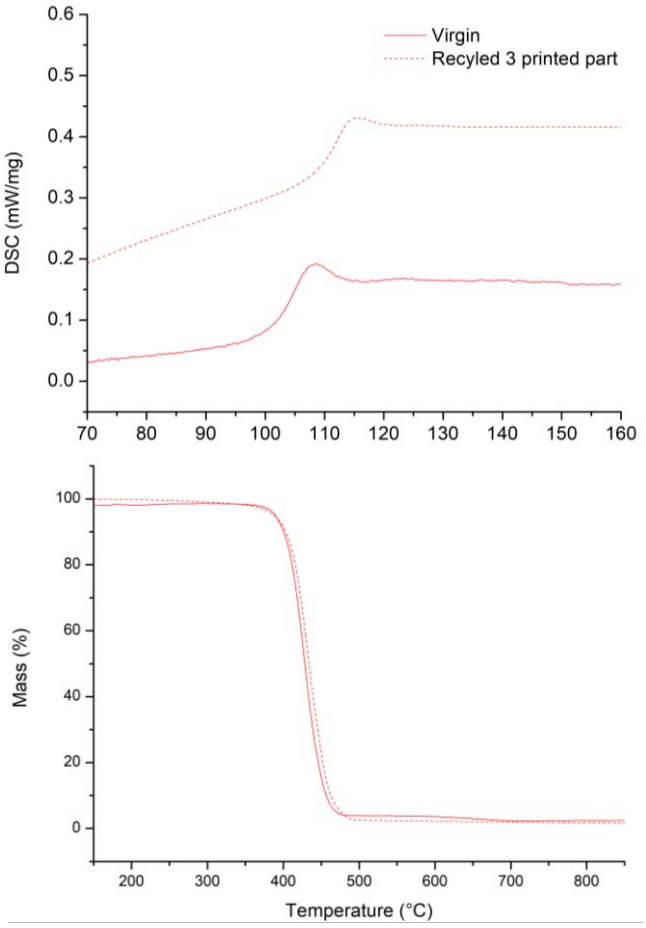

Figure 5-6 Above the DSC and below the TGA curves ABS 694 ICE-Filaments.

Table 5-3 Thermal characterization ABS 694 ICE-Filaments.

ABS 694 Ice-Filaments	Virgin	Recycled 3 printed part
T_{ONSet} (°C)	406.5	407.80
T_G (°C)	108.7	115.40
Residual mass (%)	2.13	1.26
$T_{mass\ 95\%}$ (°C)	382.85	387.86

5.1.1.3 Chemical characterization

The FTIR absorption spectra are in the attachment, the cooperation do not show any trend concerning the ratios between the values of the PB peaks and the CN peak (figure 8-5).

But, comparing the absorbency peaks, it can be seen the pellets coming from the printed parts (dashed line) have a lower absorption compared to the relative filaments (continuous line), is evident the spectra can be subdivided in two main group (figure 5-7).

Up to the second recycled material both peaks of the PB and the CN are shifting down, while an increase of the spectra of the third recycled material is evident. The infrared absorption spectra of the third recycled filament are very close to the virgin and the peak of the relative printed part is higher than the ones of printed of the other materials.

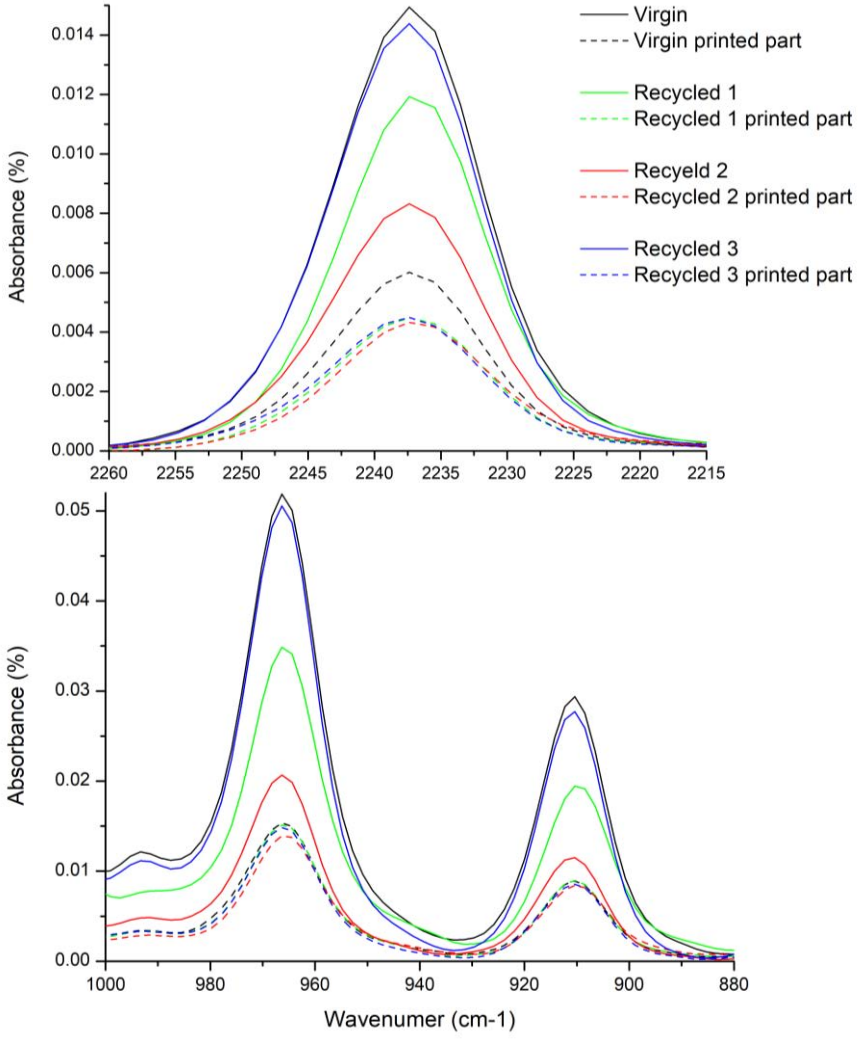

Figure 5-7 CN peaks above and PB peaks ABS 694 ICE-Filaments.

5.1.1.4 Mechanical characterization

In the figure 5-8 the most represent stress-strain curves up to the second recycled material. There are discontinuities at 4-7% of strain due to the safety take-down of the extensimeter before the brake. It is clear the recycled ABS have a similar elastic modulus, and both are higher than the virgin.

In the table 5-6 there are results of the tensile tests and impact tests up to the second recycle.

The average tensile stress at the yield and the strain at the break of recycled material are lower than the virgin, this could be associate more to a defect of the 3D printing technique, indeed the porosity and the location of the void inside the sample affect the fracture behavior; the impact strength was the less affected (table 5-6).

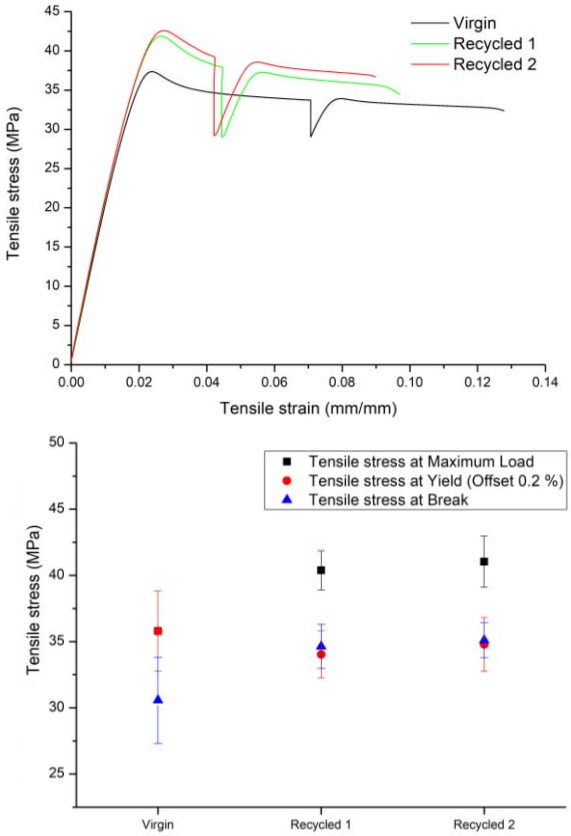

Figure 5-8 Above the main stress-strain curves, below, the results of the tensile stress at maximum load, at the yield and at the break of the ABS 694 ICE-Filaments.

Table 5-4 Tensile test results ABS 694 ICE-Filaments.

ABS 694 ICE-Filaments	Virgin	Recycled 1	Recycled 2
Modulus (MPa)	1983.72 ± 112.46	2076.45 ± 54.00	2083.07 ± 93.12
Tensile stress at Maximum Load (MPa)	35.8 ± 3.02	40.38 ± 1.47	41.04 ± 1.92
Tensile stress at Yield (MPa) (Offset 0.2 %)	35.8 ± 3.02	34.03 ± 1.78	34.79 ± 2.03
Tensile stress at Break (MPa)	30.57 ± 3.25	34.64 ± 1.67	35.11 ± 1.33
Correct strain at break ISO527 (%)	7.68 ± 1.17	5.46 ±1.30	7.91 ±1.23

The material was not enough for run both the mechanical tests for the third recycled material because there was a contamination outside of the filament use for printing the tensile samples that caused problems in the feeding system of the printer and so the specimens have defect that compromise the tensile test (6.1).

For this reason, the tensile properties of the third recycled material were not taken in account, there were not enough tensile samples for the requirements of the ISO standard, while the impact bars there was any problem.

The impact strength between the recycled ABS did not present any sensitive variation, the horizontal dashed red line at 30.24 (kJ /m^2) in the figure 5-9 represent the average strength between the three recycled ABS; it is clear the impact strength drop down after the first recycling process and then it is maintained constant until the third recycled material.

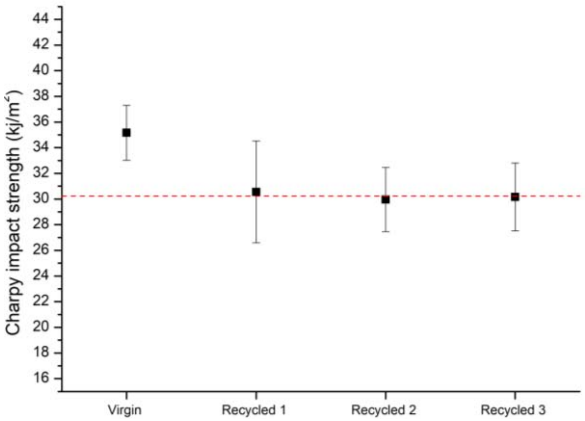

Figure 5-9 Comparison impact strength ABS 694 ICE-Filaments.

Table 5-6 Impact strength result ABS 694 ICE-Filaments.

	Impact strength (kJ /m^2)
Virgin	35.23 ± 1.09
Recycled 1	30.56 ± 3.98
Recycled 2	29.97 ± 2.5
Recycled 3	30.39 ± 2.45

5.1.2 Prusa

5.1.2.1 Rheological characterization

The melt flow index with the 2414 product number from ICE-Filaments is two times higher than 694 (table 5-7).There was a drop of index after the first printing process and then is raised up until the printing process of the second recycled ABS. The average MFI (red dotted line figure 5-10) is 11.38 (g/10 min) is slightly higher than the virgin.

Table 5-7 MFI results ABS 2414 ICE-Filaments.

Cut time: 30 (s)	MFI (g/ 10 min)
Virgin	11.00 ± 0.33
Virgin printed part	10.47 ± 0.44
Recycled 1	11.48 ± 0.60
Recycled 1 printed part	11.78 ± 0.73
Recycled 2	12.25 ± 0.66
Recycled 2 printed part	11.32 ± 0.42

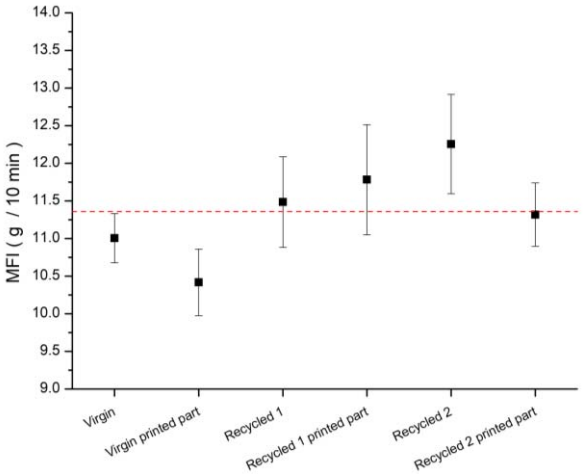

Figure 5-10 Trend MFI ABS 2414 ICE-Filaments.

For avoid the procedure problem with the rheometer explained before (5.1.1), for this characterization was used the plate-plate measuring system with the arbitrary height between the plates of 1mm; in the table 5-8 there are the settings.

Table 5-8 Rheometer setting for ABS 2414 ICE-Filaments.

Measuring system	Height (mm)	Temperature (°C)	Strain (%)	Frequency range (rad/s)
plate-plate	1	235	1%	0.1-100

Respect of the previous cone-plate measuring system was easier reach the space of 1 mm between the plates and was reduced the test time of 3 times; the ABS after the test seem less degraded.

The selection of strain was carried out tests at a constant temperature varying the strain, so the strain of 1% was chosen.

This allowed not to have a loss of linearity of the strain at medium and high frequencies (in the attachment figure 8-3)

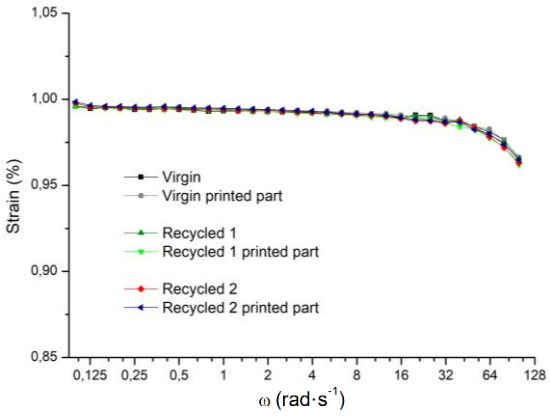

Figure 5-11 Strain in dependence of frequency ABS 2414 ICE-Filaments.

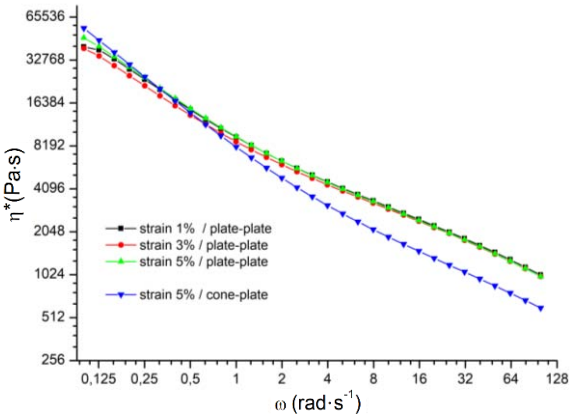

Figure 5-12 Viscosity comparison of the ABS 2414 recycled 1 in base of the measuring system and the strain %.

In the viscosity diagram in the right is visible a slightly difference in the low frequency with different percentual of strain (figure 5-12).

While the different measuring system gives low viscosity and modulus G' value at the low and medium frequency (ABS 694 curves in figure 8-2). So, the comparison of data from different measuring systems is not possible.

Comparing through the same measuring system the previous material investigated both virgin ICE-Filaments ABS, it was found that the viscosity of the 2414 is lower at all the frequency. Indeed, the MFI is two times higher than the 694 ABS.

The comparison of the viscosity results up to the second recycled printed ABS 2414 shows a difference in the low frequency while in the high frequency the curves are almost overlap (figure 5-13).

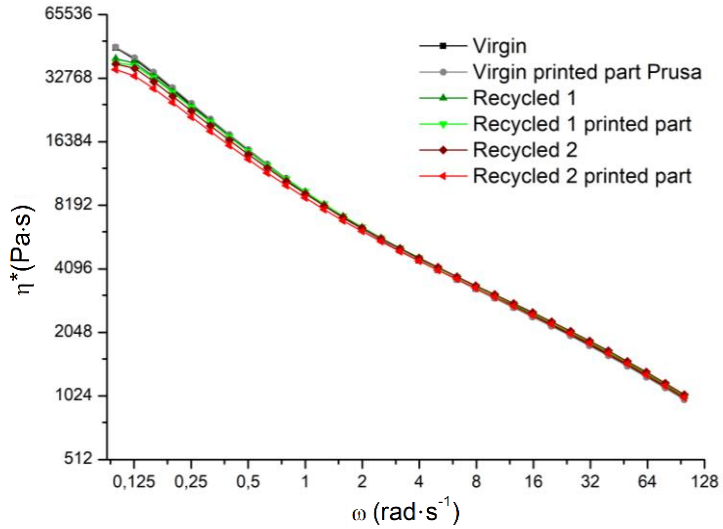

Figure 5-13 Viscosity curves ABS 2414 ICE-Filaments.

The viscosity between the virgin filament and his printed part did not present any sensitive variation while in recycled material there is a drop of the viscosity at each step.

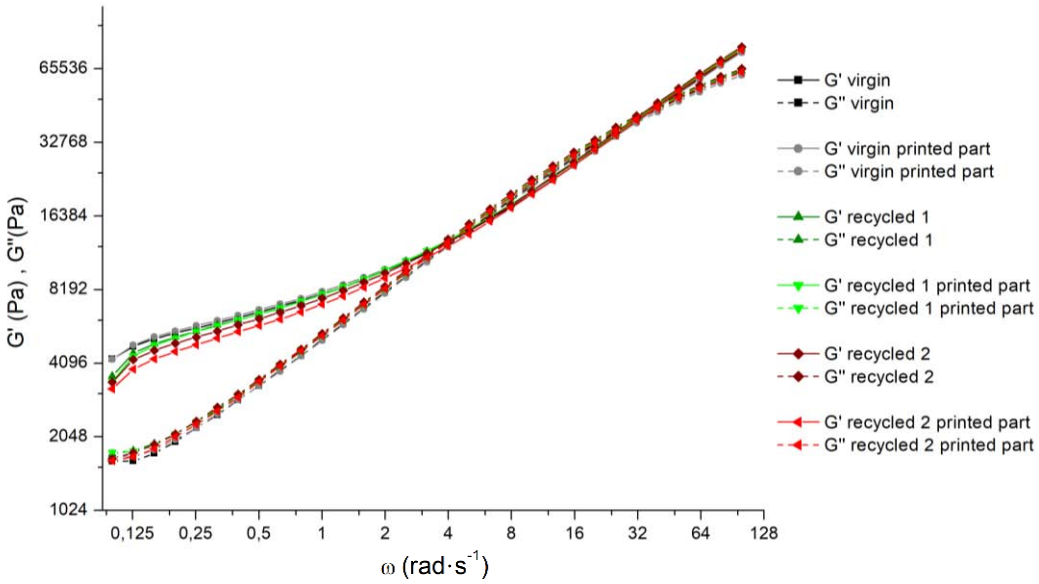

Figure 5-14 Storage modulus G' and loss modulus G'' curves ABS 2414 ICE-Filaments.

The results of the storage modulus G' have the same trend of the viscosity (figure 5-14), the curves are shifting down each recycling process while for the loss modulus G'' there is less variation between the recycled material, the curves are slightly raising up in confront of the virgin. The cross-over point between G' and G'' present a similar behaviour of the ABS 694 previously investigated; respect of the virgin, the point of the virgin printed part moved to the right and then the others cross-over points moved to the left until the second recycling loop; it is discussed more in the discussion chapter (6.2).

5.1.2.2 Thermal characterization

The results of the thermal characterization of the virgin ABS 2414 are close to the ABS 694: the $T_{mass\ 95\%}$, T_{ONSet} and the T_g are few degrees higher and the percentage of residual mass is three time bigger.

The DSC-TGA analysis was run to compare the second recycled printed material with the virgin one. The temperature range of the analysis was from 30 °C to 900 °C, there was a ramp of 10.0 (°C/min). The glass transition of the PB was not investigated. In the figure 5-15 below it can be seen the TGA curves almost overlapped, above it can be seen the glass transition temperatures of the SAN phase where the T_G of the recycled material is 1.2 °C higher.

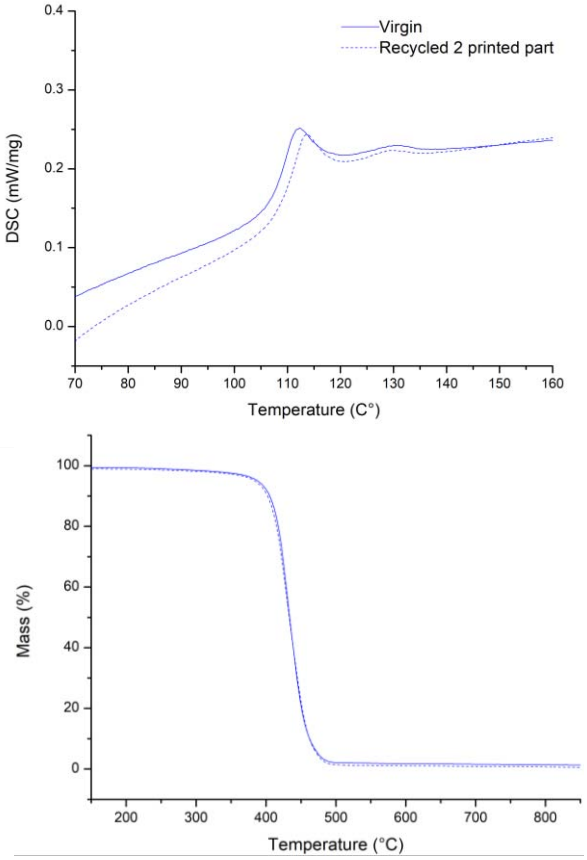

Figure 5-15 Above the DSC and below the TGA curves ABS 2414 ICE-Filaments.

There is no evidence changing in the thermal properties between the virgin and second recycled materials, the same result of the comparison of the virgin and the third recycled material of the ABS 694 (table 5-9).

Table 5-9 Thermal characterization ABS 2414 ICE-Filaments.

ABS 2414 Ice-Filaments	Virgin	Recycled 2 printed part
T_{ONSet} (°C)	408.9	405.60
T_G (°C)	112.5	113.70
Residual mass (%)	6.76	0.92
$T_{mass\ 95\%}$ (°C)	388.15	383.89

5.1.2.3 Chemical characterization

In the attachment there is the result spectra of the FT-IR analysis (figure 8-7) and the comparison between the characteristic peaks of the 694 and 2414 ICE-Filaments ABS is in figure 5-16.Comparing the infrared absorption spectra of both the ICE-Filaments ABS it is clear that the CN peak of the 2414 is lower than the 694, while the PB peaks are similar (table 5-16).

The results of the ABS 2414 up to the second recycling process are like the ABS 694 discussed before, the absorption of the filament and the relative printed part are different. Focus on the filaments there is a reduction of the peaks up the second recycled material. The second recycled printed ABS has an increasing of the absorption spectra respect the previous printed material. The comparison between both PB peaks and the CN peak is in the attachment (figure 8-6), and there is not a clear trend.

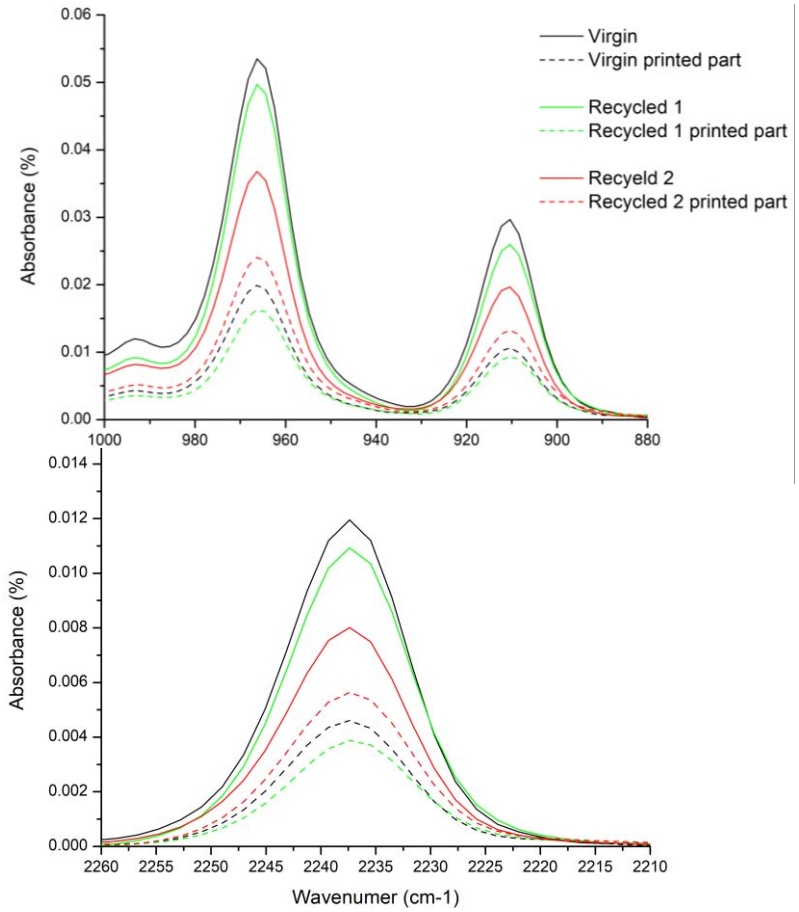

Figure 5-16 CN peaks above and PB peaks ABS 2414 ICE-Filaments.

5.1.2.4 Mechanical characterization

The tensile properties of the second recycled material are not conform to ISO standard. There was no enough specimen to reach the minimum quantity request to the ISO standard, the samples were four out of five.

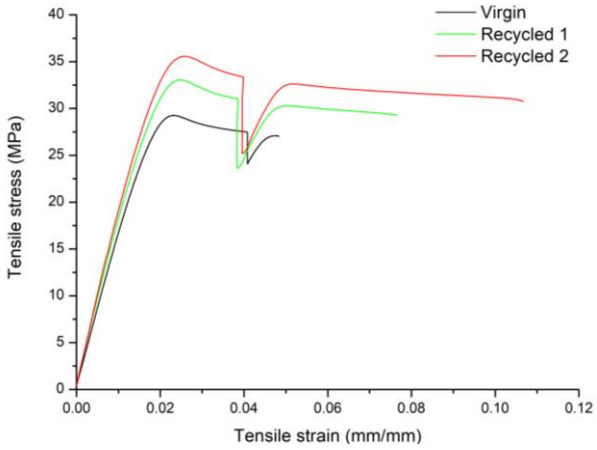

Figure 5-17 The stress-strain curves ABS 2414 ICE-Filaments.

In the figure 5-17 it is shown the most significant stress-strain curves up to the second recycled ABS.

The values of those data out of the normative are reported in in cursive and underlined in the table 5-10.

In every recycled process there was a hardening in all the tensile properties (figure 5-18).The increment in the tensile stress at the yield and the strain at the break is not just for the material. The reason why is that the recycled filaments result easier to print and so the samples present less defect (6.6).

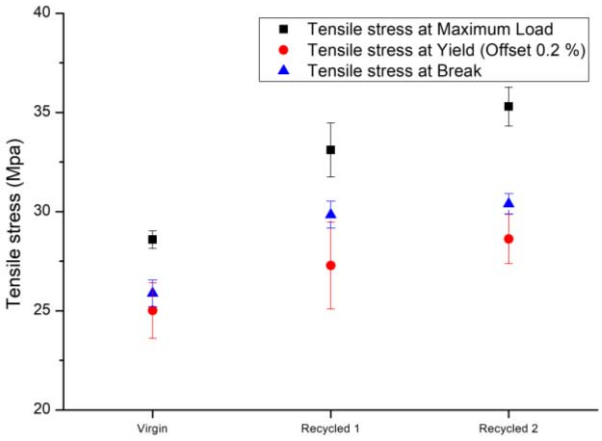

Figure 5-18 The results of the tensile stress at maximum load, at the yield and at the break of the ABS 2414 ICE-Filaments.

On the other hand, in the impact properties there is slight decrease (table 5-10).

Table 5-10 Tensile test results ABS 2414 ICE-Filaments.

ABS 2414 ICE-Filaments	Virgin	Recycled 1	Recycled 2
Modulus (MPa)	1726.12 ± 101.26	1918.88 ± 36.67	*1991.02* ± *65.58*
Tensile stress at Maximum Load (MPa)	28.59 ± 0.44	33.11 ± 1.36	*35.30* ± *0.98*
Tensile stress at Yield (MPa) (Offset 0.2 %)	25.01 ± 1.4	27.28 ± 2.19	*28.62* ± *1.24*
Tensile stress at Break (MPa)	25.88 ± 0.67	29.85 ± 0.68	*30.40* ± *0.51*
Correct strain at break ISO527 (%)	4.17 ± 0.60	4.97 ± 1.87	*7.26* ± *1.89*
Impact strength Charpy method (kJ /m^2)	29.10 ± 1.58	26.63 ± 1.53	27.98 ± 0.94

5.2 ABS Sitraplas

The follow results are for the ABS Sitraplas, it was used in both printers. The material is a recycled pellet for the injection moulding, in the beginning it was characterized then extruded to make two identical spools for the printers.

5.2.1 Rheological characterization

In the MFI tests for the ABS Sitraplas was used a 10(s) shorter cut-time (table 5-11) compared to the other ABS studied, due to the low viscosity of this material (table 8-2), indeed the tests was easier and the data obtain more useful compared to previous.

Table 5-11 MFI ABS Sitraplas.

Cut time: 20 (s)	Pellet	Filament	Prusa printed part	Spiderbot printed part
MFI (g/ 10 min)	18.36 ± 0.71	27.26 ± 1.30	27.86 ± 1.70	28.28 ± 1.33

The MFI increases of 51 % after the filament extrusion process.
The follow printing process do not have any important impact on the melt flow index (figure 5-19).
The red dashed line at 27.8 (g/10min) is the average value of the MFI between the filament and the printed parts.

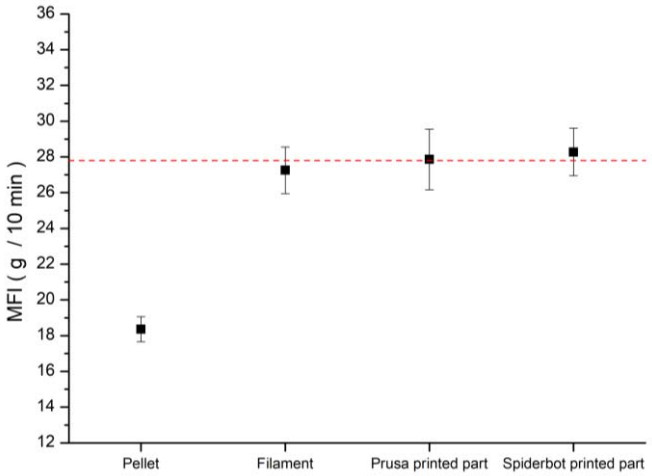

Figure 5-19 Trend of the melt flow index results ABS Sitraplas.

Table 5-12 Rheometer setting for ABS Sitraplas.

Measuring system	Height (mm)	Temperature (°C)	Strain (%)	Frequency range (rad/s)
cone-plate	0.0473	235	5	0.1-100

For this ABS it was used a cone-plate mesuring system, the same used for the ABS 694 ICE-Filaments (table 5-12). There was not any problems for reaching the standard distance between the cone-plate thanks to the low viscosity of the material. The strain curves (figure 5-21) in dependence of the frequency, indeed, is more linear than the ABS 694, but at the medium-heigh frequency there is still a lost of the linearity of the strain. Anyway the rule of Cox-Merz is always valid so all the results are reliable.
The rheometer results are in line with the MFI results. The extrusion process has the highest impact in the viscosity figure 5-20, while after the printing process it decreases more slightly for the printer without the radiant system (6.7.3).
The storage modulus G' has the same behavior of the viscosity while the lost modulus G'' is increasing after the extrusion process and then the curves are almost overlap.

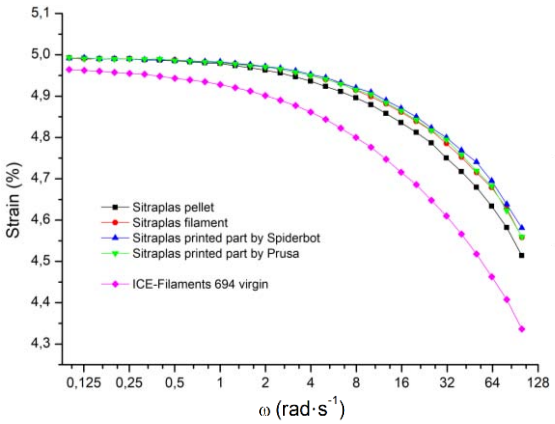

Figure 5-21 Strain in dependence of frequency ABS Sitraplas.

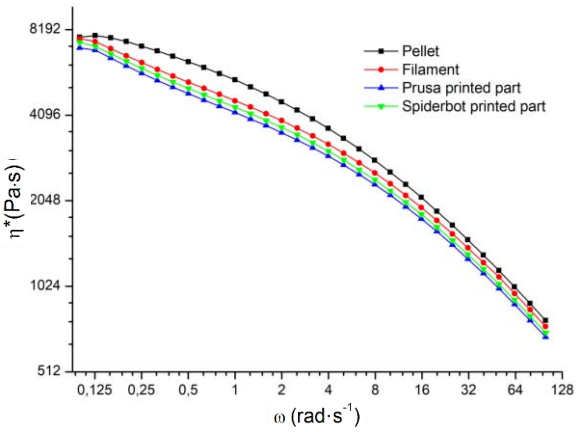

Figure 5-20 Viscosity curves ABS Sitraplas.

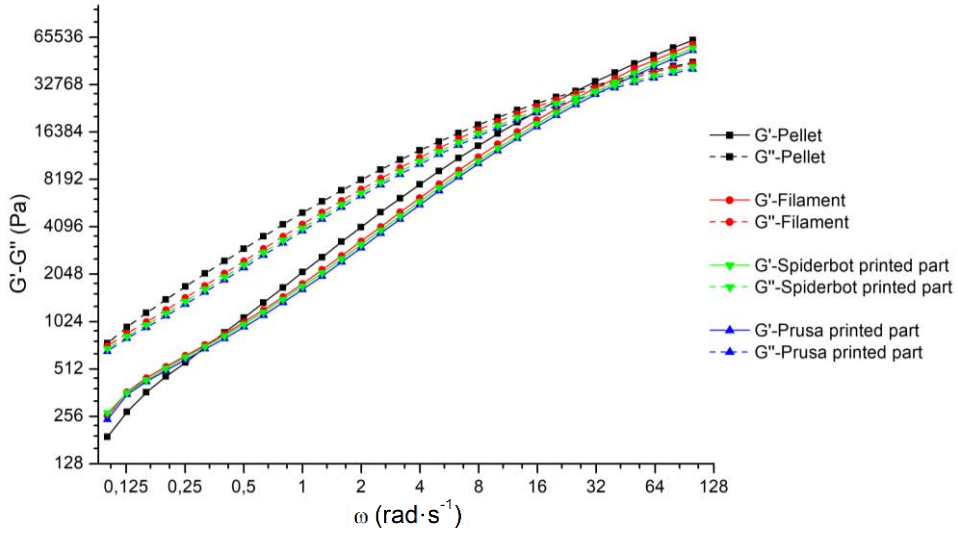

Figure 5-22 *Storage modulus G' and loss modulus G'' curves ABS Sitraplas.*

As it can be seen in the figure 5-22 the curves of the G' and G'' are shifting in the right and down, as well the cross over point between the curves. That could mean a decreasing in the molecular weight and it is a signal of predominant degradation in the SAN phase that is in accordance with a decrease in the viscosity.

5.2.2 Thermal characterization

The DSC and TGA analysis were done only for the ABS recycled pellet.

The glass transition is visible in the figure 5-23 above and below the TGA curve.

The thermal properties are close to both the virgin ABS characterised before (table 5-13).

Table 5-13 Thermal characterization ABS Sitraplas.

T_{ONSet} (°C)	T_G (°C)	Residual mass (%)	$T_{mass\ 95\%}$ (°C)
405.9	109.9	2.49	389.5

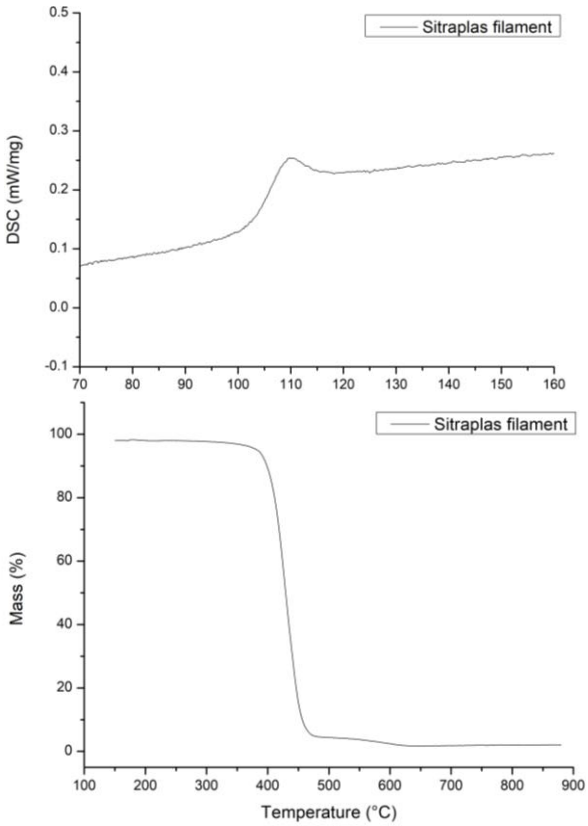

Figure 5-23 Above the DSC and below the TGA curves ABS Sitraplas.

5.2.3 Chemical characterization

The infrared spectroscopy, in the figure 5-24, shows a higher absorption spectrum for the recycled filament (red continues line) and lower for the recycled pellet and the relative printed part for both the PB and CN peaks; the same happen for the printed part of the previously materials in confront of the virgin and recycled filaments.

In the attachment the rapports BD/CN not gave any interesting trend (figure 8-4).

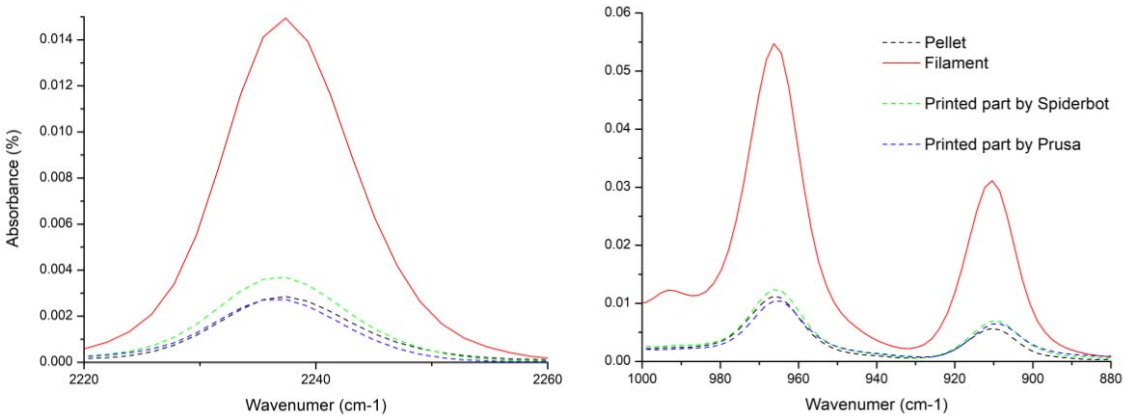

Figure 5-24 FTIR spectra of the CN peak on the left and PB peaks on the right ABS Sitraplas.

5.2.4 Mechanical characterization

The mechanical properties of the Sitraplas ABS present good tensile strength close to the virgin ABS characterized before, except for the higher elastic modulus and the low strain at the break. The difference between the two FFF machines is clear (figure 5-25). The elastic modulus is similar for both while the tensile properties of the Spiderbot samples are appreciably higher, like the strain at the break is almost two times the Prusa ones.

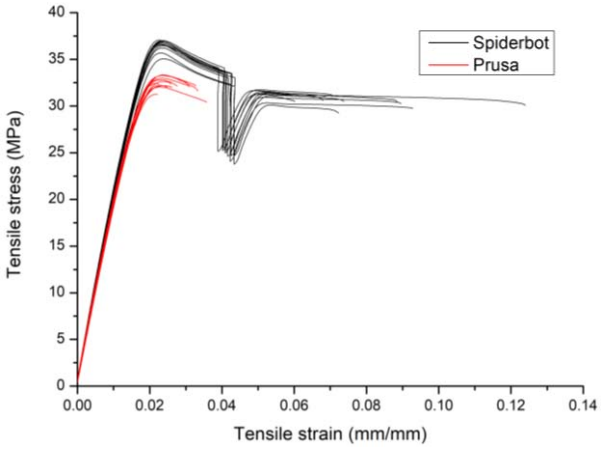

Figure 5-25 Stress-strain curves ABS Sitraplas.

The stress-strain curves of the individual tensile samples tested for both printers are very regular, which is not the case for the others recycled material tested (stress-strain curves ABS ICE-Filaments in the attachment). The impact strength is lower than the virgins and the recycled materials, almost three times, and the difference between the strength of the specimens printed with the two different FFF machines is minimal.

Table 5-10 Mechanical proprieties ABS Sitraplas.

ABS Sitraplas	Prusa	Spiderbot
Modulus (MPa)	2048.70 ± 80.19	2098.16 ± 63.12
Tensile stress at Maximum Load (MPa)	32.57 ± 0.59	36.50 ± 0.59
Tensile stress at Yield (MPa) (Offset 0.2 %)	27.84 ± 1.84	32.58 ± 0.86
Tensile stress at Break (MPa)	31.76 ± 0.57	30.90 ± 1.95
Correct strain at break ISO527 (%)	2.67 ± 0.29	5.8 ± 1.63
Impact strength Charpy method (kJ /m^2)	10.26 ± 0.40	10.80 ± 0.30

The low viscosity of the filament was useful during the printing process, the material infiltrated better through the gaps between layers and this led to benefits in the density of the printed parts (figure 5-26). Indeed, in the fracture surfaces of the samples it is visible a good bonding between the layers from both printers (red color for the Spiderbot and black color for the Prusa) compared to the other ABS studied with a higher viscosity.

The apparent areal density (subparagraph 6.5) influenced more the tensile properties than the impact strength, as confirmed by the figure 5-26.

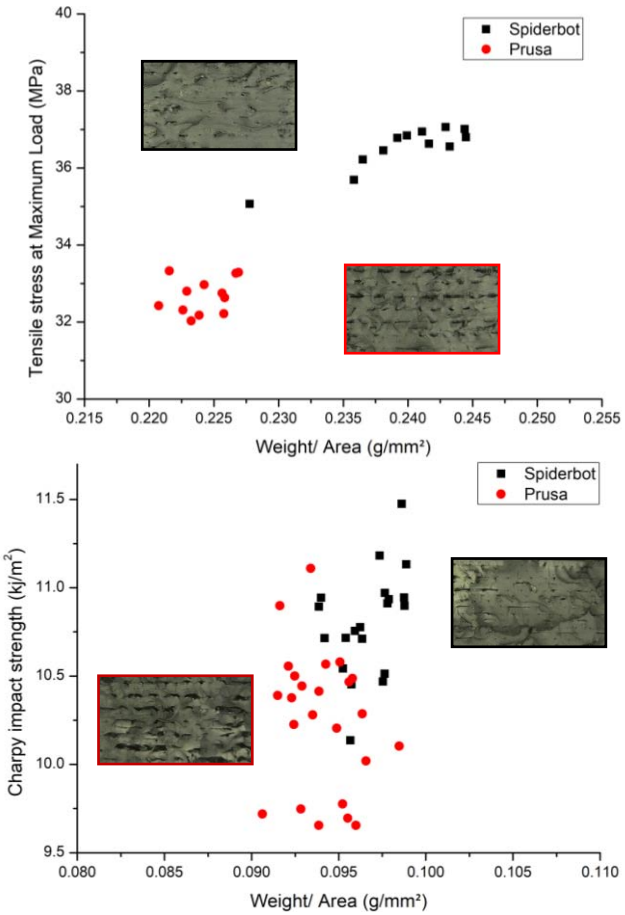

Figure 5-26 Above the tensile stress at maximum load, below the impact strength in function of the apparent areal density.

6. DISCUSSION

This session examines the results, problems and solutions applied during the recycling, the characterisation and the data processing. It discusses the filament extrusion process, the printing process and different FFF used (infrared radiant heater system effects).
The change in rheological, thermal, mechanical and morphological properties during the recycling is clarified in the following sub-chapters.

6.1 Filament extrusion process

The first extrusion process was done with the cooling bath at ambient temperature, the cooling down process was too fast that formed vacuum bubbles inside the filament (figure 6-1), because of the fast solidification of the external side. The filament results brittle and gave an obstruction problem to the feeding system of the printer. Anyway, the problem was banally solved increasing the temperature of the water up 40 °C.

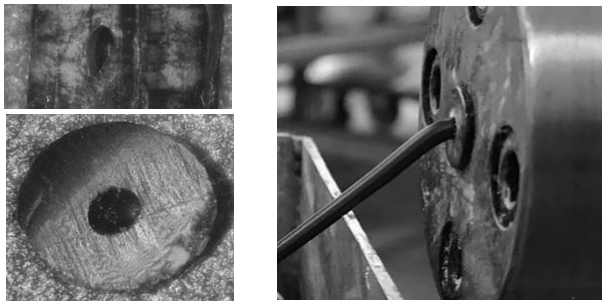

Figure 6-1 On the left two images of the vacuum bubbles inside the filament, on the right the filament inclination between the extruder head ant the cooling bath cooling bath.

Figure 6-2 Different shapes of the pellet, in order from the right: pellet for the injection moulding, pellet from the FFF filament and pellet from the printed part.

During the extrusion process it was difficult to maintain the diameter of the filament close to 1.75 mm, the shapes of the input pellet influenced the behaviour of the flow in output.
The recycled pellets came from the rest of the mechanical samples and objects printed for have enough material for the next recycling. Those objects are cylinders with a higher layer height (0.4 mm) and a lower infill (50 %) than the mechanical samples, the process setting, which can affect the degradation of the material were the same.
The average diameter obtained in the recycled process was 1.70 mm with a deviation standard of 0.1. The filament roundness was affected by the inclination of the outgoing filament between the extruder and the bath, was obtained an average of 90% of roundness instant head a 95% from the filament producers.

In the last extrusion process for the third 694 ABS recycled there was an external contamination around the filament; the PP used for cleaning the equipment was present in a small quantity in the barrel, it was attached to the external part of first meters of the filament. When it was printed, the contamination deposed into the PTFE tubes, an in the other feeding system components where the filament passed, causing the obstruction of the feeding system. This caused under extrusion problems, so the samples had defects and voids, the average apparent areal density was significantly reduced below standards and no one printed samples was useful. The filament was selected and discarded. For this reason, there was not enough material to print enough tensile test specimens for the mechanical characterization of the third recycled ABS (694 ICE-Filaments).

6.2 Printing process

The choice of temperature was based on the level of the bonding between the layers evaluated qualitatively through the dissection of the samples and the microscopic control of the section and based on the impact strength of the ABS. The layer bonding increased with the extrusion temperature thanks to a decrease of the viscosity and a better infiltration of the melt material between the layers (figure 6-3).

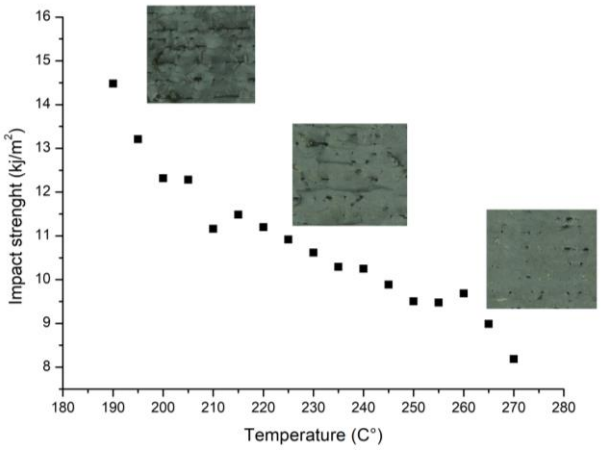

Figure 6-3 Impact strength in dependence of the temperature.

It is known that the thermal degradation of ABS affected more the impact strength and the elongation, so it was chosen a temperature with a compromise between porosity and impact strength at the break. Different impact test using the samples printed at nozzle temperature from 190 °C to 270 °C were run, and so it was selected the temperature of 235 (°C) for the printing process.

The temperature of the bed was chosen based on the T_g of the SAN phase.

As said before, due to the bad shape of the pellet, it was difficult to obtain a constant diameter of 1.75 mm, the deviation standard of the recycled filament was two times the one of the filaments producers and the roundness was 4% lower than the virgin one, so that affected the layer deposition and flow and the resulting density of the samples.

The warpage problem was more controllable after each recycling process, the decrease of the viscosity helped the layer bonding and there was less thermal expansion at the base of the printing part, so the recycled materials were easier to print compared to the virgin. The printed part became more yellow after each filament extrusion process and printed process. It was more evident in the printed with the infrared radiant system.

6.3 Rheological properties

The melt flow index has not shown any trend for both the ABS ICE-Filaments during the recycling process, the same conclusion was found in those researches of the reprocessing ABS for the injection moulding [18] [17]. However, it is to consider that the average values of MFI regarding the reprocessed materials are higher than the corresponding virgin ones.

The ABS Sitraplas was the only material that presented good results from MFI due to its low viscosity, while the high viscosity of the other materials tested influenced the MFI results, and the irregular shape of the pellet has further accentuated the problem; for this reason, data obtained from the rheometer are more trustable.

In the ABS Sitraplas, there was a significant increase of the melt flow index after the extrusion process and an imperceptible variation after the printing processes, which is also confirmed by the rheometer analysis.

Moreover, as it can be seen by the results of the rotational rheometer, for both the ABS ICE-Filaments, in each thermal step there is a change in the rheological properties.

The viscosity and G’ are more influenced by the filament extrusion process than by the 3D printing process.

The viscosity curves and the both modulus curves decreases until the second recycling.

The storage modulus G’ and lost modulus G’’ give information regarding the degradation of the SAN and the PB phases, the crossover point of the curves is useful to understand the changing in the molecular mass during the recycling process.

There is a correlation between the molecular mass, the viscosity and the crossover point at the low frequency (figure 6-4).

The research [48] demonstrates an increasing in the storage modulus G ' and in the viscosity correlated to an increasing in the molecular weight of the SAN phase, with the

same percentage of rubber. Also, if the molecular weight increases, it corresponds to change to the left of the cross over point.

The same correlation between molecular weight (MW) and crossover point was found in [49] for the PS material. Moreover, it was found a correlation between the height of the point and the MW distribution (figure 6-4).

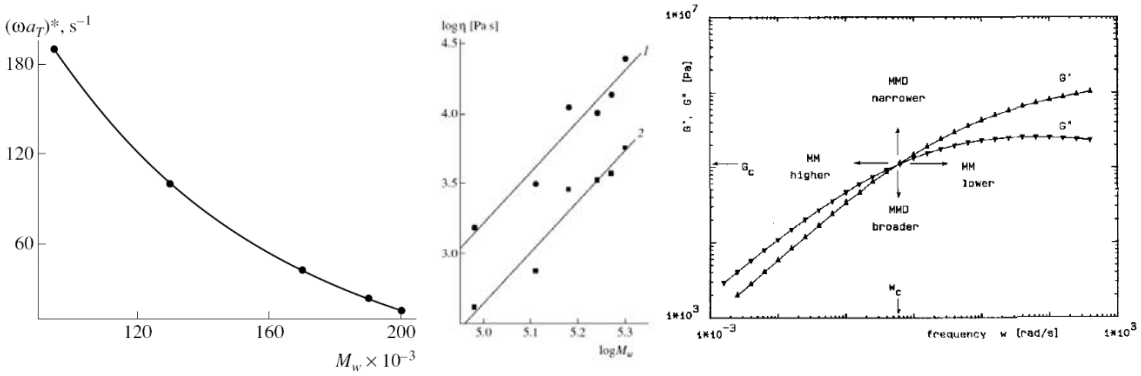

Figure 6-4 In the right the intersection point of storage and loss moduli gives information regarding the MMD and the Mw; in the centre the appearance viscosity as a function of the Mw; in the left the frequency of the crossover point in dependence of the Mw.

The study of [47] investigate the influence of grafting degree on the rheological properties, with different percentage of rubber inside the SAN matrix. It was found a relationship between the grafting and the mechanical rheological properties. As concerned the rubber phase when the grafting degree increases, the viscoelastic functions first decrease and then increase. As it can be seen in the figure 6-5 in the right, the storage modulus is decreasing and then increasing in base of the graft and the rubber content.

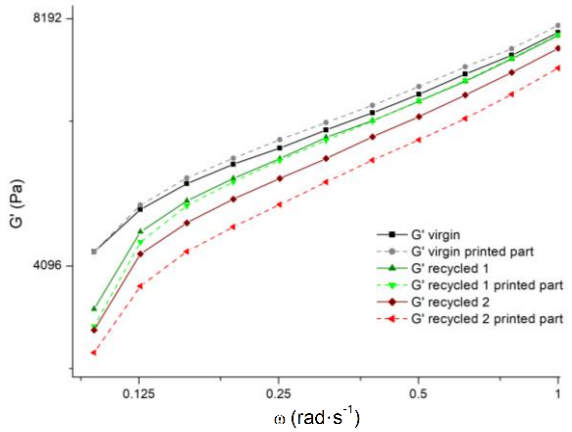

Figure 6-6 The modulus G' in dependence of the frequency for the ABS 2414 ICE-Filaments.

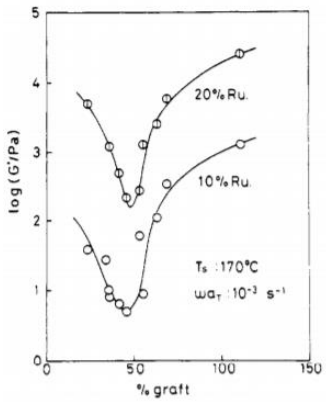

Figure 6-5 The storage modulus G' plotted against the % graft and the content of rubber.

Taking in account the crossover points of the 2414 ICE-Filaments ABS (figure 6-6) after the first printing process it moves to the right (probably due to an important loss in the molecular mass of the SAN phase) and then moves to the left up to the third last

printing process of the second recycled ABS (could be an increase in molecular mass probably due to the predominant crosslinking of the rubber phase).

Anyway, the viscosity follows the crossover point with an opposite behaviour than expected, the match between the degradation of the two phases showed a decrease in viscosity probably due mainly to SAN phase while it is less significant the increase in the molecular mass due to the cross-linking of PB assumed by the evolution of the crossover point, until the second recycling process.

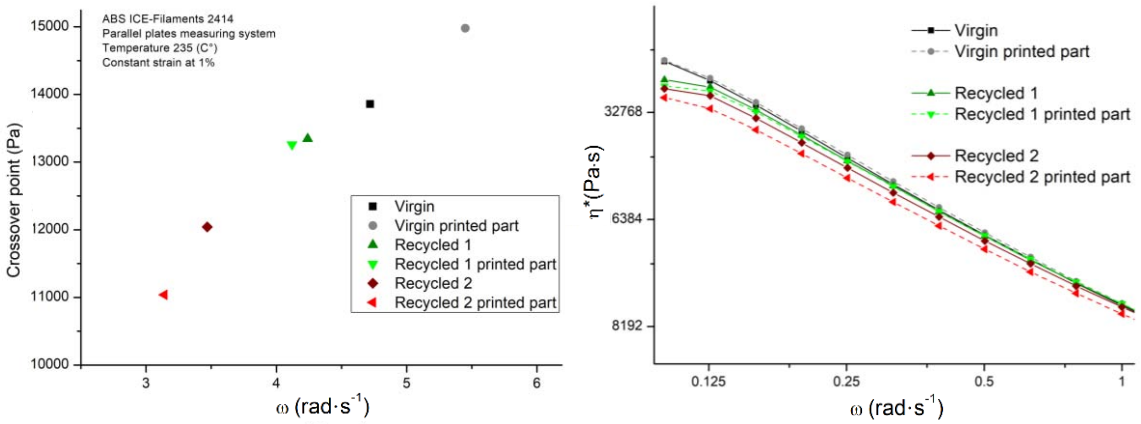

Figure 6-7 In the left the cross over points, in the right the complex viscosity (2414 ICE-Filaments ABS).

For the ABS 694 ICE-Filaments, the results of the rheological properties up the third recycled material are in line with the ABS 2414; but the third recycled printing parts showed an increase of the modulus and the viscosity that could be correlated to an important level of grafting, enough to influence the rheological properties more than the degradation of the SAN phase even if the crossover point has reversed behaviour going to position itself above all the others and rightmost.

So it could be concluded that, the change in the rheological behaviour for the degradation of the ABS are influenced more by the degradation of the SAN phase until the second recycling process [49] then by the degradation of the PB phase after the third recycling process [50].

6.4 Thermal properties

The results of the thermal analysis carried out with the DSC showed a slight increase in the Tg of the SAN and no other significant variations due to the recycling process, the same result was found also in this research [18] .

In figure 6-8 there is a comparison of the TGA and DSC curves.

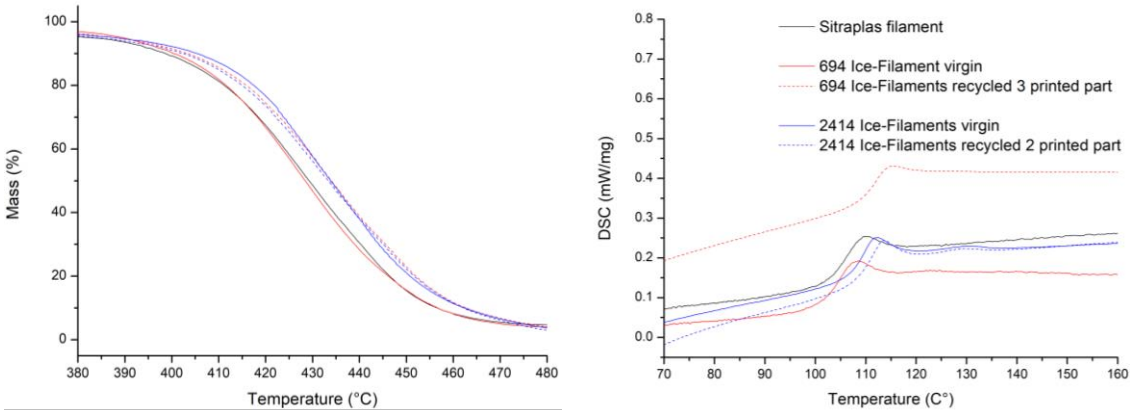

Figure 6-8 In the left the thermogravimetric curves and in the right the T_g of the SAN phase, of all the ABS samples.

It was not possible to investigate the TG of the PB because it is limited to the equipment used to reach temperatures down to -50 (°C). The research carried out by Pérez et al. [17] do not show relevant changes in the glass transition temperatures of the polybutadiene due to the recycling process with the plastic injection technology, it is supposed to be the same with the 3D printing technology.

In the table 6-1 there are the properties of each ABS thermal characterized; the properties of recycled materials do not differ much from virgin, there is a small increase in the T_G of the SAN phase, more pronounced for the recycled material reprocessed tree times, which could be related to less freedom of the polymer chain than the virgin.

Table 6-1 Thermal proprieties of all the ABS characterized.

	T_{ONSet} (°C)	T_G (°C)	Residual mass (%)	$T_{mass\ 95\%}$ (°C)
Recycled pellet Sitraplas	405.90	109.90	2.49	389.5
Filament 694 ICE-Filaments virgin	406.50	108.70	2.13	382.85
Printed part 694 ICE-Filaments recycled 3	407.80	115.40	1.26	387.86
Filament 2414 ICE-Filaments virgin	408.90	112.50	6.76	388.15
Printed part 2414 ICE-Filaments recycled 2	405.60	113.70	0.92	383.89

The TGA showed a general decrease in residual mass, maybe for losing of some addictive during the reprocessing, or like the ABS 2414 recycled two times showed a decrease more than seven times maybe for some measurement error in the virgin.

6.5 Chemical properties

The BD/CN ratios, from the infrared spectrometry, did not show any relevant trend between the recycled materials (figure 8-4, figure 8-5, figure 8-6 in the attachment).

Looking at all the PB and CN peaks of the materials is evident a distinction between the spectra collected from the printed parts and recycled filaments.

Paying attention only to the recycled filaments there is an effective reduction of the peaks of SAN and PB until the second recycling.
The percentage of photodegradation can be measured through the carbonyl index (1724 cm^{-1}) indicating changes in chemical structure associated with oxidation.
Through the ratio of spectrometric indices of the carbonyl group and the starting polymer, for both materials, did not present significant trend in the process.
Another chemical inspection was carried out through the SEM, using the EDX detector, in order to investigate the dispersion of polybutadiene inside the matrix.
The chemical component that distinguishes the SAN and PB phases is nitrogen, but unfortunately, the peak of the nitrogen spectrum is very close to that of carbon, present logically in both phases, so the mapping created by the EDS has not led to any results.
During the mapping test for the ABS of ICE-Filaments traces of calcium have been found in recycled materials even small amounts of iron and aluminium due to the reprocessing (figure 6-15).
It would be necessary to section the specimen with a crymicrotome or use the transmission electron microscope or an etching technique.

6.6 Mechanical and morphological properties

As explained previously, the flow in 3D printing process depends on the diameter and the roundness of the filament, overflow or low flow affect the density of the final part. For this problem, it was applied a selection criterion on the appearance density of the mechanical samples to discard the parts with a higher porosity and defects.
Ker Chin Ang et all. [51] investigated on the mechanical properties and porosity relationships in the FFF part. They found a correlation between porosity and the mechanical properties. A sample research was carried out on the specimens to calculate the porosity respect of the transverse area (figure 6-9). The samples were cut and refined with the

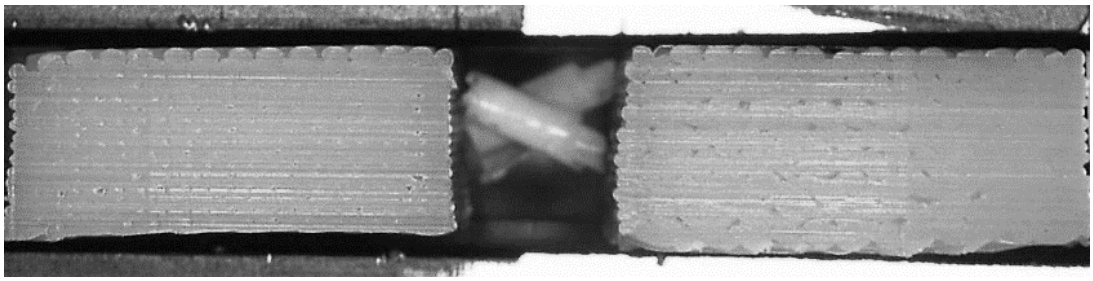

Figure 6-9 Section of tensile sample, on the left the Spiderbot one, on the right the Prusa one.

microtome and was taken the image of the transversal area with the digital microscope, then was processing the images with ImageJ (open-source software) for estimate the porosity. So, the printer with the radiant system has average porosity of 7 % compared to the resistant section, while Prusa was 12%. This assumes a lower sample weight than the ideal weight. It was considered the ideal weight as the volume of the ISO standard sample multiplied by the density provided by the material data sheet. Assuming a relationship between the weight and the transverse area of the specimens, the ideal weight was divided by the transversal area of the specimens, resulting in a theorical apparent areal density value.

$$\text{Theorical apparent areal density (tensile sample)} = \frac{\text{Volume sample} * \text{Density}}{\text{Transversal area}} = \frac{9.602 * 1.03}{40} = 0.247 \ \frac{\text{g}}{\text{mm}^2}$$

$$\text{Theorical apparent areal density (impact sample)} = \frac{\text{Volume sample} * \text{Density}}{\text{Transversal area}} = \frac{3.197 * 1.03}{32} = 0.103 \ \frac{\text{g}}{\text{mm}^2}$$

Considering the information collected for the porosity of the virgin specimens based on the printer, a lower limit of acceptability based on the apparent areal density was set, at 10% for Spiderbot and at 15% for Prusa.

Considering the results obtained with Spiderbot, the apparent areal density for the virgin ABS 2414 differs between 4.5% and 8% from the theorical; whereas the Sitraplas ABS has an apparent viscosity between 7%-10% (Prusa 10%-13%), this is a positive verification of the selection criteria impose. An expected correlation has been found between the apparent areal density and the tensile strength of the material, while for impact there is no influence. An example is the figure 6-10 considering the ICE-Filaments ABS 694 printed by the Spiderbot; the red dashed line represents the theorical value, the black dashed line the lower limit of acceptability.

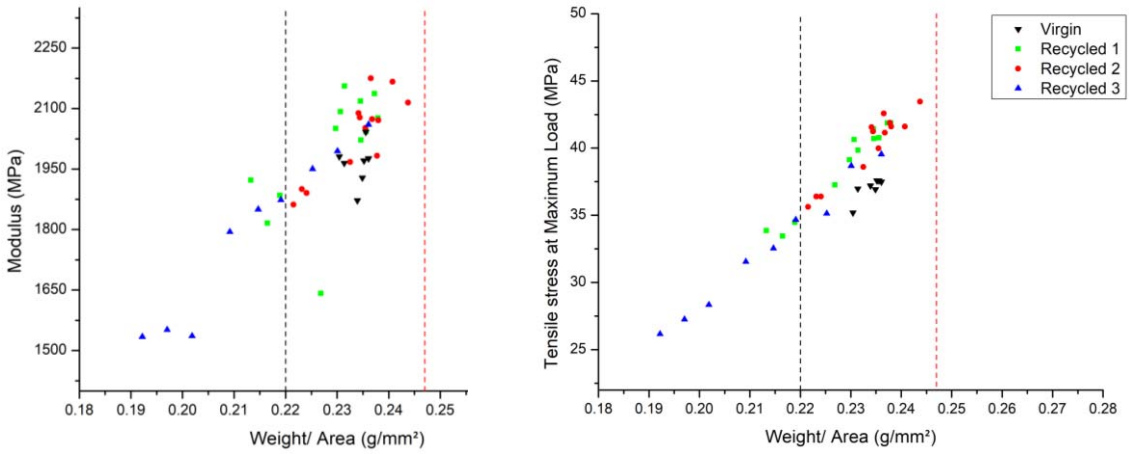

Figure 6-10 Modulus and tensile stress at maximum load in dependences of the apparent areal viscosity.

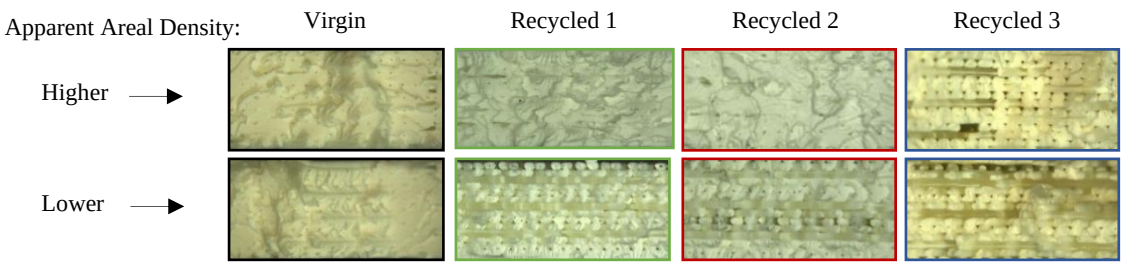

Figure 6-11 Fracture section of the tensile bones.

In figure 6-11, in first line there are the fracture surfaces of the tensile samples with a higher apparent areal density, in the second line with a lower apparent areal density.
In the tensile samples the failure occurred at whitened areas from plastic deformation where some evidence of localized infill delamination was observed.
The fractures surfaces were further analysed with an optic microscope and displayed. The fracture mechanisms were predominantly brittle with localized micro-shearing on each layer face (figure 6-11).
Depending on the breaking point of the tensile specimen, the curves exhibit different behaviour. Specimens that break near the end of the gauge length have defects due to a problem of the deposition technology, the layer seams. This seam happened when the printer moves up to the next step of the deposition process. The standard process for printing one layer is as follows: inner perimeters > outer perimeter > infill > layer change; in each step there is a connecting point between those trajectories. If there is a loss in the flow of the printer (example for problems with the volume of the filament) at the time when there is the beginning or the end of the layer deposition (where the scar forms) there could be a lack of material that physically is a notch that causes a concentration of tensions. Those points are the weaker in the part, as was saw in the tests that this samples breaks with a 45° fracture maybe due to the infill strategy used. Depending on the inclination of the fracture, there are curves with different elastic modulus, yield maximum stress, and strongly the elongations (figure 6-12).

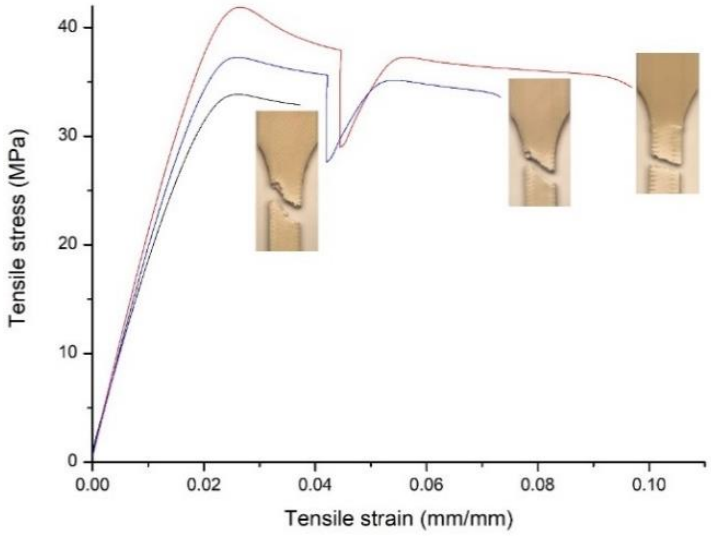

Figure 6-12 Stress-strain curves ABS 694 ICE-Filaments recycled 1 in base of the fracture angle.

The samples with a fracture after the gauge length was not considered, anyway almost all of them present a low apparent areal density and a defect in the layer bonding.
The tensile strength of the filament fused deposition printed specimens depended much more heavily upon the fiber-to-fiber fusion and any air gap resulting between the fibers, as opposed to the strength of the material themselves, in fact, there was no appreciable shrinkage of the neck of the specimen before breakage.
The mechanical characterization during the recycling processes has shown a hardening of the mechanical properties given by an increase in the elastic modulus, tensile strength and yield strength up to the second recycling (table 5-6 and table 5-10).
The impact resistance properties do not show a tendency towards apparent areal density (figure 6-13), is thus more heavily dependent on the strength of the ABS monofilament than from the bonding between the internal structure, as confirmed from figure 6-13 and figure 6-14.

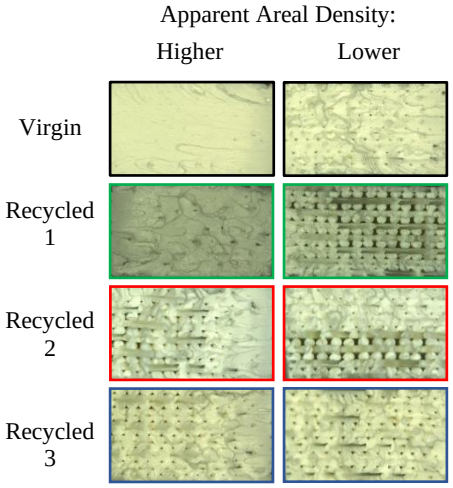

Figure 6-13 Fracture surfaces of the impact strength, in the left with the higher apparent areal density in the right with the lower.

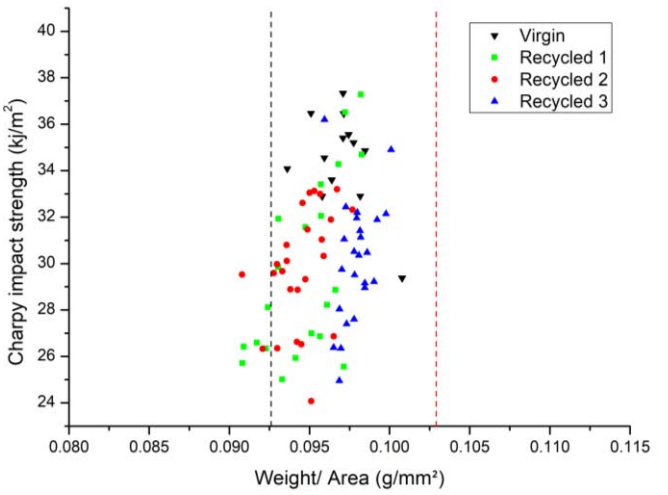

Figure 6-14 Charpy impact strength in dependences of the apparent areal density.

The fracture surfaces of impact samples are increasingly sharp and brittle each recycling, the virgin showed more deformation. As expected, the impact resistance decreased already after the first printing process, and then remained unexpectedly constant until the third recycling (table 5-6). A possible decrease in the impact properties of ABS, in addition to crosslinking in the rubbery part, is the variation in dispersion of rubber particles inside the SAN matrix, as explained before. For the virgin ABS 694 filament, for the printed part of the ABS 694 first recycled and for the ABS 694 third recycled filament, were investigated the morphology at the SEM (figure 6-15).

The sample were dissected after immersion in liquid nitrogen to obtain a net rupture surface, but unfortunately, it was not possible to observe the difference phase and the distribution of the rubber phase, as explained before (6.6).

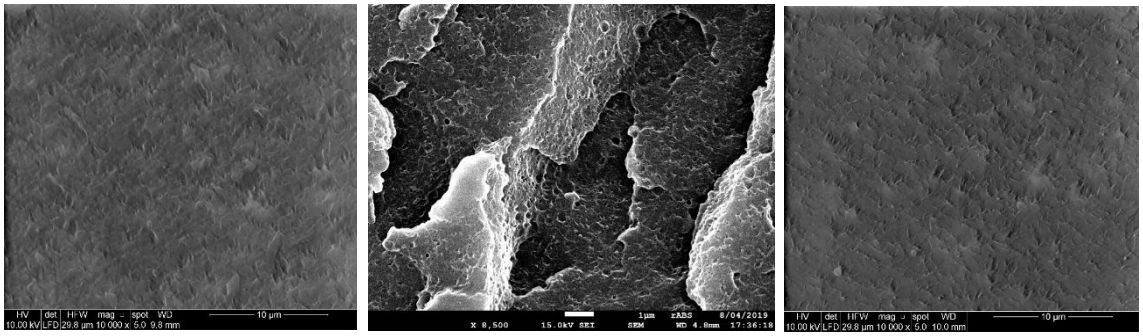

Figure 6-15 SEM microscopies, in the left the ABS 694 ICE-Filaments virgin, in the middle the relative recycled 1 printed part, in the right the relative filament recycled 3.

6.7 Infrared radiant heaters system effects

In this sub-paragraph it is evaluated the effects of the infrared radiant system in the mechanical properties and the additional thermal degradation they could cause. The material used was the virgin ABS 2414 ICE-Filaments characterized for both printers.
The differences between the printers that could affect the properties of the printed part are listed below:

- Feed-system:

  Both printers have the double gear pull system. The Spiderbot has a bowden extrusion system and a bigger stepper motor in respect the conventional desktop printer. The Prusa has a direct drive system, the torque supplied by the electric motor sometimes do not cover the required, so giving under extrusion problems.

- Hot chamber and infrared radiant system:

  The temperature of the material inside the Spiderbot depends on the temperature of the infrared radiant heaters. To have a 55 (°C) in the chamber the radiant must work at 235(°C), it is 117.5(°C) at the part. Over the Tg of the SAN phase the material become too much soft and makes the layer base unstable for the deposition process. An ideal temperature for the ABS in the chamber is around 70 (°C) but that requests a radiant temperature over 300 (°C), it means 150 (°C) at the

part, around 30 (°C) higher than the SAN T_g .The positive effect of this system depends more on the radiant contribute than on the chamber one.

Anyway, the Spiderbot with his chamber maintains the work environment controlled, while the Prusa work is an open ambient and it is influenced by the changes in the working ambient.

- Head cooling system:

  Spiderbot has a liquid cooling head that maintains a lower temperature in the hot-end up to the nozzle than the Prusa, which as an air one. Having here a controllable and low temperature give the possibility to use a higher pressure in the feeding system and it helps to avoid problems of under extrusion, entanglement, obstruction in the hot-end.

6.7.1 Mechanical properties improvements

In the match between the printers, the infrared radiant system and the hot chamber being the main difference in the deposition process, the dimensional stability of the mechanical samples was therefore greater, less thermal expansion and a significant improvement in all the mechanical properties and in the density (figure 6-16).

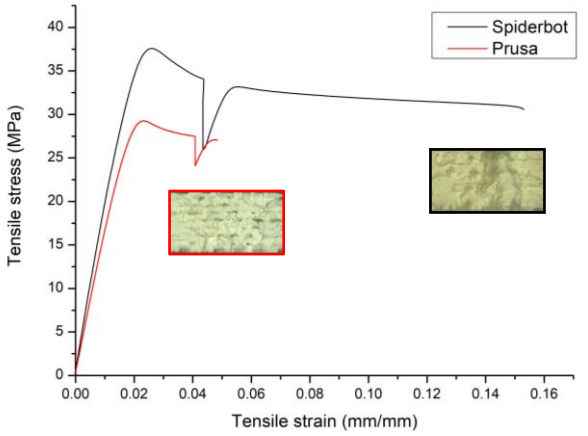

Figure 6-16 Stress-strain curves and fracture surface of the 2414 ICE-Filaments ABS based on the printers.

The samples printed with the radiant system has more pronounced yellowing . About the fracture surfaces of the Prusa tensile specimens, there is a markable delamination between the layers not present in the Spiderbot one, this difference is less evidence in the recycling materials (figure 6-17). The fracture surfaces are brittle with a lower deformation sign in both cases.

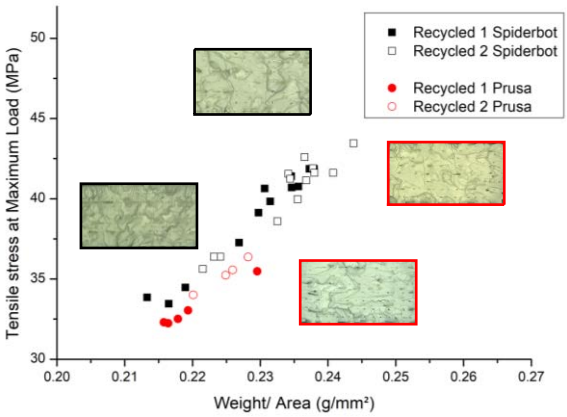

Figure 6-17 Tensile stress at the maximum load in dependence of the viscosity, competition between the recycled material for both printers.

The infrared radiant system increases of the 17% the impact strength (table 6-3).

Table 6-4 Mechanical proprieties ABS 2414 ICE-Filaments printed by Prusa and Spiderbot.

MECHANICAL PROPERTIES ICE-Filaments 2414	Prusa	Spiderbot *Hot chamber + Radiant system*
Modulus (MPa)	1726.12 ± 101.26	1962.08 ± 52.01
Tensile stress at Maximum Load (MPa)	28.59 ± 0.44	36.99 ± 0.84
Tensile stress at Yield (MPa) (Offset 0.2 %)	25.01 ± 1.4	32.08 ± 1.72
Tensile stress at Break (MPa)	25.88 ± 0.67	30.47 ± 0.49
Correct strain at break ISO527 (%)	4.17 ± 0.60	9.37 ± 2.1
Charpy impact test (kJ /m^2)	29.10 ± 1.58	34.52 ± 2.06

6.7.2 Thermal degradation

From the spectrographic results the material printed with the infrared radiant system has a decrease in the peaks of the polybutadiene, the nitrile and the carbonyl (figure 6-18) .
It is expected that the CN (nitrile) does not change with the processing and recycling, but the CO (carbonyl-1730 cm^{-1}) would increase and the BD bands (966 cm^{-1} and 911 cm^{-1}) decrease with the degradation. However, as the CN band is lower, the CO and BD bands are also lower and this does not necessarily means BD degradation.

The MFI do not present important variations between the printed materials and the virgin, it is marginally higher for the Spiderbot printed part and slightly lower for the Prusa printed part (table 6-4).

Table 6-7 MFI ABS 2414 ICE-Filaments.

Cut time: 30 (s)	MFI (g/ 10 min)
Virgin	11.00 ± 0.33
Prusa printed part	10.42 ± 0.44
Spiderbot printed part	11.22 ± 0.50

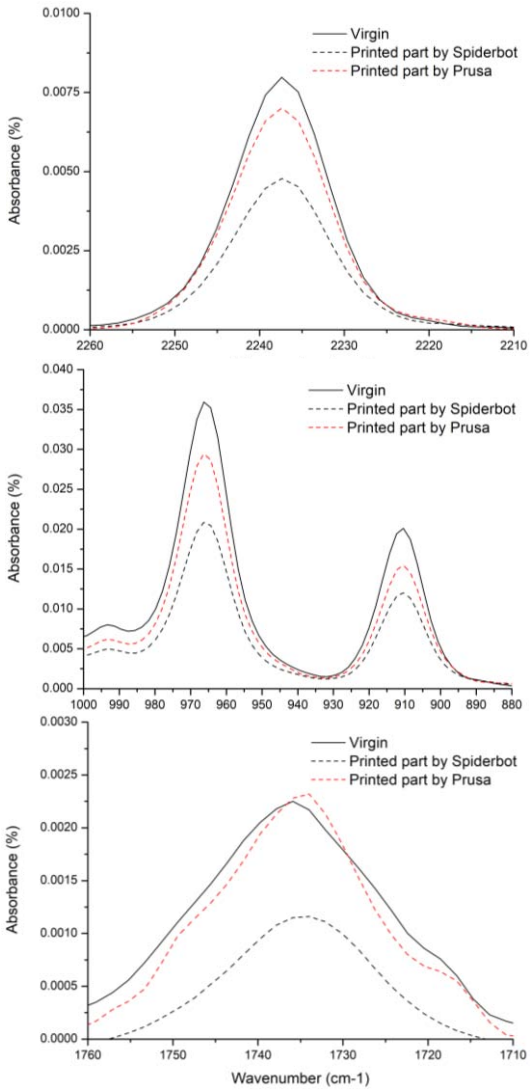

Figure 6-18 The most important FTIR spectra of the 2414 ICE-Filaments ABS.

The results from the rotational rheometer at an isothermal temperature of 235 °C, in constant strain (1%) and with the plate-plate measurement system, showed in the low frequencies a slightly increase of the viscosity (figure 6-19) only for the ABS printed with the radiant system, could be for a thin crosslink of the rubber phase. Even the curves concerning G' and G''' are marginally higher in the low frequency (figure 6-20) but in the medium and high frequency the viscosity and both moduli are almost identical (figure 8-4 and figure 8-5).

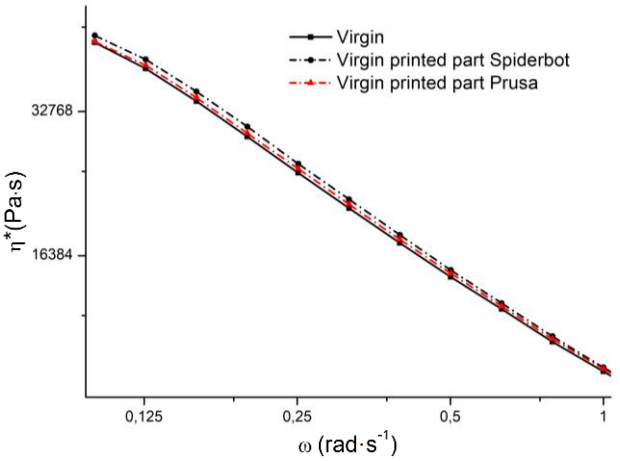

Figure 6-19 Viscosity curves at low frequency ABS 2414 ICE-Filaments virgin and printed by Prusa and Spiderbot.

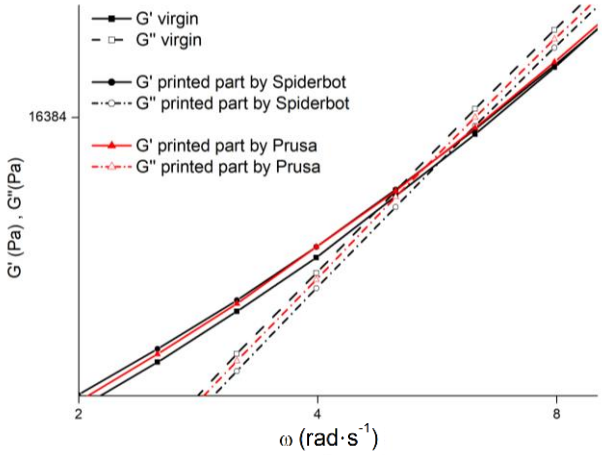

Figure 6-20 G' and G'' curves of ABS 2414 ICE-Filaments, a magnification of the cross over points.

The cross over point from both printers moved to the right and up, but between the low and medium frequency the curves of the both printer parts are overlap and the difference of the position of the point is due to the modulus G''. For this reason, it is difficult to use the information given by the cross-over point to understand if the printers with the radiant system have degraded more the molecular mass respect of the printer without this system. In any case, the movement to the right of the points corresponds to a decrease in molecular mass due to the degradation of the SAN.

So, it can be concluded that there has not been a relevant degradation in the chemical and rheological properties given by the infrared radiant heaters system, compared to a conventional printer.

7. CONCLUSION

It can be concluded that the recycling of ABS plastic for FFF technologies is possible and until the second reprocessing the material maintains good rheological, thermal, chemical and mechanical propriety. The main characteristic of this material, i.e. the resistance to impact, has an acceptable decrease for subsequent reuses and the printed process result easier with less warpage and a lower thermal contraction.

The recycling process carried out in the various ABS plastics, regardless of the type of 3d printer used, has shown a match between the degradation of SAN and PB with a different influence on the general properties.

As far as rheological properties are concerned, it was not possible to obtain a clear trend from the results of the melt flow index, however in general each melt of the recycled material shows an increase.

On the other hand, the results of the tests performed with the rotational rheometer show a clear decrease in viscosity and storage modulus G' up to the second recycling process, which shows a significant decrease after the extrusion process of the filament compared to the printing process.

The data of the crossover points between the two modules of recycled materials suggest an increase in the molecular mass of the ABS, up to the second recycling, due to cross-linking of the rubbery phase, while the loss of viscosity and the reduction of the G' is associated in the literature to the degradation of the polymeric chains of the SAN.

It is assumed in the rheological properties of the melt that the degradation of the SAN matrix plays a predominant role, up to the second recycling, and the melt is not affected by the cross-linking of the rubbery part, which instead from the third recycling influences heavily going to increase G' and complex viscosity.

Probably the effect of grafting and cross-linking of the material needs to exceed a certain threshold before influencing the viscoelastic dynamics of the material.

The thermal analysis showed an increase in the glass transition temperature of SAN probably due to limits of the mobility of the polymer chains.

Infrared spectroscopic analysis has shown a difference between absorption into materials from moulded parts and filaments.

There is an actual decrease in the peaks concerning the PB and CN of the filaments up to the second recycling, the third recycled filament has an imported increase in absorption with a value similar to virgin.
The mechanical properties have had a hardening of the maximum stresses, at break and of the module until the second recycling; a behaviour associated with the increase of the molecular mass due to the crosslinking of the PB. The impact resistance decreased immediately after the first recycling and then stabilized up to the third reprocessing, which can be associated more than the degradation of the rubber phase to the non-homogeneous distribution of rubber particles within the SAN matrix.
The printing process was more controllable with each recycling; the decrease in viscosity helped the bonding, the deposition of the layer was more effective having a melt that infiltrated better between the voids; even the layers shrinking and the warpage were reduced more and more going to facilitate the process.
A visible change in colour was seen qualitatively after each thermal process.
As far as the impact of the infrared radiant system on the general properties of the material is concerned, it showed more benefits than the degradation it could cause.
The chemical properties of the material showed a greater reduction of the absorption peaks of the PB, CN and carbonyl than a conventional printer without this system.
Rheological properties have a slight increase in viscosity and a greater right-side shift of the crossover points between modules, so more accentuated decrease in molecular mass.
The general mechanical properties are increased of 24%, the fracture surfaces show a much greater bonding between layers than the printer without the radiant system.
A higher yellowing was observed in the samples printed with the radiant system.
For the next studies it is recommended to investigate the variation in the distribution of rubber particles due to reprocessing using appropriate etching techniques or by equipping a transmission electron microscope preparing the sample with a cryogenic equipment to preserve the shape of rubber particles. More in-depth research is recommended on the behaviour of PB cross-linking and grafting with the SAN phase due to thermo-mechanical degradation.
Therefore, the closed-loop recycling of ABS used in AM is an attractive strategy for the re-utilization of supporting structures and defective parts, supporting the circular economy concept.

8. ATTACHMENT

Materials

Table 8-1 Data sheet ABS by ICE-Filaments.

Properties	Standards	Test condition	Value	Unit
Specific Gravity	ISO 1183		1.03	g/cc
MFR	ISO 1133	220°C/10kg	5.5	cm^3 / (10 min)
Tensile strength at yield	ISO 527	50 mm/min	44	MPa
Elongation at break	ISO 527 ½	50 mm/min	9	%
Tensile Modulus	ISO 527	1 mm/min	2000	MPa
Impact Strength Charpy Method	ISO 179	23°C	35	KJ/m2
Printing Temperature			220-260	°C
Melting Temperature	ISO 294		245 ± 10	°C
Vicat Softening Point	ASTM D 1525	50°C/h; 50N	103	°C
Filament size			1.75 ± 0.05	mm
Filament Roundness			≥ 95	%

Table 8-2 Data sheet ABS by Sitraplas.

Properties	Standards	Test condition	Value	Unit
Specific Gravity	ISO 1183		1.05	g/cm^3
Melt Volume-Flow rate (MVR)	ISO 1133	220 °C/ 10Kg	15	cm^3/ (10 min)
Tensile strength	ISO 527 -1, -2	50 mm/min	35	MPa
Elongation at break	ISO 527 -1, -2	50 mm/min	35	%
Tensile stress at break	ISO 527 -1, -2	50 mm/min	25	MPa
Yield strain	ISO 527 -1, -2	50 mm/min	4	MPa
Tensile Modulus	ISO 527 -1, -2	1 mm/min	2200	MPa
Impact Strength Charpy Method	ISO 179-1eA	23°C	10	KJ/m2
Vicat Softening Point	ISO 306	50°C/h; 50N	95	°C

Printer technical data

Table 8-3 Technical data Spiderbot.

Architecture	Delta
Extruder type	Bowden Dual Drive
Chamber Temp.	max 90°C heat by infrared ovens
Type of Radiant infrared	
Radiant Temp.	Up to 450°C
Print bed Temp.	max 150°C
Max Extruder Temp.	470°C
Cooling system print head	Liquid
Build Volume	Ø 220 mm x 180 mm
Filament diameter	1.75mm
Nozzle diameter	0.3 to 0.8 mm
X, Y, Z resolution	0.01mm
Build plate	Ø 220 mm
Connectivity	Ethernet via Repetier Server
Build plate leveling	Manual
Calibration	Autocalibration 21-point 3d mapping
Mother board	32-bit Ultratronics
Firmware	
Open Software/Hardware	GNU GPLv3
Print Bed	Heated, Fixed, PEI Coating
Motor	
Belt	
Belt pulleys	
Extruder pulley	
Driver	1/128e step drivers
Velocity	
Layer height	0.15 to 0.45 mm depending on nozzle
Extruder type	Bowden
Standard nozzle diameter	Ø 0.5mm
Nozzle diameter used	Ø 0.5mm

Table 8-4 Technical data Prusa.

Architecture	Cartesian
Build volume	250 x 210 x 210mm
Filament diameter	1,75 mm
Cooling system print head	Forced air
X, Y, Z resolution	0.01mm
Build plate	250x210
Connectivity	SD Card, WI-FI, USB
Build plate leveling	Automatic
Calibration	Automatic + skew axes compensation
Mother board	EINSY RAMBo
Max. Extruder Temperature	300°C
Max. Print Bed Temperature	120°C
Firmware	Marilyn
Open Software/Hardware	GNU GPLv3
Print Bed	Heated, Removable, PEI Coating
Motor	NEMA 17
Belt	GT2
Belt pulleys	16t
Extruder pulley	Bontech Pulley Drive Gear
Driver	Trinamic 256 microstep
Velocity	200+ mm/s
Layer height	From 0.05mm
Extruder type	Direct
Chamber	Ambient temperature
Standard / used nozzle	Ø 0.4mm – Ø 0.5mm

Data sheet nozzle

TABLE							
SKU	A	B	C	D	E	F	# Dots
V6-NOZZLE-175-150	0.15	0.30	0.18?	2.0	2.6	0.10	?
V6-NOZZLE-175-250	0.25	0.63	0.38	2.0	2.6	0.10	0
V6-NOZZLE-175-300	0.30	0.75	0.45	2.0	2.6	0.10	1
V6-NOZZLE-175-350	0.35	0.88	0.53	2.0	2.6	0.15	2
V6-NOZZLE-175-400	0.40	1.00	0.60	2.0	2.6	0.20	3
V6-NOZZLE-175-500	0.50	1.25	0.90	2.0	2.6	0.20	6
V6-NOZZLE-175-600	0.60	1.50	1.20	2.0	2.6	0.25	4
V6-NOZZLE-175-800	0.80	2.00	1.60	2.0	2.6	0.30	5

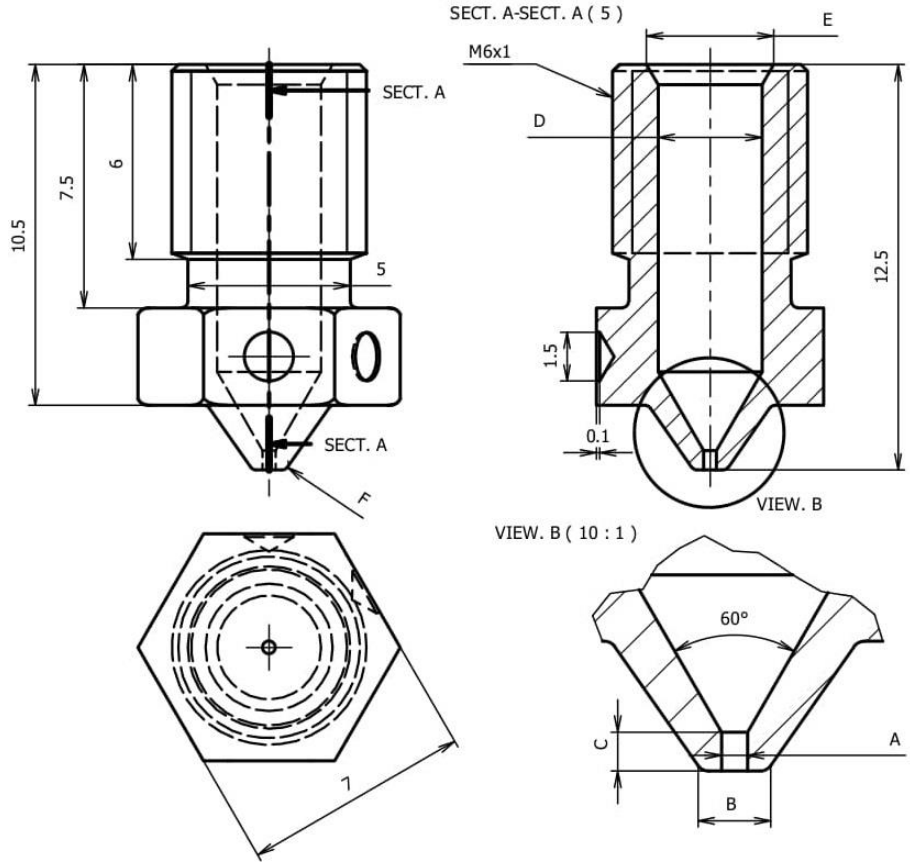

Figure 8-1 Nozzle technical data.

Slicer setting

Table 8-5 Cura slicer setting.

CURA SETTINGS	Spiderbot ICE-Filaments ABS	Spiderbot SitraPlas ABS	Prusa ICE-Filaments ABS	Prusa SitraPlas ABS	Unit
Initial/Top/Bottom layer height	0.25	0.25	0.25	0.25	mm
Line width (Outer/Inner) initial/ Top/Bottom/Infill	0.5	0.5	0.5	0.5	mm
Wall thickness (1 wall line)	0.8	0.8	0.8	0.8	mm
Outer wall wipe distance	0.25	0.25	0.25	0.25	mm
Top/Bottom/Initial/ Infill layer pattern	LINE	LINE	LINE	LINE	
Top/Bottom line directions	[45, -45]	[45, -45]	[45, -45]	[45, -45]	
Outer before inner walls	yes	yes	yes	yes	
Fill gaps between walls	everywhere	everywhere	everywhere	everywhere	
Initial layer horizontal expansion	0.15	0.15	0.15	0.15	mm
Z seam alignment	Random	Random	Random	Random	
Infill density	100	100	100	100	%
Connect infill lines	yes	yes	yes	yes	
Infill line directions	[90, 45, 90, -45]	[90, 45, 90, -45]	[90, 45, 90, -45]	[90, 45, 90, -45]	
Infill overlap	0.4	0.25	0.3	0.3	mm
Skin overlap	0.3	0.35	0.3	0.3	mm
Infill wipe distance	0.125	0.125	0.125	0.125	mm
Infill layer thickness	0.25	0.25	0.25	0.25	mm
Skin removal width and expand distance Top/Bottom	0.5	0.5	0.5	0.5	mm
Maximum skin angle for expansion	90°	90°	90°	90°	
Maximum width for expansion	0	0	0	0	mm
Default/Initial/Final/ Initial layer temp.	235	235	235	235	°C
Bed temperature	112	112	112	112	°C
Flow	104	113	104	114	%
Initial Flow	120	135	120	140	%
Enable Retraction/ Retract at layer change	yes	yes	yes	yes	
Retraction distance	9	8.5	0.8	0.8	mm
Retraction retract/Prime speed	20	20	35	35	mm/s
Retraction extra prime amount	2.5	2.5	0.2	0.4	mm^3

Retraction minimum travel	4	4	0.8	0.8	mm
Maximum retraction count	200	200	90	90	
Minimum extrusion distance windows	9	8.5	0.8	0.8	mm
Nozzle switch retraction distance	4.5	4.5	16	16	mm
Nozzle switch retraction/ Retract/Prime speed	20	20	20	20	mm/s
Print / Infill Speed	35	35	35	35	mm/s
Wall/Wall Outer and Top/ Bottom Speed	17.5	17.5	17.5	17.5	mm/s
Wall inner Speed	35	35	35	35	mm/s
Initial/ Travel speed and Maximum Z speed	50	50	50	50	mm/s
Initial/ Travel print speed	40	40	40	40	mm/s
Number of slower layers	2	2	2	2	
Maximum speed for flow equalization	60	60	60	60	mm/s
Travel setting	Default	Default	Default	Default	
Build Plate Adhesion Type	Raft	Raft	Raft	Raft	
Raft Extra Margin	3	3	3	3	
Raft Smoothing	2	2	2	2	
Raft Air Gap / Initial Layer Z overlap	0.13	0.12 / 0.18	0.3 / 0.19	0.3 / 0.19	mm
Raft Top Layers	2	2	2	2	
Raft Layer Thickness	0.25	0.25	0.25	0.25	mm
Raft Top Line Width/ Spacing	0.5	0.5	0.5	0.5	mm
Raft Middle Thickness	0.3	0.3	0.3	0.3	mm
Raft Base line width	1	1	1	1	mm
Raft base line spacing	2	2	2	2	mm
Raft Top/ Middle Print Speed	40	40	40	40	mm/s
Raft Base Print Speed	17.5	17.5	17.5	17.5	mm/s
Raft Fan Speed	0	0	0	0	%
Cooling/ Support/Mesh Fixes/ Special Modes/Experimental	NO	NO	NO	NO	

Underlined the different settings between the printers.

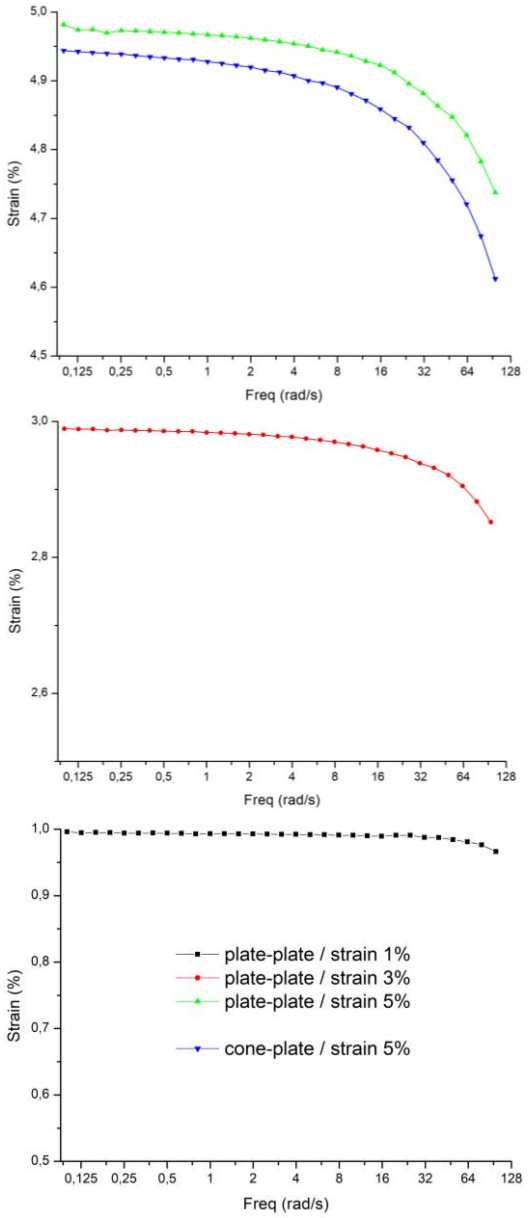

Figure 8-2 Strain tests of the ABS 2414 recycled 1 and the comparison of the measuring system.

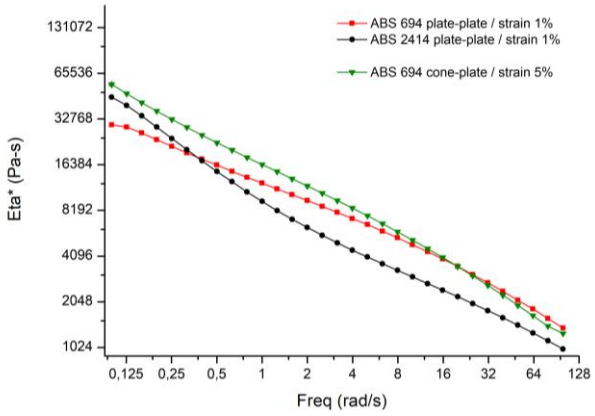

Figure 8-3 Viscosity comparison ABS 694 and 2414, different measuring system and strain %.

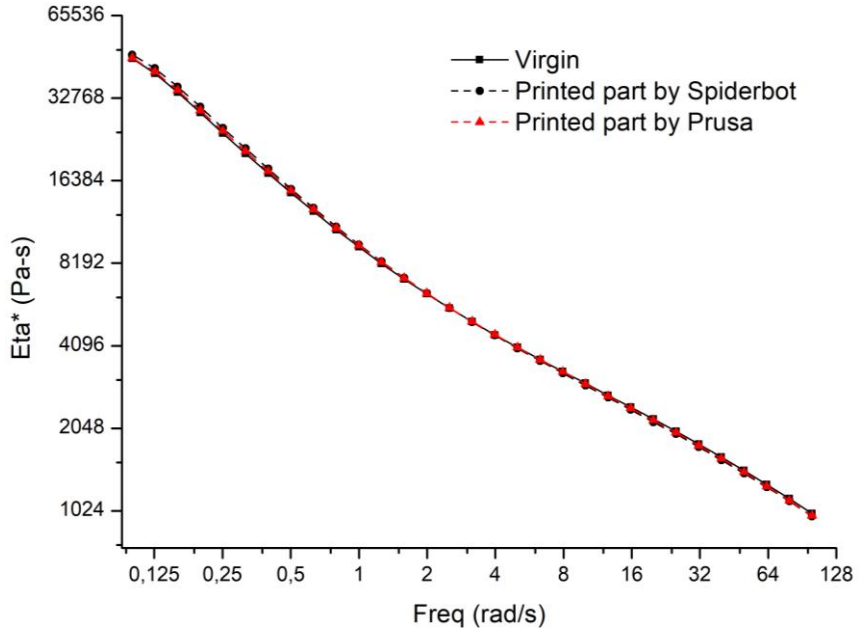

Figure 8-4 Viscosity curves ABS 2414 ICE-Filaments virgin and printed by Prusa and Spiderbot.

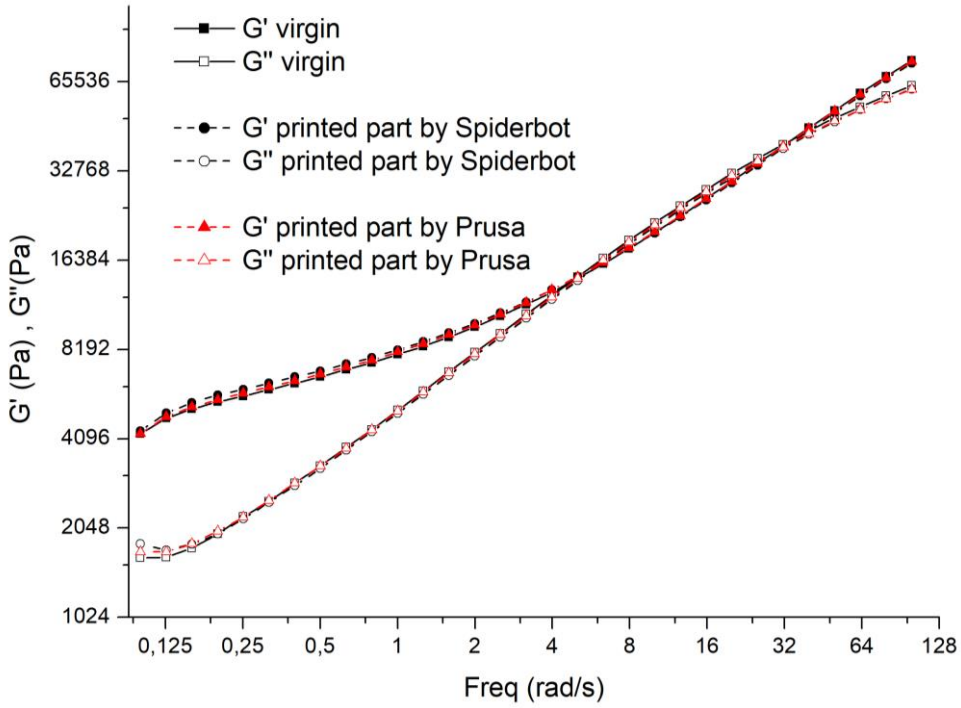

Figure 8-5 G' and G'' curves of ABS virgin printed by Prusa and Spiderbot.

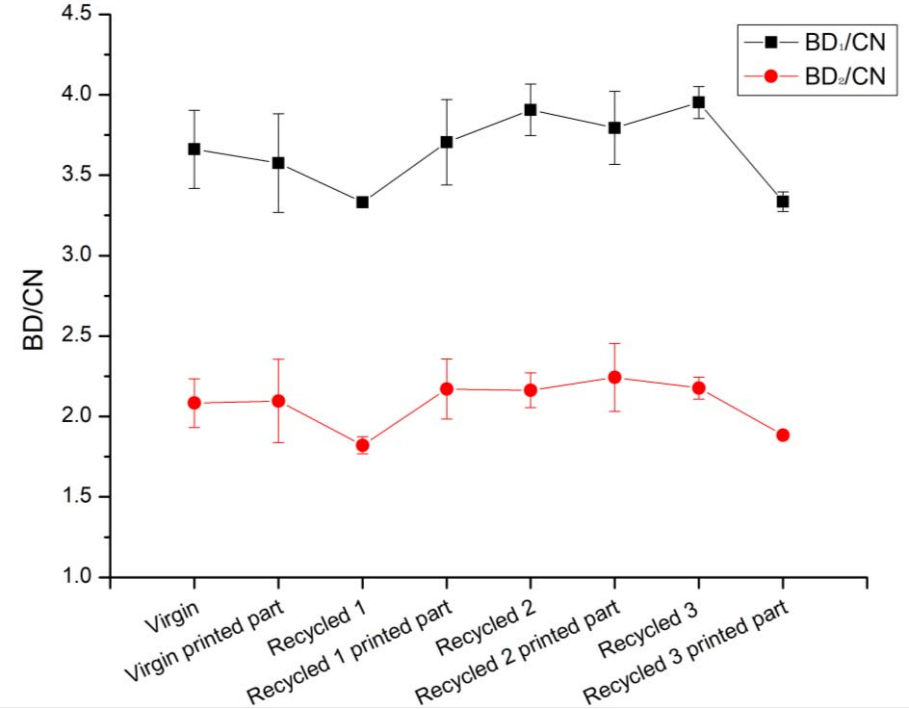

Figure 8-6 BD/CN ABS 694 ICE-Filaments printed by Spiderbot.

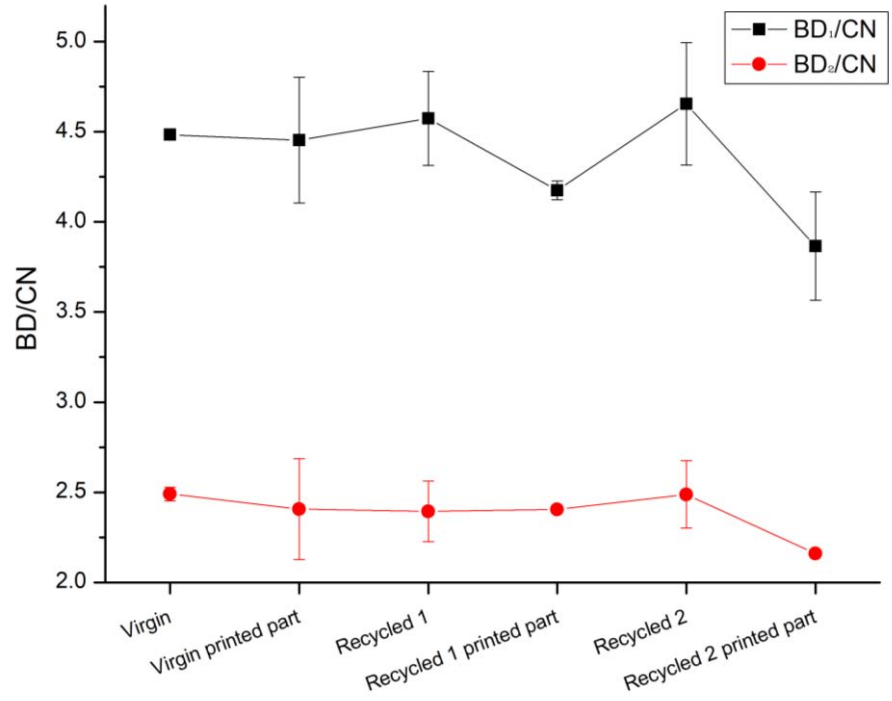

Figure 8-7 BD/CN ABS 2414 ICE-Filaments printed by Prusa.

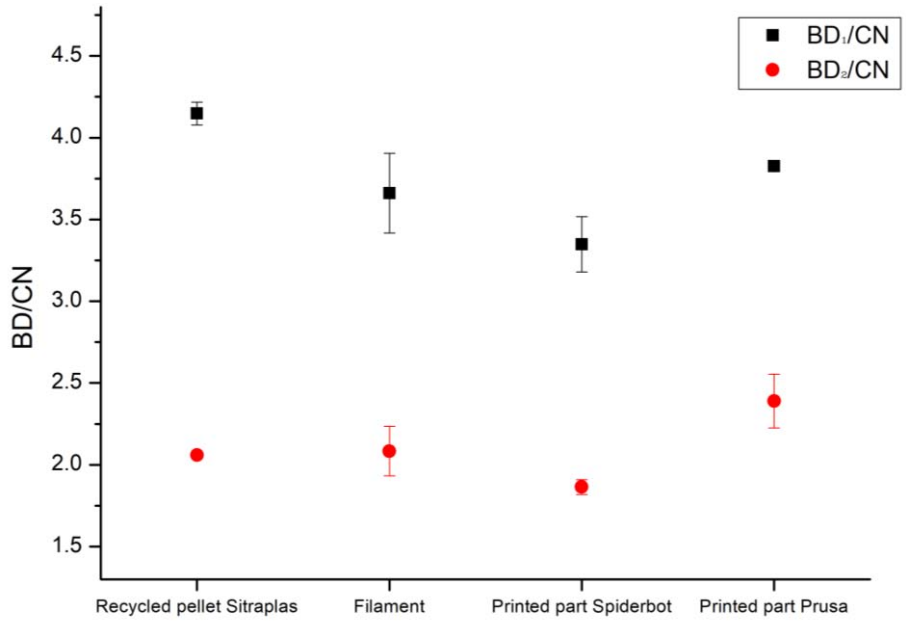

Figure 8-8 ABS 2414 ICE-Filaments virgin.

Table 8-6 IR ABS characteristic peaks.

Peak/ cm^{-1}	**Attribution**
758	ω S CH_2 ring bends
911	ω - CH 1,2 PB
966	ω - CH 1,4 PB
1071	v - PS ring modes
1156	v - PS ring modes
1181	v - PS ring modes
1355	ω - CH 1,2 PB and 1,4 PB
1453	δ_s - CH_2 scissoring
1494	v_{as} - PS ring modes
1583	v - PS ring modes
1602	v - PS ring modes
1639	v - CH 1,2 PB
2237	v_s - CN
2800-3000	v_s, v_{as} - Aliphatic CH stretching
3000-3200	v_{as} Aromatic CH stretching

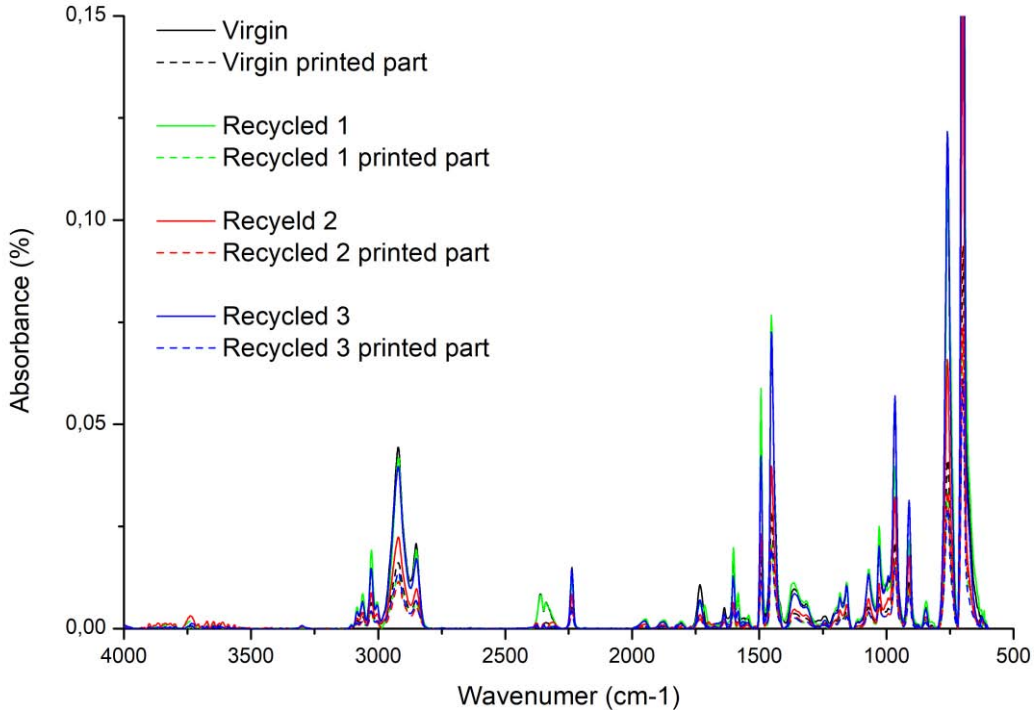

Figure 8-9 Infrared spectrum ABS 694 ICE-Filament up to the third recycle.

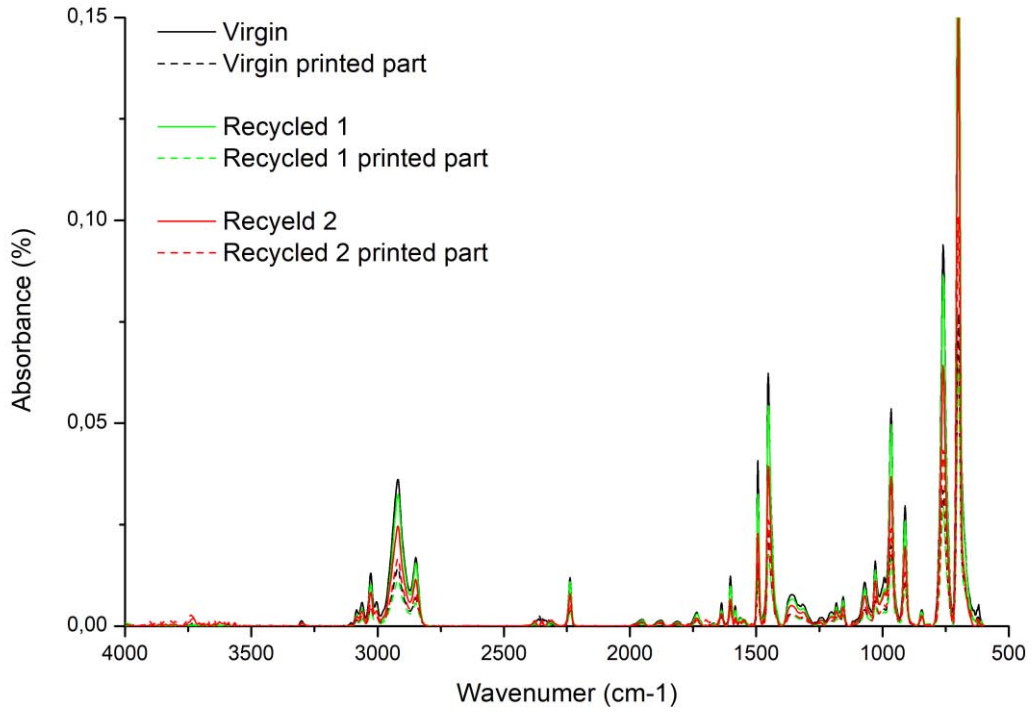

Figure 8-10 Infrared spectrum ABS 2414 ICE-Filament up to the second recycle.

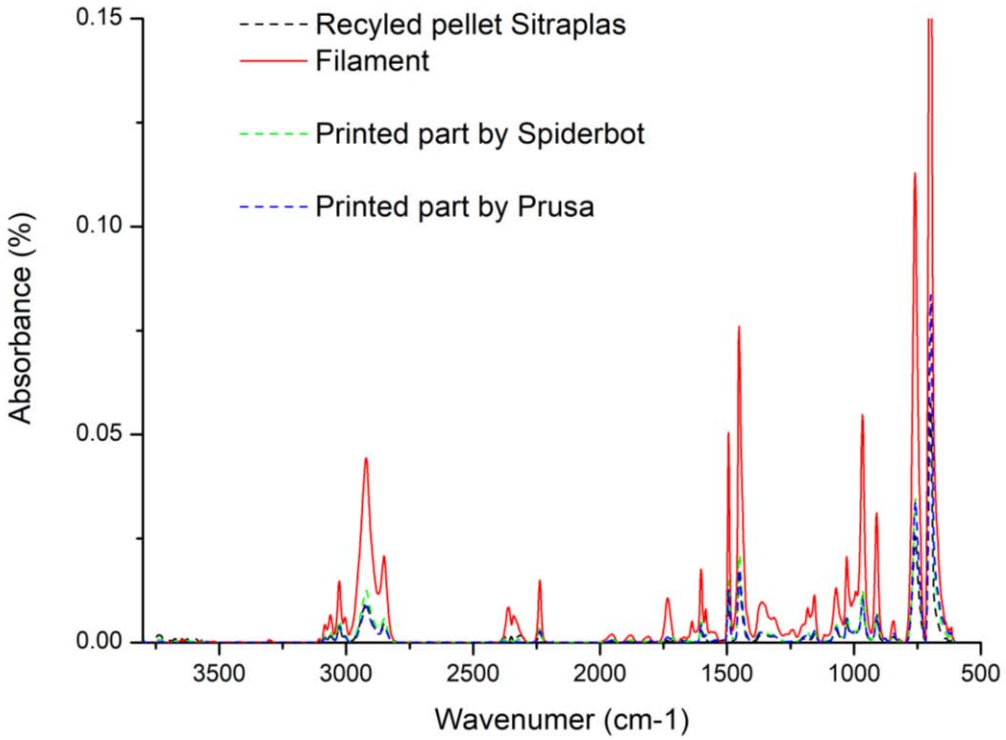

Figure 8-11 Infrared spectrum ABS Sitraplas.

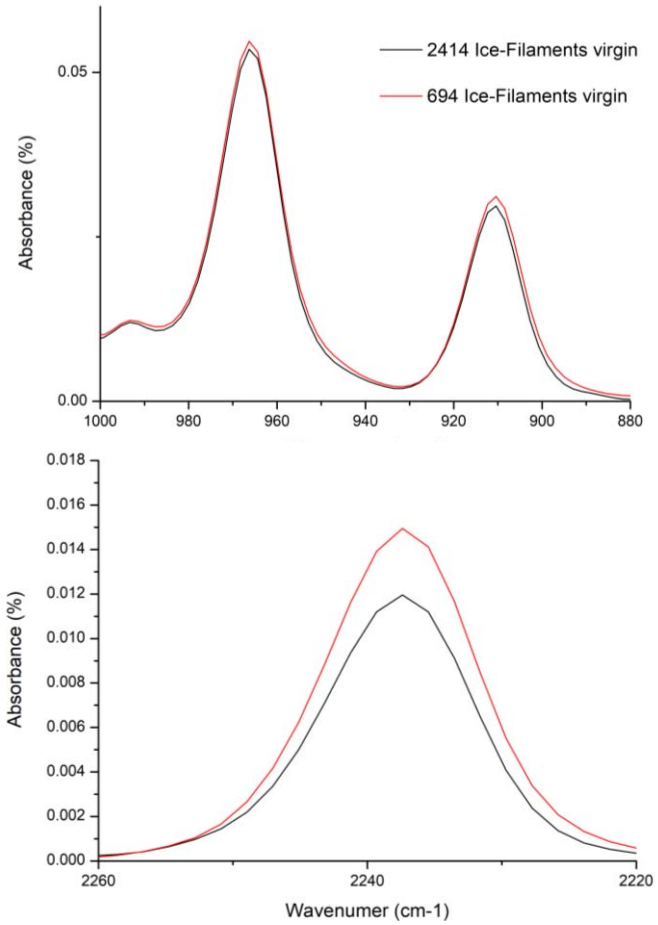

Figure 8-12 Comparison between PB and CN infrared absorption peaks of the ABS ICE-Filaments 694 and 2414 virgins.

Mechanical properties in dependence of the apparent areal density

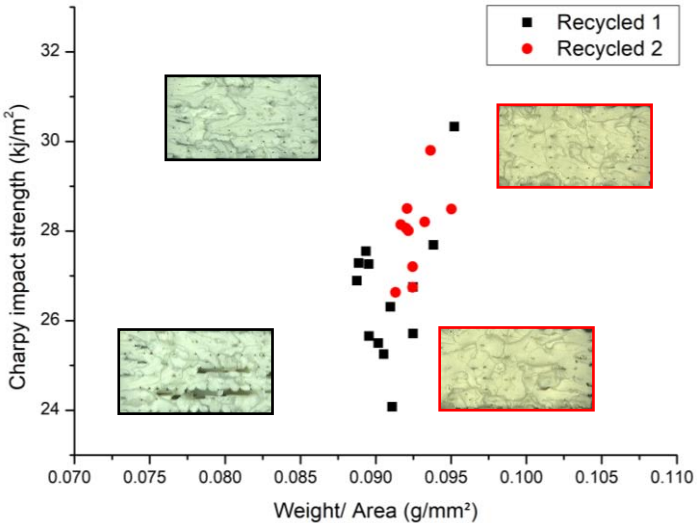

Figure 8-13 Impact strength in function of the apparent areal viscosity of the recycled ABS Ice-Filaments 2414 printed by Prusa.

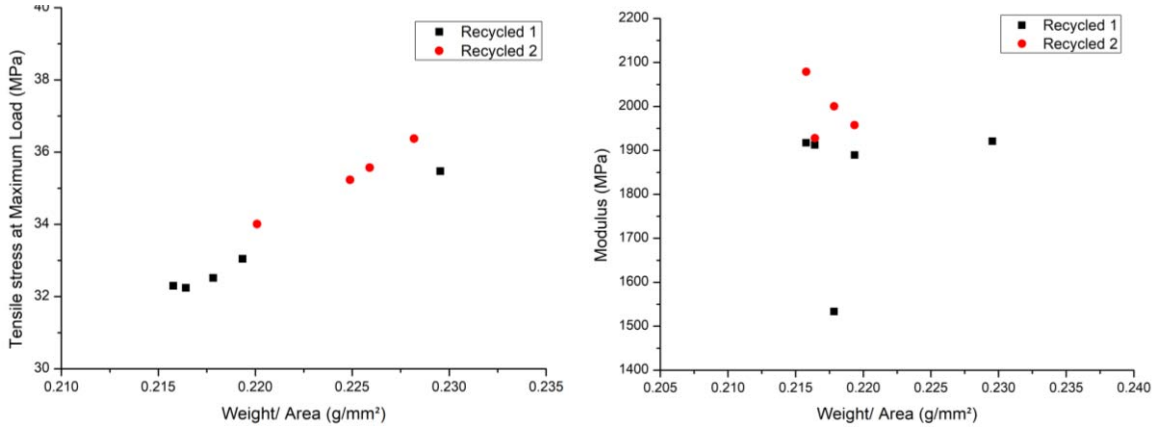

Figure 8-14 Tensile stress at maximum load and modulus in function of the apparent areal viscosity of the recycled ABS ICE-Filaments 2414 printed by Prusa.

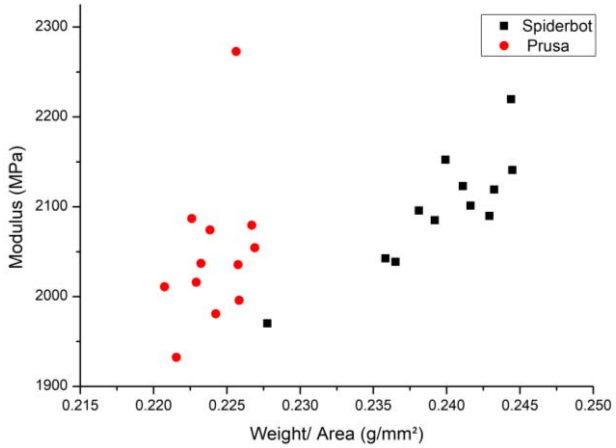

Figure 8-15 Modulus in function of the apparent areal viscosity of the recycled ABS Sitraplas.

Stress – Strain Curves ABS-ICE Filaments Spiderbot

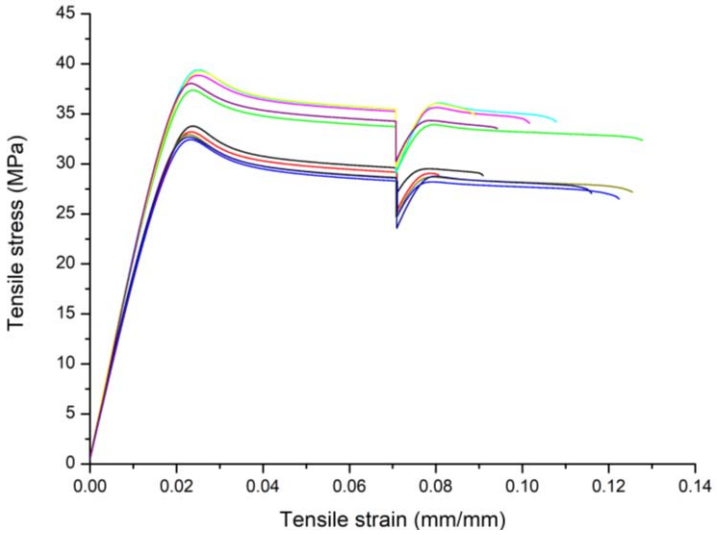

Figure 8-16 ABS 694 ICE-Filament virgin.

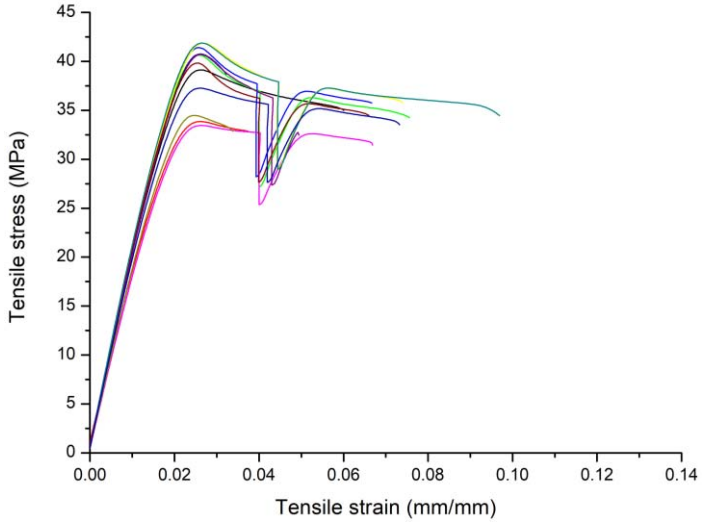

Figure 8-17 ABS 694 ICE-Filaments recycled 1.

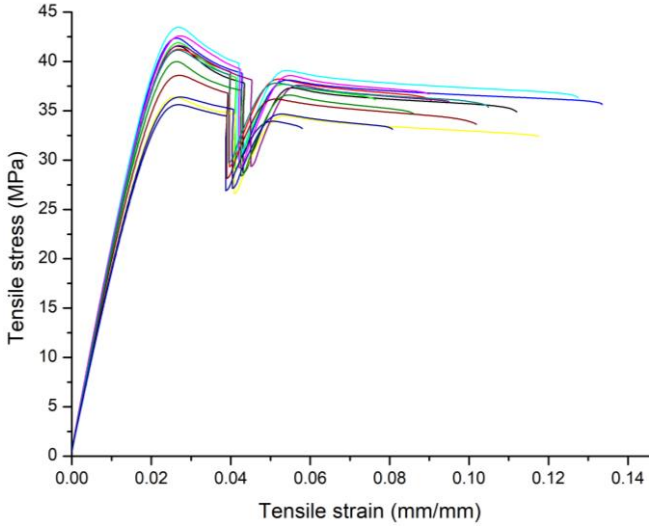

Figure 8-18 ABS 694 ICE-Filaments recycled 2.

Stress – Strain Curves ABS-ICE Filaments Prusa

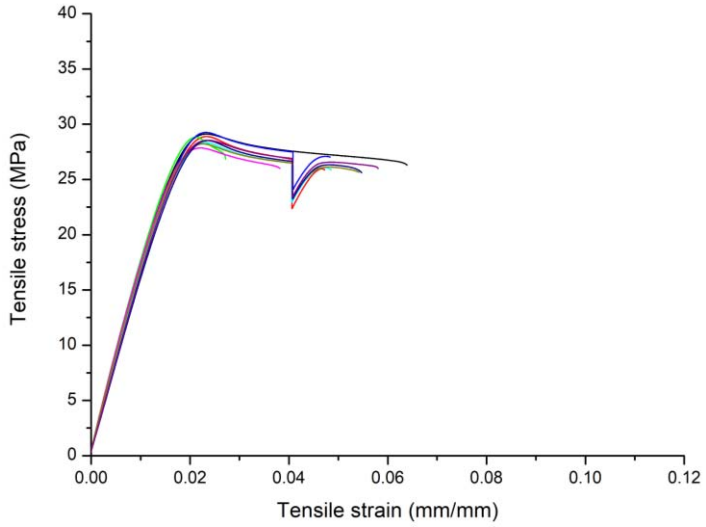

Figure 8-19 ABS 2414 ICE-Filaments virgin.

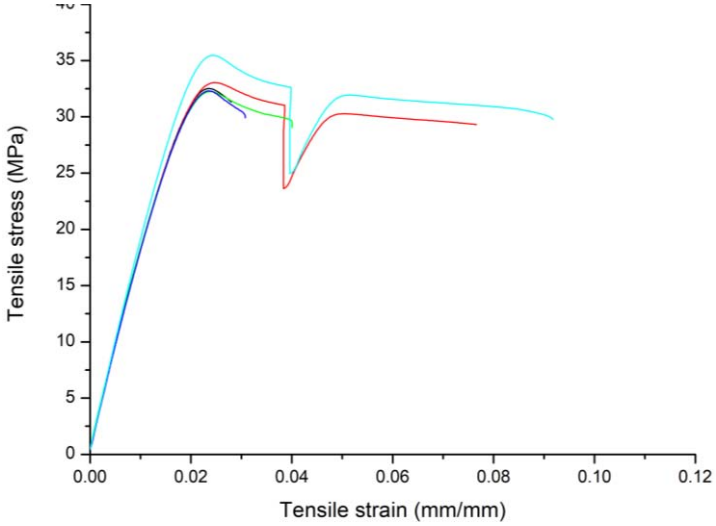

Figure 8-20 ABS 2414 ICE-Filaments recycled 1.

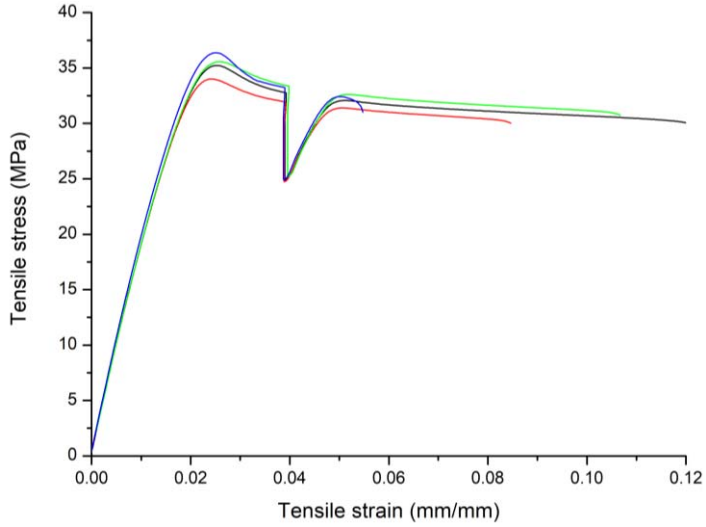

Figure 8-21 ABS 2414 ICE-Filaments recycled 2.

Filament contamination

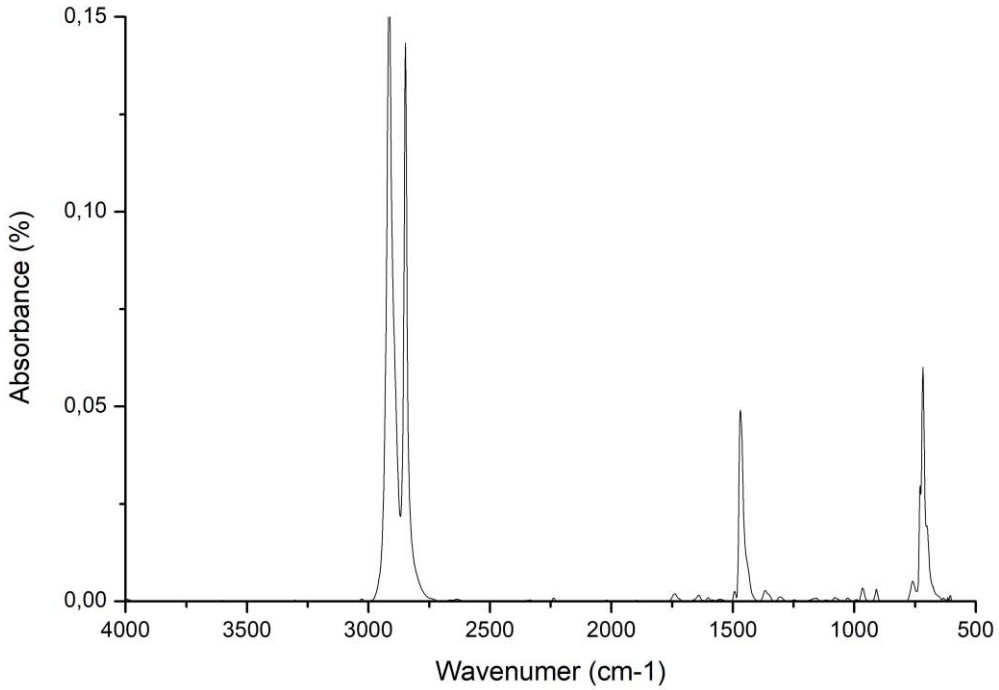

Figure 8-22 Absorption spectra of the contamination of the third recycled filament (ABS 694 ICE-Filaments).

Figure 8-23 Contamination around the filament.

Figure 8-24 Failed printed due to the problem at the feeding system, gave from the contamination.

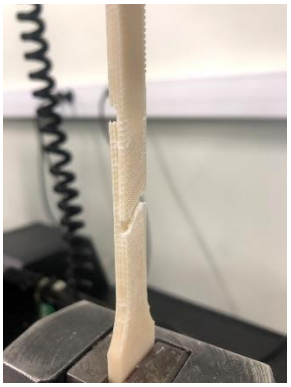

Figure 8-25 Premature fracture of a tensile bone with defects due to problem of under-extrusion.

9. BIBLIOGRAPHY

[1] www.ec.europa.eu/programmes/horizon2020/en/what-horizon-2020

[2] R. Geyer, J. Jambeck, and K. Law, “Production, Use, And Fate Of All Plastics Ever Made,” Sci. Adv., vol. 3, no. 7, pp. 25–29, 2017.

[3] www.ec.europa.eu/environment/circular-economy.

[4] J. Faludi, C. Bayley, S. Bhogal, and M. Iribarne, “Comparing Environmental Impacts Of Additive Manufacturing Vs Traditional Machining Via Life-Cycle Assessment”, Rapid Prototyp. J., vol. 21, no. 1, pp. 14–33, 2015.

[5] R. Song, C. Telenko, and G. W. Woodruff, “Material Waste of Commercial Fdm Printers Under Realstic Conditions”, Solid Free. Fabr., no. 2015, pp. 1217–1229, 2016.

[6] I. Gibson, D. Rosen, B. Stucker, "Additive Manufacturing Technologies", Second Edition, pp. 1-6, 43-50, 147-153, 2015.

[7] www.stratasys.com/fdm-technology.

[8] P. J. Ba, “Sustainability in extrusion-based additive manufacturing technologies”, pp. 65–78, 2016.

[9] www.reprap.org/wiki/RepRap

[10] M. Dawoud, I. Taha, and S. J. Ebeid, “Mechanical behaviour of ABS: An experimental study using FDM and injection moulding techniques”, J. Manuf. Process., vol. 21, pp. 39–45, 2016.

[11] www.3dhubs.com/knowledge-base/fdm-3d-printing-materials-compared-

[12] C. S. Davis, K. E. Hillgartner, S. H. Han, and J. E. Seppala, “Mechanical Strength Of Welding Zones Produced By Polymer Extrusion Additive Manufacturing”, Addit. Manuf., vol. 16, pp. 162–166, 2017.

[13] AA.VV., “Polimeri Stirenici Termoplastici”, Encicl. degli Idrocarb. TRECCANI, vol. II, pp. 837–862, 2003.

[14] www.filaments.directory/en/trends.

[15] A. E. Albrecht, C. J. West, and L. B. Flohr, “Market Statistics”, Journal of the American Statistical Association, vol. 18, no. 137. p. 136, 2006.

[16] T. Boronat, V. J. Segui, M. A. Peydro, and M. J. Reig, “Influence Of Temperature And Shear Rate On The Rheology And Processability Of Reprocessed ABS In Injection Molding Process”, J. Mater. Process. Technol.,

vol. 209, no. 5, pp. 2735–2745, 2009.

[17] J. M. Pérez et al., “Effect Of Reprocessing And Accelerated Weathering On ABS Properties”, J. Polym. Environ., vol. 18, no. 1, pp. 71–78, 2010.

[18] P. A. T. E.-K. Karahaliou, “Stability of ABS Compounds Subjected to Repeated Cycles of Extrusion Processing E.-K.,” vol. 47, no. 22, 2012.

[19] J. K. K. and C. K. Kang, “Polymer-Plastics Technology and Engineering,” Polym. Plast. Technol. Eng., vol. 34, p. 875, 1995.

[20] L. B. Brennan, D. H. Isaac, and J. C. Arnold, “Recycling Of Acrylonitrile-Butadiene-Styrene And High-Impact Polystyrene From Waste Computer Equipment”, J. Appl. Polym. Sci., vol. 86, no. 3, pp. 572–578, 2002.

[21] D. Hirayama and C. Saron, “Morphologic And Mechanical Properties Of Blends From Recycled Acrylonitrile-Butadiene-Styrene And High-Impact Polystyrene”, Polymer (Guildf)., vol. 135, pp. 271–278, 2018.

[22] S. S. W. Grellmann, “Deformation and Fracture Behaviour of Polymers,” Springer Sci. Bus. Media, 2001.

[23] S. Wu, “Chain structure, phase morphology and toughness relationship in polymer blends,” Polym. Eng. Sci., vol. 30, p. 753,764, 1990.

[24] A. Margolina and S. Wu, “Percolation Model For Brittle-Tough Transition In Nylon/Rubber Blends”, Polymer (Guildf)., vol. 29, no. 12, pp. 2170–2173, 1988.

[25] X. Bai, B. K. Stein, K. Smith, and D. H. Isaac, “Effects of Reprocessing on Additives in ABS Plastics , Detected by Gas Chromatography / Mass Spectrometry”, vol. 28, no. 1, pp. 1–14, 2011.

[26] J. Shimada and K. Kabuki, “The Mechanism Of Oxidative Degradation Of ABS Resin. Part I. The Mechanism Of Thermooxidative Degradation”, J. Appl. Polym. Sci., vol. 12, no. 4, pp. 655–669, 2003.

[27] K. S. Xiaojuan Bai, D.H. Isaac, “Reprocessing Acrylonitrile–Butadiene–Styrene Plastics: Structure–Property Relationships,” vol. 47, no. 22, 2012.

[28] M. I. Mohammed, A. Das, E. Gomez-kervin, D. Wilson, and I. Gibson, “EcoPrinting : Investigating The Use Of 100 % Recycled Acrylonitrile Butadiene Styrene (ABS) For Additive Manufacturing,” Solid Free. Fabr. Symp., pp. 532–542, 2017.

[29] P. Zhao, C. Rao, F. Gu, N. Sharmin, and J. Fu, “Close-Looped Recycling Of

Polylactic Acid Used In 3D Printing: An Experimental Investigation And Life Cycle Assessment," J. Clean. Prod., vol. 197, pp. 1046–1055, 2018.

[30] P. Cirp et al., "A Comparison Between Mechanical Of Specimens 3D Printed With Virgin And Properties Recycled PLA A New Methodology To Analyze The Functional And Physical 3D Printed With Virgin Recycled PLA A Architecture Of Martorelli Product ", Procedia CIRP, vol. 79, pp. 143–146, 2018.

[31] F. A. C. Sanchez, "Methodological Proposition To Evaluate Polymer Recycling In Open-Source Additive Manufacturing Contexts", Doctoral Dissertation, 2016.

[32] R. Goutham, T. R. Veena, and S. P. K. R, "ScienceDirect Study on mechanical properties of recycled Acrylonitrile Butadiene Styrene (ABS) blended with virgin Acrylonitrile Butadiene Styrene (ABS) using Taguchi method," Mater. Today Proc., vol. 5, no. 11, pp. 24836–24845, 2018.

[33] www.icefilaments.com/material/abs

[34] www.sitraplas.de/en/products/sitralacr-abs

[35] ISO, "Plastics: Determination Of The Melt Mass-Flow Rate (MFR) And Melt Volume-Flow Rate (MVR) Of Thermoplastics", ISO/DIS 1133, 2011.

[36] ISO, "Plastics: Determination Of The Melt Volume-Flow Rate (MVR) And Melt Mass-Flow Rate (MFR) Of Thermoplastics Materials", ISO 1133, 2009.

[37] ISO, "Plastics: Differential Scanning Calorimetry (DSC)", ISO 11357-6, 2018.

[38] ISO, "Plastics: Methodol. Assess. Polym. photoageing by FT-IR UV-visible Spectrom", ISO 10640, 2009.

[39] www.spiderbot.eu/spiderbot-4-0-ht

[40] www.prusa3d.com

[41] Angelo Gennaro, "Materie Plastiche: Testing Fisico-Meccanici", HOEPLI, pp. 72, 2012.

[42] G. Gozzelino, "Materie plastiche", HOEPLI, pp. 105-119, 2017.

[43] ISO, "Plastics: Determination Of Tensile Properties, Part 1", ISO 527-1, 1996.

[44] ISO, "Plastics: Determination Of Tensile Properties, Part 2", ISO 527-2, 1993.

[45] ISO, "Plastics: Charpy impact Properties", ISO 179-1, 1998.

[46] www.nanoscience.com/techniques/scanning-electron-microscopy

[47] H. A. Barnes, Rheology: Principles, Measurements and Applications, vol. 86, no. 3. 1996.

[48] V. E. Dreval, G. B. Vasil, E. K. Borisenkova, and V. G. Kulichikhin, “Rheological and Mechanical Properties of ABS Plastics Prepared by Bulk Polymerization”, no. January, 2006.

[49] H. Ag, “Characterization Of Polymer Molecular Mass Distribution”, vol. 341, pp. 324–341, 1992.

[50] S. Effect, “Dynamic Viscoelastic Properties of ABS Polymers in the Molten” ,vol. 2213, no. 20, pp. 2208–2213, 1987.

[51] K. C. Ang, K. F. Leong, and C. K. Chua, “Investigation Of The Mechanical Properties And Porosity Relationships In Fused Deposition Modelling-Fabricated Porous Structures”, vol. 2, no. July 2005, pp. 100–105, 2006.